Vibration Response of the Polar Supply and Research Vessel the S.A. Agulhas II in Antarctica and the Southern Ocean

by
Keith Ian Soal

Thesis presented in fulfilment of the requirements for the degree of Master in Mechanical Engineering in the Faculty of Engineering at Stellenbosch University

Supervisor: Dr. A. Bekker

December 2014

Declaration

By submitting this thesis electronically, I declare that the entirety of the work contained therein is my own, original work, that I am the sole author thereof (save to the extent explicitly otherwise stated), that reproduction and publication thereof by Stellenbosch University will not infringe any third party rights and that I have not previously in its entirety or in part submitted it for obtaining any qualification.

Date: .....

Abstract

Vibration Response of the Polar Supply and Research Vessel the S.A. Agulhas II in Antarctica and the Southern Ocean

K. Soal

Thesis: MEng (Mechanical)

November 2014

Full scale measurements were conducted on the polar supply and research vessel the S.A. Agulhas II during a 78 day voyage from Cape Town to Antarctica in 2013/2014. Investigations were conducted into the effect of vibration on human comfort and the structural dynamic response of the vessel. Vibration measured in the bridge of the vessel is found to have little effect on human comfort for a standing person and is classified as not uncomfortable according to BS ISO 2631-1. Structural fatigue as a result of vibration is found to reach levels where damage is possible in the stern and where damage is probable in the bow during open water navigation, according to ship vibration guidelines by Germanischer Lloyd. Multivariate statistical analyses are performed to investigate the relationships between multiple predictor variables and vibration response. Factor analysis revealed data structure from which specific physical phenomena could be identified. Multivariable linear regression models are developed to predict vibration response and are found to provide more accurate predictions in open water than in ice. The 2-node, 3-node and 4-node normal bending modes of the structure are identified using operational modal analysis while the vessel was moored in the harbour. The natural frequencies, damping ratios and mode shapes are estimated and compared using LMS Operational PolyMAX and ARTeMIS CCSSI. A comparison of operational modal analysis results to the STX Finland finite element model show that the vessel's modes occur at lower frequencies than numerically predicted. Clear potential is identified to further investigate structural vibration and operational modal analysis algorithm development in future research.

Uittreksel

("Vibration Response of the Polar Supply and Research Vessel the S.A. Agulhas II in Antarctica and the Southern Ocean")

K. Soal

Tesis: MIng (Meganies)
November 2014

Volskaal metings was op die poolvoorsienings en navorsingskip die S.A. Agulhas II uitgevoer tydens 'n 78 dae reis van Kaapstad tot Antarktika in 2013/2014. Ondersoeke is uitgevoer met betrekking tot die effek van vibrasie op menslike gemak en die strukturele dinamiese reaksie van die vaartuig. Vibrasie wat in die brug van die skip gemeet is, het min invloed op menslike gemak vir 'n staande persoon en word geklassifiseer as nie ongemaklik volgens BS ISO 2631-1. Strukturele vermoeidheid as gevolg van vibrasie bereik vlakke waar skade moontlik is in die spieël en waar skade waarskynlik is in die boog tydens navigasie in oop water, volgens skip vibrasie riglyne deur Germanischer Lloyd. Meerveranderlike statistiese ontledings is uitgevoer om die verhoudings tussen verskeie voorspellerveranderlikes en vibrasieterugvoer te ondersoek. Faktorontleding het data struktuur openbaar waaruit spesifieke fisiese verskynsels geïdentifiseer kan word. Multi-veranderlike lineêre regressiemodelle was ontwikkel om vibrasie reaksie te voorspel en lewer meer akkurate voorspellings in oop water as in ys. Die 2-nodus, 3-nodus en 4-nodus normale buig modes van die struktuur is geïdentifiseer met behulp van operasionele modale analise terwyl die skip vasgemeer in die hawe is. Die natuurlike frekwensie, demping verhoudings en mode vorms is beraam en vergelyk met behulp van LMS operasionele Polymax en ARTeMIS CCSSI. 'n vergelyking van operasionele modale analise resultate en 'n STX Finland eindige element model toon dat die vaartuig se modusse voorkom by laer frekwensies as wat numeries voorspel word. Duidelike potensiaal is geïdentifiseer om strukturele vibrasie en die ontwikkeling van operasionele modale analise algoritmes te ondersoek in toekomstige navorsing.

Acknowledgements

It has been an incredible privilege to work on the S.A. Agulhas II during two voyages to Antarctica. The people that I have come to know during long voyages at sea, as well as those in the consortium, at conferences and at the University of Stellenbosch have not only made significant contributions to my work but also to my character.

I would firstly like to thank my supervisor Dr Annie Bekker for her wisdom and support throughout this project. She is a passionate and motivated woman from whom I have learnt so much. I would also like to thank Prof Joerg Bienert for his technical expertise in Operational Modal Analysis (OMA) and for allays being willing to answer all my questions. To Kim McMahon, Brendan Boulle and Fourie Gildenhuys for their help during long days and nights spent instrumenting the vessel and their 'gees' throughout the voyage. To Oom Ferdi Zietsman, Jacques Muiyser, Daan Nel, Cheif Engineer Alan, Captain Gavin Syndercombe, Captain Knowledge Bengu and their crews, Alan Robertson, Bigboy Joseph and Jeremy Pietersen for their help and advice during different stages of this project. I would also like to thank the Department of Environmental Affairs of South Africa for the opportunity to conduct measurements on their ship, as well as the project partners namely STX Finland, Aalto University, the University of Oulu, Aker Arctic, Rolls-Royce, DNV and Wärtsilä. And of course a very big thank you to the National Research Foundation for the project funding. Finally to my family for their amazing support in the pursuit of my passion in mechanical engineering. And most importantly to God upon whom I base my life.

Dedications

This thesis is dedicated to my mom Esther, dad Bruce and sister Hayli, and to my God.

Contents

List of Figures

List of Tables

Nomenclature

Variables

a_w	Weighted rms acceleration
$\underline{\boldsymbol{C}}$	Damping matrix
$\underline{\boldsymbol{F}}$	State transition matrix
$\boldsymbol{F_n}$	Underlying factors
$\underline{\boldsymbol{H}}$	Observation matrix
g_i	Operational reference factor
i	Sample index
$\underline{\boldsymbol{I}}$	Identity matrix
k	Multiplying factor
$\underline{\boldsymbol{K}}$	Stiffness matrix
$\underline{\boldsymbol{L}}$	Observation matrix
$\underline{\boldsymbol{L_n}}$	Factor loadings
$\underline{\boldsymbol{M}}$	Mass matrix
n	Number of modes
N	Total number of samples
p, q	Estimators
$\underline{\boldsymbol{R}}$	Correlation matrix
$\underline{\boldsymbol{S_{yy}}}$	Cross Spectrum
t	Time
T_s	Duration of the sampled motion
$\boldsymbol{v}$	Excitation
v_i	Mode shape
$\boldsymbol{V_k}$	Residual
VDV_w	Weighted VDV acceleration
$x(i)$	Sampled data values

$\boldsymbol{X}$	Observable random vector
$\boldsymbol{Y}$	Measured data
$\boldsymbol{Y_n}$	Response variables
y_k	Measured signal
$\boldsymbol{Z_n}$	Predictor variables
β	Unknown regression coefficients
ω	Frequency
ω_k	Weighting
ω_i	Eigenfrequency
$\underline{\boldsymbol{\mathcal{H}}}$	Hankel matrix
$\underline{\boldsymbol{\mathcal{O}}}$	Observability matrix
$\boldsymbol{\lambda}$	Eigenvalues
$\boldsymbol{\varphi_\lambda}$	Eigenvectors
λ_i	Poles
$\boldsymbol{\epsilon}$	Error
$\boldsymbol{\mu}$	Mean
ζ_i	Damping ratio
$\bullet^*$	Complex conjugate

Acronyms

bpp Between Perpendiculars

CCSSI Crystal Clear Stochastic-subspace Based Identification

CF Crest Factor

CFD Computational Fluid Dynamics

CMU Central Measurement Unit

COMNAP Council of Managers of National Antarctic Programs

DEA Department of Environmental Affairs

DAQ Data Acquisition System

DFT Digital Fourier Transform

DNV Det Norske Veritas

DOF Degree of Freedom

EMA Experimental Modal Analysis

FE Finite Element

FFT Fast Fourier Transform

FIR Finite Impulse Response

FRF Frequency Response Function

IRF Impulse Response Function

ISO International Organization for Standardization

GL Germanischer Lloyd

MAC Modal Assurance Criterion

MEMS Micro-electro-mechanical systems

MSA Multivariate Statistical Analysis

NMISA National Metrology Institute of South Africa

NRF National Research Foundation

OMA Operational Modal Analysis

OVDV Overall Vibration Dose Value

PSRV Polar Supply and Research Vessel

PSD Power Spectral Density

PVTV Point Vibration Total Value

rms Root Mean Square

SANAE South African National Antarctic Expedition

SANAP South African National Antarctic Program

SCADAS Supervisory Control and Data Acquisition

SDS Scientific Data System

Stb Starboard

UTC Coordinated Universal Time

VDV Vibration Dose Value

Chapter 1

Introduction

Antarctica and the Southern Oceans are unique and complex environments which provide key scientific insights into the intricate functioning of our global Earth system (Alfred Wegener Institute, 2014). The South African National Antarctic Program (SANAP) maintains bases on Antarctica as well as Marion and Gough Islands in the Southern Ocean from which it conducts scientific research. Scientists conducting research in these environments rely on polar supply and research vessels (PSRVs) to serve as floating laboratories and to transport cargo, equipment, fuel and personnel. The S.A. Agulhas II is a state-of-the-art PSRV, and the work horse of SANAP. The vessel was designed to provide logistical and research support for scientists in Antarctica and the Southern Ocean.

PSRVs operating in the Antarctic and Southern Oceans are exposed to extreme and unpredictable conditions, and encounter a number of excitation mechanisms. These excitation mechanisms include the ship's engines, propellers and machinery as well as waves, wind and ice. PSRVs are therefore designed to operate in both large swells in the Southern Ocean, often in excess of 8 m as seen in Figure 1.1a, as well as in first-year and multi-year level ice, pack ice, ridged ice and iceberg infested waters, shown in Figure 1.1b, in the oceans surrounding Antarctica. This results in a hybrid design for both open water and ice navigation, which has various implications. In order to efficiently break through ice, PSRVs have thick rounded keels with no protuberances for stability which can lead to heavy rolling even in light seas (Kujala, 2011). Another implication is that the stern must be raised out of the water to allow ice to pass between the propellers and the hull. In conjunction with a wide stern this can result in stern slamming during open water navigation.

Advances in the various fields of marine engineering have allowed optimal and efficient modern ship designs. Utilising lightweight materials for construction and

(a) 8 m swells in the Southern Ocean. (b) Pack ice in Antarctica.

Figure 1.1: The S.A. Agulhas II.

implementing state-of-the-art high power propulsion systems, engineers are able to optimize the power to weight ratio (Orlowitz and Brandt, 2014). The consequence of various excitation mechanisms, a hybrid design and a large power to weight ratio is significant dynamic response. These dynamic responses result in vibration propagating through the ship structure, which may exacerbate structural fatigue, damage equipment as well as impair the well-being, efficiency and health of people on-board (Asmussen *et al.*, 2001). Since polar regions, and the Antarctic in specific, are so remote, passengers, scientists and crew often spend months on-board, living and working in this dynamic environment. The habitability of polar vessels is therefore an important design consideration in order to prevent human fatigue which could result in damage of the ship structure and possible loss of life.

Full scale measurements have played an important role in understanding the dynamic responses of ice going vessels (Nyseth *et al.*, 2013). Measurements are compared to relevant standards such as BS ISO 20283-2:2008 (2008) and BS ISO 2631-1:1997 (1997). These standards provide guidelines for the measurement, evaluation and reporting of structural vibration and habitability in terms of vibration. The current lack of high quality data has been cited as one of the most important factors limiting further understanding of the effects of various excitation mechanisms on ship dynamic responses (Dinham-Peren and Dand, 2010). The importance of full scale measurements was recognised by STX Finland and resulted in the formation of an international consortium. The consortium members include Aker Arctic, STX Finland, DNV, Rolls-Royce, Wärtsilä, The Department of Environmental Affairs, of South Africa, Smit Vessel Management Services, Aalto University, the University of Oulu and the University of Stellenbosch. The project aim is to create a scientific basis for the design of ice going ships with regards to ship hull, propulsion, power requirement and comfort for passengers and crew on-board.

The aim of this thesis is to perform full scale measurements on-board the PSRV S.A. Agulhas II to investigate the vibration response of the vessel in Antarctica and the Southern Ocean. Analyses will be conducted into the effect of the vessels dynamic response on human comfort as well as structural fatigue. Multivariate statistical techniques are proposed to investigate the effect of multiple predictor variables on the measured vibration response. Factor analysis will allow investigation into the structure among the measured variables while multi-variable linear regression is proposed for the development of a predictive vibration response model. Operational Modal Analysis (OMA) is proposed to investigate the modal parameters of the vessel. These include the natural frequency, damping ratio and mode shape.

The vibration performance analysis begins with the relevant theory in the literature study in Chapter 2. Chapter 3 then presents the full scale measurements which includes a description of the S.A. Agulhas II, the measurement equipment and setup, a description of the voyage, the consortium measurement equipment and the data analysis method. Chapter 4 presents the human vibration analyses, and Chapter 5 the structural vibration analyses. Chapter 6 presents the multivariate statistical analysis (MSA) results and Chapter 7 the Operational Modal Analysis (OMA) results. Chapter 8 presents the main conclusions, and recommendations are then made for future research in Chapter 9.

Chapter 2

Literature Study

Exploration of the Southern Polar regions began in the late 17 hundreds as a result of a postulated southern continent, as well as by earlier discoveries that proved that if there was indeed a great southern continent, that it was not attached to Africa (Mills, 2003). Captain James Cook of the British Royal Navy was the first to cross the Antarctic Circle on the 17th January 1773 aboard HMS Resolution and HMS Adventure (BBC, 2014). Cook's vessels were wind powered wooden sailing ships, which limited his progress further south into the Antarctic pack ice.

The first sighting of the Antarctic continent was made on the 27th January 1820 by Fabian von Bellingshausen a Captain in the Russian Imperial Navy on his flagship Vostok (Ward, 2001). The Vostok was a wooden sailing vessel with a copper-sheathed hull which allowed him to penetrate deeper into the pack ice. The American, Captain John Davis, is believed to be the first explorer to land on an ice free part of the Antarctic Peninsula on the 7th February 1821 on his sailing vessel named Cecilia (Lagerbom, 2014). The first undisputed landing occurred on the 24th January 1895 by Norwegian Henrik Johan Bull on his ship the Antarctic (Mills, 2003). The Antarctic was a steam powered sailing ship built specifically for ice navigation.

Polar exploration then headed inland, with Norwegian explorer Roald Amundsen on his ship Fram, being the first to reach the South Pole on the 14th December 1911 (Encyclopeadia Britannica, 2014). Fram was a wooden sailing vessel with an unusually wide and shallow hull to allow her to ride up on the ice instead of being crushed. The Fram was also the first polar exploration vessel to be fitted with a diesel engine. Significant scientific polar exploration was conducted by Captain Robert Falcon Scott on his ship the Terra Nova before his death while attempting to reach the pole (Fiennes, 2004).

The Irish polar explorer Sir Ernest Henry Shackleton led three expeditions, the most famous of which was on his ill-fated ship the Endurance. The Endurance, shown in Figure 2.1a was designed for polar conditions and was considered the strongest wooden ship ever built (Lansing, 2007). During Shackleton's 1915 Antarctic expedition the Endurance was stuck in ice for 10 months, and was eventually crushed by ice floes and sank. These are but a few of the early polar explorers who relied on ships to reach the Antarctic continent.

(a) The Endurance (Preston, 2013).

(b) The S.A. Agulhas II (STX Finland).

Figure 2.1: Antarctic exploration, research and supply vessels of 1912 and 2012.

While large advances in technology have occurred between James Cook's HMS Resolution, Ernest Shackleton's Endurance and modern steel hulled, diesel-electric propulsion vessels such as the S.A. Agulhas II seen in Figure 2.1b, Antarctic institutes and their scientists continue to rely on polar supply and research vessels. In order to carry on supporting current polar supply and research as well as to provide new opportunities, new ships are currently being investigated and designed by various countries including Germany, China, United States of America and Australia (COMNAP, 2014). The hull structure of these vessels is designed and optimised using advanced finite element (FE) and computational fluid dynamic (CFD) simulations. These designs are then tested, and the numerical simulations are validated through full scale measurements.

2.1 Full Scale Measurements

Results of full scale vibration measurements conducted on ships operating in open water is scarce, and on ships operating in ice is, until very recently, almost non-existent. The current lack of high quality data has been cited as one of the most important factors limiting further understanding of dynamic ship responses (Dinham-

Peren and Dand, 2010). Advances in electronics and computing have enabled the development of accurate and compact transducers and data acquisition systems. This has created opportunities to study various phenomena at full scale during normal operating conditions.

Full scale measurements have recently been conducted by Lubbad *et al.* (2013) on the Swedish icebreaker Oden in the Arctic. The main scientific scope of this research was to study sea ice. This included the physical and mechanical properties of sea ice and icebergs, the various methods of forecasting ice conditions and numerical modelling of ice behaviour. Investigations were also conducted into the performance and manoeuvrability of Oden in different ice and open water conditions. The effects of ice loading on the hull and shaft line as well as the vibration response of the vessel were however not investigated.

Full scale measurements by Suominen *et al.* (2013) on the South African PSRV S.A. Agulhas II during sea trials in the Baltic Sea focused on the measurement and analysis of both the ice mechanical-properties as well as its effect on hull and shaft line loading. The effects of vibration on human comfort were also evaluated in the bridge of the vessel. The main findings of these measurements were that ice loading on the hull is high and at times exceeds the PC 5 class limit values but remains below the DNV ICE-10 limits. Human vibration levels in the bridge were found to range from barely noticeable to not uncomfortable for the duration of the trial. Vibration measurements were however limited to 16 second durations and were recorded manually, resulting in gaps in the measured data. During sea trials the vessel also performs controlled manoeuvres which may differ significantly from actual operation.

Belov and Spiridonov (2012) review ship vibration based on experimental investigations of ice ships in Russia started in the 1980's in their paper titled features of ship vibration in ice conditions. Key findings include that the ice field surrounding the ship hull increases it's damping characteristics, but does not decrease the vibration level. This is because of the forces of the hull and ice interaction which have a continuous spectrum. The forces are also found to excite the first few hull modes in the range 2 Hz to 8 Hz. It is also found that vibration levels increase significantly in ice as compared to open water.

Full scale OMA investigations into the dynamic behaviour of marine structures were performed by Rosenow (2007) in his PhD thesis. Despite the thesis being published in German, figures showing the experimental setup as seen in Figure 2.2a were influential in guiding the measurement setup described in Chapter 3.

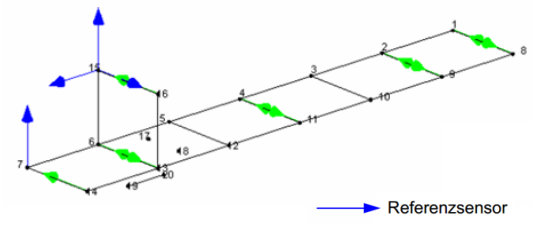

(a) Measurement model and sensor positioning (Rosenow, 2007).

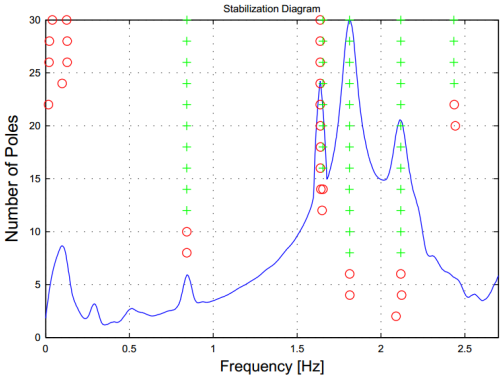

(b) Stabilisation diagram for 18 knots condition (Orlowitz and Brandt, 2014).

Investigations into the effect of different operating conditions on the modal parameters in open water using OMA was conducted by Orlowitz and Brandt (2014) as part of his PhD. Full scale measurements were performed during sea trials for three different operating conditions, namely 10 knots, 18 knots and while at anchor. Twenty six measurement points were recorded across the main deck and deck house to investigate the normal bending and torsional modes of the vessel. Five modes are identified by the stable "+" poles in the stabilization diagram shown in Figure 2.2b. The modes are identified as: mode 1 vertical bending, mode 2 horizontal bending, mode 3 vertical bending, mode 4 torsion, mode 5 vertical bending. The natural frequencies and damping ratios are then computed and compared for the three cases. The key findings are that the natural frequencies decrease and the damping ratios increase with increasing cruising speed. The vertical bending modes also show the most significant dependency on cruising speed. These results are in contradiction to those of scaled model tests by Coppotelli *et al.* (2008), and highlight the importance of experimental results in the verification of scaled models.

Model scale testing provides an alternative to full scale measurements. The advantages of model scale testing include lower instrumentation costs and the ability to test various modifications to a proposed design relatively quickly and inexpensively. Disadvantages include inaccurate models, boundary conditions and excitation forces as well as errors of scale. The advantages of full scale measurements during normal operation are that actual boundary conditions and excitation forces are responsible for the measured dynamic response. The disadvantages include expensive equipment which often limit the extent of the measurement setup. A further limiting factor is the cost of acquiring measurement time on vessels which often have busy schedules planned years in advance.

Full scale and model scale testing together with FE and CFD simulations have allowed large advances in the state-of-the-art in modern ship design. Despite these advances, humans are still ultimately responsible for the decision making and safety of vessels at sea. Investigations into the effect of vibration on the human body is therefore just as important as the effects of vibration on structural fatigue.

2.2 Human Vibration

The human body is a complex, active, intelligent and dynamic structure (Griffin, 1990). Its response to dynamic or vibratory motion is equally complex and there are no simple or easily predictable consequences. Shipping provides a complex dynamic environment in which seafarers and passengers are exposed to various vibration stimuli from machinery on board as well as the vessels motion through the water. A further dimension is added to these dynamic environments when ships encounter ice during their normal operation.

2.2.1 Whole Body Vibration

Whole body vibration occurs when the body is supported on a surface which is vibrating (Griffin, 1990). This thesis will consider standing whole body vibration of the ship's officers only. This assumption is based on observations that the captain and his officers spend a large amount of their time standing in the bridge while navigating in open water, and spend almost all their time standing during ice navigation. Human vibration measurements and analyses are conducted according to BS ISO 2631-1, which is described below.

2.2.2 BS ISO 2631-1:1997 Mechanical Vibration and Shock - Evaluation of Human Exposure to Whole-body Vibration

The primary purpose of BS ISO 2631-1 is to define methods of quantifying whole-body vibration. BS ISO 2631-1 does not contain vibration exposure limits, but rather evaluation methods which may be used as the basis for limits which may be prepared separately. BS ISO 2631-1 states that the primary quantity of vibration magnitude shall be acceleration. The frequency range considered is 0,5 Hz to 80 Hz for health, comfort and perception.

In order to better understand whole body vibration and its effects on the human body, it is important to understand how the various influential factors combine. These factors include vibration frequency, magnitude, direction and duration.

2.2.3 Vibration Frequency

Human response to whole body vibration is highly dependent on the vibration frequency. Low frequencies, below 1 Hz or 2 Hz cause most parts of the body to move up and down together, essentially representing rigid body motion. Frequencies above 2 Hz can cause amplification of vibration within the body (Griffin, 1990). The influence of vibration frequency is accounted for by frequency weighting the vibration signal.

Vibration signals are weighted by equivalent comfort contours. The BS ISO 2631-1 equivalent comfort contours are presented in Figure 2.3a with the W_d filter for weighting horizontal (+X) and lateral (+Y) vibration and the W_k filter for weighting vertical (+Z) vibration. These contours define the values by which the vibration magnitude at each frequency is to be multiplied, in order to weight it according to its effects on the body. A digital filter developed by Rimell and Mansfield (2007) allows vibration to be weighted in the time domain, and is discussed in Chapter 4.

2.2.4 Vibration Magnitude

Vibration magnitude can be reported as either displacement, velocity or acceleration. While velocity is more directly related to the energy involved in the motion, acceleration is regarded as the standard measurement unit (Griffin, 1990). The magnitude can also be classified according to its peak-to-peak acceleration or more commonly its root mean square (rms) which is calculated as follows:

$$rms = \left[\frac{1}{N}\sum x^2(i)\right]^{\frac{1}{2}} \tag{2.2.1}$$

Where $x(i)$ is the sampled data values and N is the total number of samples. If all motions were deterministic the rms value would always provide accurate results which are independent of the period of exposure. Real world vibration, and vibration on board ships in particular, is however often stochastic in nature, and in these cases the vibration dose value provides a more accurate measure of the total severity (Griffin, 1990). A simple measure which can be used to indicate the conditions where rms values are not appropriate is the ratio between the peak

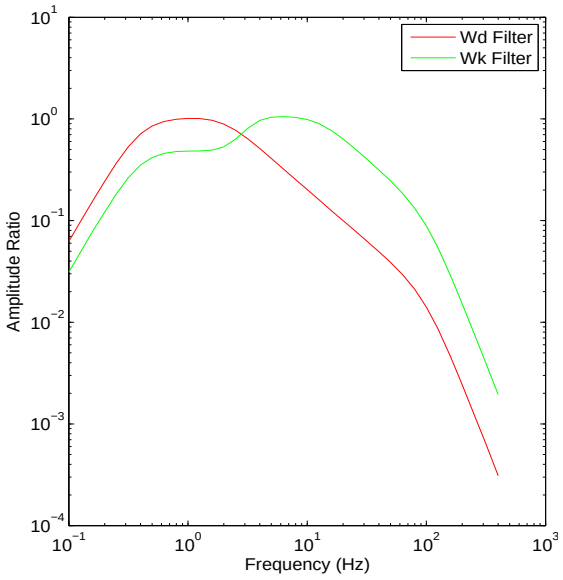

(a) Frequency weighting filters.

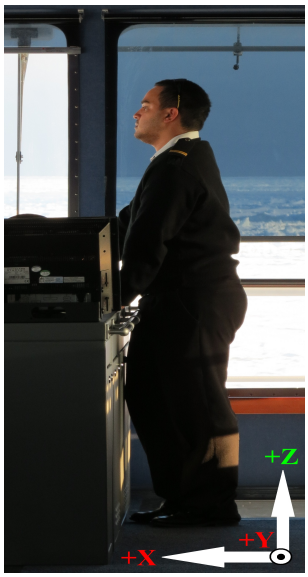

(b) Coordinate system.

Figure 2.3: BS ISO 2631-1 frequency weighting filters and a navigating officer with the basicentric coordinate system.

acceleration and the rms acceleration, which is known as the crest factor (CF), and defined as follows:

$$CF = \frac{peak\ acceleration}{rms\ acceleration} \tag{2.2.2}$$

This is usually calculated after the signal has been frequency weighted. If the crest factor is higher than 9 it is generally accepted that the rms value is a less useful measure of the vibration severity (BS ISO 2631-1:1997, 1997). Griffin (1990) notes that for the assessment of some effects of transient, shock and non-stationary motions the root mean quad (rmq) and the vibration dose value (VDV) appear more appropriate than either rms or peak values. The VDV is calculated as follows:

$$VDV = \left[\frac{Ts}{N}\sum x^4(i)\right]^{\frac{1}{4}} \tag{2.2.3}$$

Where $x(i)$ is the sampled data values, N is the total number of samples and T_s is the duration of the sampled motion. The occurrence of slamming during open water navigation and ice impacts during ice navigation may therefore result in the VDV being the most appropriate metric for ship vibration analyses.

2.2.5 Vibration Direction

The response of the human body to vibration depends on both the direction of the vibration and the position of the body which is excited (Griffin, 1990). A basicentric biodynamic coordinate system according to BS ISO 2631-1, see Figure 2.3b, is used to standardize the vibration direction and position of the body.

Vibration in the three orthogonal coordinate axis can be combined to determine a representative overall vibration value. The point vibration total value (PVTV) of weighted rms accelerations is calculated as follows based on BS ISO 2631-1:

$$a_v = (k_x^2 a_{wx}^2 + k_y^2 a_{wy}^2 + k_z^2 a_{wz}^2)^{\frac{1}{2}} \tag{2.2.4}$$

Where a_{wx}, a_{wy}, a_{wz} are the weighted rms accelerations with respect to the orthogonal axes, and k_x, k_y, k_z are the multiplying factors. The overall vibration dose value (OVDV) of weighted VDV accelerations is calculated as follows by Griffin (1990):

$$OVDV = (k_x^4 VDV_{wx}^4 + k_y^4 VDV_{wy}^4 + k_z^4 VDV_{wz}^4)^{\frac{1}{4}} \tag{2.2.5}$$

Where VDV_{wx}, VDV_{wy}, VDV_{wz} are the weighted VDV accelerations with respect to the orthogonal axes, and k_x, k_y, k_z are the multiplying factors.

2.2.6 Vibration Duration

The effects of whole body vibration are also dependent on the duration of exposure. Many classification societies publish guidelines which stipulate how long a person may be exposed to various levels of vibration each day. The measurement duration for classification purposes is important and must be clearly stated.

BS ISO 2631-1 states that the duration shall be sufficient to ensure reasonable statistical precision and to ensure that the vibration is typical of the exposures which are being assessed. It is also important to recognise that measurement results of the same vibration excitation can differ due to different measurement durations. The response of the human body does however not vary according to these chosen measurement durations.

Investigations into human comfort on board the S.A. Agulhas II have been conducted by Bekker (2013) in the Baltic Sea and Soal and Bekker (2013) in Antarctica. Research by Soal and Bekker (2013) was published at the 48th United Kingdom Conference on Human Responses to Vibration and is presented in Appendix A. In this research, vibration was measured in the bridge of the S.A. Agulhas II during a 76 day voyage during 2012/2013 to Antarctica. The vibration data was then human weighted and compared to relevant standards. Results

indicate low vibration levels in the bridge of the vessel. Despite low human vibration levels in the bridge, vibration problems can still occur on the structure in areas were the human limit values do not apply. This leads to investigations into structural vibration.

2.3 Structural Vibration

Ships are exposed to a number of excitation mechanisms which can cause structural vibration. Excitation mechanisms include engines, electric motors and other machinery, propellers and the sea. Vessels operating in the Antarctic and Southern Oceans are exposed to wave and ice excitation which each create different dynamic forces. The vibration response of the structure is dependent on these dynamic forces as well as the dynamic characteristics of the structure. The dynamic characteristics of the structure include the natural frequencies, damping ratios and mode shapes. These characteristics are in turn dependent on the ship loading condition, draft and speed.

Ship vibration can be classified as global vibration, vibration of substructures and local vibration. Global vibration deals with the dynamic response of large ship structures such as the hull in the frequency range from about 0,5 to 10 Hz (Asmussen *et al.*, 2001). A ship's hull will respond to excitation forces and moments as a freely supported non-uniform beam in water (Filcek, 2006), exhibiting vertical and transverse bending as well as torsional modes. Vibration of substructures account for the vibration of large subsystems such as the superstructure, masts, engine systems and shaft lines. Superstructure vibration may be caused by excitation from the ship hull or wind excitation. Local vibration includes vibration of plate fields, stiffeners and panels as a result of global or substructure vibration. It is important that the global structure, substructure and local structure be designed such that their natural frequencies do not overlap during normal operating conditions, in order to avoid excessive vibration which may result in fatigue damage.

2.3.1 BS ISO 20283-2:2008 - Mechanical vibration - Measurement of vibration on ships - Part 2: Measurement of structural vibration

BS ISO 20283-2:2008 (2008) provides guidelines and requirements for the measurement, diagnostic evaluation and reporting of structural vibration of ships which are excited by the propulsion plant. The primary focus of the standard is on global vibration, which in terms of this standard includes the hull girder, superstructure

and aft body. Brief notes are provided in an annex on local vibration. The standard does not consider transient ship vibration phenomena such as wave slamming excitation. Torsional shaft and crankshaft vibration are also not considered.

2.3.2 Measurement Conditions and Manoeuvres

It is recommended by BS ISO 20283-2 that measurements be performed on the first ship of a series for comparison with theoretical predictions as well as measurement results from other ships. It is specified that the sea state during measurements shall be below 3 (ISO 6954:2000, 2000). If sea states exceed 3 it should be recorded, and the signal should be high pass filtered above 2 Hz. The loading condition during sea trials should preferably be that of the normal operating conditions, but at a minimum, the propeller should be fully immersed.

For the determination of operational mode shapes and natural frequencies, measurements should be conducted in free route runs, which are constant speed runs with helm adjustment of $\pm$ 2° or less and no throttle adjustment. The speed range should should be within 30 % to 100 % of the maximum continuous rated power. Ships with controllable pitch propellers should be operated at the normal shaft rotational speed with at least 20 increments of the pitch. Data should be recorded for at least 60 s during each measurement run. BS ISO 20283-2 also states that if quasi-continuous operating conditions have not been ensured during speed-up trials, separate measurements with a 3 minute duration must be conducted at nominal as well as maximum vibration response speeds.

2.3.3 Measurement Locations

Measurement Locations should reflect the focus on the determination of global operational deflection shapes, important natural vibration modes and dominant vibration excitation mechanisms (Filcek, 2006). Sensors should thus be located to measure the theoretically predicted or expected global mode shapes, as well as the energy and frequency content of the main vibration excitation sources.

2.3.4 Signal Acquisition, processing and storage

BS ISO 20283-2 states that transducers shall be calibrated in the laboratory, and that the full system including all cabling shall be checked in the field before and after conducting measurements. It is recommended that multi-channel equipment be used. Vibration transducers are required to be capable of measurement from 1 Hz to 80 Hz with a magnitude accuracy of $\pm$ 5% and a frequency resolution of at least 0,125 Hz. It is recommended that a flat top or Hanning window be

used for the calculation of frequency spectra. The stable mean averaging mode shall be used for the Fourier Transform as mean values and not extreme values are of interest. The standard also states that the measured vibration levels shall preferably be documented in terms of peak value of the vibration velocity.

2.4 Modal Analysis

In order to understand the measured vibration response, it is important to investigate the dynamic characteristics of the ship's structure. Modal analysis is the study a structure's dynamic characteristics, and involves testing structures with the objective of obtaining a mathematical description of their dynamic or vibration behaviour (Ewins, 1984). The fundamental idea behind modal testing is that of resonance (Inman, 2014). If a structure is excited at one of it's resonant frequencies, its response exhibits two distinct physical phenomenon:

1. As the excitation frequency approaches the structure's natural frequency, the magnitude of the vibration response approaches a sharp maximum.
2. The phase of the response shifts by 180° as the frequency passes through resonance, and is 90° at resonance.

These physical phenomena are used to determine the modal parameters of a structure. The modal parameters of interest are the natural frequency, damping ratio and mode shape. The natural frequency is the frequency at which the above resonance phenomenon occur. The damping ratio indicates the amount of vibration energy dissipated through either friction (coulomb) damping or viscous damping. Mode shapes are vectors which describe the relative motion between two or more degrees of freedom (Inman, 2014). Mode shapes provide a graphical representation of how the structure is bending, compressing or twisting at its natural frequencies.

2.4.1 Experimental Modal Analysis (EMA)

Traditional Experimental Modal Analysis (EMA) makes use of measured input excitation and vibration response to determine the modal parameters through the frequency response function (FRF) or impulse response function (IRF) (Zhang *et al.*, 2005). EMA is however limited to the analysis of structures which are able to be excited by measurable excitation forces from electromagnetic shakers or modal hammers. Large structures such as buildings, bridges, large ships etc. are unable to be analysed using traditional EMA. EMA is also often performed under laboratory conditions which mean that the structure is not exposed to its normal

operating excitation forces and boundary conditions.

2.4.2 Operational Modal Analysis (OMA)

Since the early 1990's Operational Modal Analysis (OMA) has drawn great attention in civil engineering due to its ability to analyse large structures such as bridges, buildings, towers and offshore structures (Zhang *et al.*, 2005). OMA is an output only modal analysis technique, which uses the structure's normal operating conditions as the input excitation to determine its modal parameters. The major benefits of OMA during normal operation include (Structural Vibration Solutions):

- True structural boundary conditions.
- Actual excitation forces which include harmonics.
- No artificial excitation forces are required.
- No interruption to normal operation.
- Independent of the size of the structure.
- Modal parameters describe the true service state of the structure .

Further applications of OMA due to its in operation analysis include non-destructive testing, damage detection, vibration level documentation and fatigue analysis (Structural Vibration Solutions). Limitations of OMA include:

- Unscaled mode shapes.
- Unscaled excitation forces.
- Harmonic contamination.

Unscaled mode shapes mean that modal participation factors can not be calculated. Research is however currently under way to address this and methods have been proposed to accurately scale these output only mode shapes (Brincker and Andersen, 2003; Khatibi *et al.*, 2009; Aenlle *et al.*, 2009; Parloo *et al.*, 2002). Due to the response only measurements it is also not possible to calculate the magnitude of the excitation forces. Harmonics due to rotating machinery introduce spurious modes which may be incorrectly identified. Research into harmonic reduction tools is being conducted by Structural Vibration Solutions.

2.4.3 OMA Framework

The theoretical OMA framework, see Figure 2.4, is based on the assumption that the input excitation driving the combined system is a Gaussian white noise stochastic process (Structural Vibration Solutions). This means that the input excitation has the same energy at all frequencies, and therefore all modes are excited equally. However in the real world it is not usually possible to excite all frequencies with the same energy. To compensate for this, the unknown excitation forces are modelled as the result of the assumed white noise passed through a linear, time invariant excitation filter.

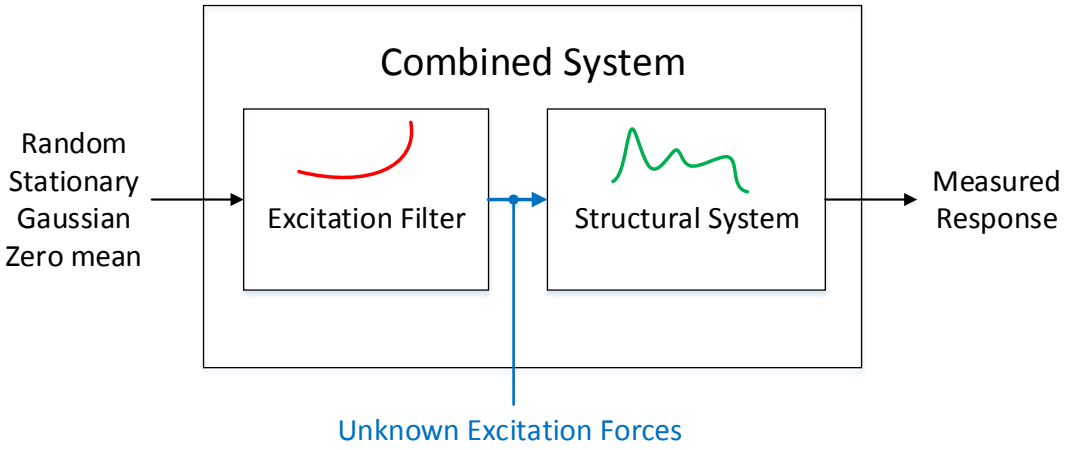

Figure 2.4: The stochastic framework used in OMA (Structural Vibration Solutions).

The measured response therefore consists of a combination of the structural system as well as the excitation filter. The implication of this framework is that the modes of the combined system contain information about the:

- Structural system (Physical modes)
- Excitation forces (Non-physical modes)
- Noise (Non-physical modes)
- Harmonics (Non-physical modes)

2.4.4 Modal Identification Techniques

There are various techniques to identify the modal parameters from output only measurements. Time domain techniques include the Natural Excitation Technique (NExT), Auto-Regression Moving Average (ARMA), Stochastic Realization-based and Stochastic Subspace-based techniques (Zhang *et al.*, 2005). Frequency domain techniques include the Frequency Domain Decomposition (FDD) and Least Squares Complex Frequency (LSCF) techniques (Zhang *et al.*, 2005). Each technique has its own advantages and disadvantages, suiting different applications. The two OMA solvers used in this thesis are:

1. LMS Test.Lab Operational PolyMAX.
2. Structural Vibration Solutions (SVS) ARTeMIS Crystal Clear Stochastic Subspace based Identification (CCSSI).

Operational PolyMAX is a frequency domain algorithm while CCSSI is a time domain algorithm. LMS and SVS specialise in the development of vibration analysis software and both companies OMA algorithms have found application in a wide variety of engineering structures. A summarised mathematical description of the main steps from Goursat *et al.* (2010); Döhler *et al.* (2012) and Janssens *et al.* (2014) follows.

2.4.5 Operational PolyMAX

Pre-processing of the data begins by computing the correlation $R_i \in \mathbb{R}^{lxl}$ between the measured signals $y_k \in \mathbb{R}^l$ as follows:

$$R_i = \frac{1}{N} \sum_{k=0}^{N-1} y_{k+i} y_k^T \tag{2.4.1}$$

where k is the sample index, N is the total number of samples and i is the correlation sample index also called the time lag. A cross spectrum is then used to convert the data to the frequency domain. This is achieved by computing the Digital Fourier Transform (DFT) of the weighted correlation matrix or the so-called weighted correlogram. The cross spectrum is calculated as follows:

$$S_{yy}(\omega) = \sum_{k=1}^{L} w_k R_k e^{(-j\omega k \Delta t)} \tag{2.4.2}$$

where L is the maximum number of time lags at which the correlations are estimated and w_k is the weighting. Since the correlations at negative time lags

($k < 0$) contain redundant information, only the positive time lags need to be considered. This leads to the following *half spectra*:

$$S_{yy}^{+}(\omega) = \frac{w_0 R_0}{2} + \sum_{k=1}^{L} w_k R_k e^{(-j\omega k \Delta t)} \tag{2.4.3}$$

In order to reduce the bias in the damping estimates, an exponential window rather than a Hanning window is applied to the correlation functions before computing the DFT. The Operational PolyMAX method then estimates the modal model from the half spectra as follows:

$$S_{yy}^{+}(\omega) = \sum_{i=1}^{n} \frac{\{v_i\} < g_i >}{j\omega - \lambda_i} + \frac{\{v_i^*\} < g_i^* >}{j\omega - \lambda_i^*} \tag{2.4.4}$$

where n is the number of modes, $\bullet^*$ is the complex conjugate of a matrix, $\{v_i\} \in \mathbb{C}^l$ are the mode shapes, $< g_i > \in \mathbb{C}^l$ are the operational reference factors which replace the modal participation factors and λ_i are the poles, which occur in complex-conjugate pairs. The poles are related to the Eigenfrequencies ω_i and damping ratios ζ_i as follows:

$$\lambda_i, \lambda_i^* = -\zeta_i \omega_i \pm j\sqrt{1 - \zeta_i^2}\omega_i \tag{2.4.5}$$

A stabilization diagram is constructed as an intermediate step in the analysis. This allows the user to select the stable physical poles. The data is then re-synthesised based on the right hand side of Equation 2.4.4 and the modal properties of the selected poles are displayed.

2.4.6 ARTeMIS CCSSI

The behaviour of the mechanical system is assumed to be described by a stationary linear dynamic system:

$$\begin{aligned} \underline{\boldsymbol{M}}\ddot{\boldsymbol{Z}}(\boldsymbol{t}) + \underline{\boldsymbol{C}}\dot{\boldsymbol{Z}}(\boldsymbol{t}) + \underline{\boldsymbol{K}}\boldsymbol{Z}(\boldsymbol{t}) &= \boldsymbol{v}(\boldsymbol{t}) \\ \boldsymbol{Y}(\boldsymbol{t}) &= \underline{\boldsymbol{L}}\boldsymbol{Z}(\boldsymbol{t}) \end{aligned} \tag{2.4.6}$$

where $\boldsymbol{Z}$ is the displacement of the degrees of freedom, $\underline{\boldsymbol{M}}, \underline{\boldsymbol{C}}$ and $\underline{\boldsymbol{K}}$ are the mass, damping and stiffness matrices, t is the time $\boldsymbol{v}$ is the excitation, $\boldsymbol{Y}$ is the measured data and $\underline{\boldsymbol{L}}$ is the observation matrix, which can be written as a discrete state-space model as:

$$\begin{aligned} \boldsymbol{X_{k+1}} &= \underline{\boldsymbol{F}}\boldsymbol{X_k} + \boldsymbol{V_k} \\ \boldsymbol{Y_k} &= \underline{\boldsymbol{H}}\boldsymbol{X_k} \end{aligned} \tag{2.4.7}$$

where $\boldsymbol{X}$ and $\boldsymbol{Y}$ are state-space vectors, $\underline{\boldsymbol{F}}$ is the state transition matrix, $\underline{\boldsymbol{H}}$ is the observation matrix and $\boldsymbol{V_k}$ is the residual.

The data driven SSI algorithm with Unweighed Principal Components (UPC) is then used to estimate the Eigenvalues and Eigenvectors from the output only measurements ($\boldsymbol{Y_k}$). Firstly p and q variables are chosen with $p+1 \geq q$ that indicate the quality of the estimators. The block data matrices are then created as follows:

$$\underline{\mathcal{Y}^{+}}=\frac{1}{\sqrt{N}}\begin{pmatrix} Y_{q+1} & Y_{q+2} & \cdots & Y_{N+q} \\ Y_{q+2} & Y_{q+3} & \cdots & \vdots \\ \vdots & \vdots & \ddots & \vdots \\ Y_{q+p+1} & Y_{q+p+2} & \cdots & Y_{N+p+q} \end{pmatrix}, \underline{\mathcal{Y}^{-}}=\frac{1}{\sqrt{N}}\begin{pmatrix} Y_{q}^{(ref)} & Y_{q+1}^{(ref)} & \cdots & Y_{N+q-1}^{(ref)} \\ Y_{q-1}^{(ref)} & Y_{q}^{(ref)} & \cdots & Y_{N+q-2}^{(ref)} \\ \vdots & \vdots & \ddots & \vdots \\ Y_{1}^{(ref)} & Y_{2}^{(ref)} & \cdots & Y_{N}^{(ref)} \end{pmatrix} \tag{2.4.8}$$

Where $Y_k^{(ref)}$ are the reference sensors. The Hankel matrix can then be computed as follows:

$$\underline{\mathcal{H}_{p+1,q}^{data}} = \underline{\mathcal{Y}_{p+1}^{+}\mathcal{Y}_{q}^{-T}}(\underline{\mathcal{Y}_{q}^{-}\mathcal{Y}_{q}^{-T}})^{-1}\underline{\mathcal{Y}_{q}^{-}} \tag{2.4.9}$$

In practice only the left matrices of a singular value decomposition (SVD) of $\underline{\mathcal{H}}$ are needed. This is calculated using a thin LQ factorization:

$$\begin{pmatrix} \underline{\mathcal{Y}_{-}} \\ \underline{\mathcal{Y}_{+}} \end{pmatrix} = \begin{pmatrix} \underline{\boldsymbol{R_{11}}} & 0 \\ \underline{\boldsymbol{R_{21}}} & \underline{\boldsymbol{R_{22}}} \end{pmatrix} \begin{pmatrix} \underline{\boldsymbol{Q_1}} \\ \underline{\boldsymbol{Q_2}} \end{pmatrix} \tag{2.4.10}$$

Where $\underline{\mathcal{H}}$ is defined as $\underline{\mathcal{H}} = \underline{\boldsymbol{R_{21}}}$. The matrix $\underline{\mathcal{H}}$ can then be factorised as $\underline{\mathcal{H}} = \underline{\mathcal{O}\mathcal{X}}$, where $\underline{\mathcal{O}}$ is known as the observability matrix and is obtained by SVD and truncated at the desired model order n:

$$\underline{\mathcal{H}} = \begin{pmatrix} \boldsymbol{U_1} & \boldsymbol{U_2} \end{pmatrix} \begin{pmatrix} \boldsymbol{\Delta_1} & \\ & \boldsymbol{\Delta_2} \end{pmatrix} \boldsymbol{V^T}, \underline{\mathcal{O}} = \boldsymbol{U_1}\boldsymbol{\Delta_1^{1/2}} = \begin{pmatrix} \underline{\boldsymbol{H}} \\ \underline{\boldsymbol{HF^2}} \\ \vdots \\ \underline{\boldsymbol{HF^p}} \end{pmatrix} \tag{2.4.11}$$

From the observability matrix $\underline{\mathcal{O}}$ the matrix $\underline{\boldsymbol{H}}$ in the first row and the state transition matrix $\underline{\boldsymbol{F}}$ from least squares can be determined. The Eigenvalues ($\boldsymbol{\lambda}$) and Eigenvectors ($\boldsymbol{\varphi_\lambda}$) can then be obtained by solving:

$$det(\underline{\boldsymbol{F}} - \boldsymbol{\lambda}\underline{\boldsymbol{I}}) = 0,\ (\underline{\boldsymbol{F}} - \boldsymbol{\lambda}\underline{\boldsymbol{I}})\boldsymbol{\phi_\lambda} = 0,\ \boldsymbol{\varphi_\lambda} = \underline{\boldsymbol{H}}\boldsymbol{\phi_\lambda} \tag{2.4.12}$$

2.5 Multivariate Statistical Analysis

Multivariate statistical analysis (MSA) refers to statistical techniques which allow investigations into the relationships between multiple variables recorded at the same time. MSA is performed in order to gain further insight into the influence of variables such as ice, wave, wind, motor power, hull loading etc., on the ship's structural dynamic response as well as the effect on human vibration comfort. The objectives of multivariate methods include (Johnson and Wichern, 1988):

1. Reducing and simplifying large data sets.
2. Sorting and grouping data into meaningful subsets.
3. Investigating the relationships among variables.
4. Developing models for data prediction.
5. Constructing and testing hypotheses.

Multivariate methods are based on a probability model known as the multivariate normal distribution (Johnson and Wichern, 1988). The normal distribution is a commonly occurring probability distribution describing data which tends to be around a central value with no bias to the left or right hand side (Weisstein, 2014). The importance of the multivariate normal distribution lies in the central limit theorem which says that the mean of a sufficiently large number of independent random variables will be approximately normally distributed (Annis, 2014). The multivariate normal distribution can therefore be used to describe or approximate data sets of real valued random variables.

Statistical analyses have been performed on full scale data sets to optimize the hull form of the bulbous bow of ships by Wagner *et al.* (2014). A data set consisting of vessel speed and draught is used from a comparable ship over a duration of three years and eight months. Four operational profiles are identified to derive an objective function. Two parameters of the bulbous bow, namely length and width, are selected for optimization. The weighted effective power is then optimized using the speed, draught and bulbous bow dimensions. The key results are a largest reduction in the weighted effective power of the optimised hull by 3,75 %. The authors also recommend including more factors such as weather predictions and the price of fuel in future models. A factor which is possibly missing from this research, and is an important function of the bulbous bow is its effect on ship stability. It is stated that "multi-objective hull form optimization typically leads to a reduced, less distinctive bulbous bow", which in terms of drag and weighted

effective power makes sense, but disregards the effects on vessel stability.

The focus of this thesis will be on development of predictive vibration response models based on full scale data. Statistical techniques used include principal component analysis, factor analysis and multi-variable linear regression, and are reviewed below. To the best of the authors knowledge, there is currently no published literature pertaining to statistical analyses of vibration response based on comprehensive full scale data sets recorded in ice and open water on board research vessels over long voyage durations.

2.5.1 Principal Component Analysis

Principal component analysis is concerned with explaining the variance-covariance structure through a few linear combinations of the original variables (Johnson and Wichern, 1988). Its objectives are to reduce the number of variables when they are highly correlated, to a smaller number of principal components which account for most of the variance (Suhr, 1994). Principal component analysis serves as an intermediate step in multiple regression analysis and factor analysis (Johnson and Wichern, 1988).

2.5.2 Factor Analysis

Factor analysis is a method for investigating whether a number of variables of interest $X_1, X_2, ..., X_n$ are linearly related to a smaller number of underlying, but unobservable, random quantities called factors $F_1, F_2, ..., F_k$ (Tryfos, 1997; Johnson and Wichern, 1988). The purpose of factor analysis is to describe the covariance relationships among many variables in order to identify underlying structure (Johnson and Wichern, 1988). Variables in each factor grouping are highly correlated among themselves, and highly orthogonal to the other factors. The orthogonal factor model can be written as

$$\boldsymbol{X} = \boldsymbol{\mu} + \underline{\boldsymbol{L_n}}\boldsymbol{F_n} + \boldsymbol{\varepsilon} \tag{2.5.1}$$

where $\boldsymbol{X}$ is the observable random vector, $\boldsymbol{\mu}$ is the mean of the variables, $\underline{\boldsymbol{L_n}}$ is the factor loadings, $\boldsymbol{F_n}$ is the underlying factors and $\boldsymbol{\varepsilon}$ is the error terms.

Factor analysis is best explained using an example, in this case adjusted from Tryfos (1997). Students attending an MBA program must take courses in finance, marketing and business policy. Let the marks for these courses be represented by X_1, X_2, X_3 respectively. It can then be postulated that the grades obtained for these three courses are functions of a certain number of underlying factors. Based

on our intuition we can identify that finance is highly quantitative, while marketing and policy are highly qualitative. Performing a factor analysis on a data set of MBA grades can then confirm or disprove the hypothesis that two unique factors F_1, F_2 exist.

The interpretation of each factor can then provide insight into the structure of the data, and in the ship specific context can then be identified as a specific physical phenomenon such as ice excitation and vibration response in the stern for example.

2.5.3 Multi-variable Linear Regression

Regression analysis is the statistical methodology for predicting values of one or more *response* (dependent) variables from a collection of *predictor* (independent) variables (Johnson and Wichern, 1988). The classical multivariate linear regression model can be written as

$$\boldsymbol{Y_n} = \boldsymbol{Z_n}\beta + \boldsymbol{\varepsilon} \tag{2.5.2}$$
$$E(\varepsilon) = 0, \text{ and } Cov(\varepsilon) = \sigma^2 I$$

where $\boldsymbol{Y_n}$ is the response variables, $\boldsymbol{Z_n}$ is the predictor variables, β is the unknown regression coefficients and $\boldsymbol{\varepsilon}$ is the error terms.

Multivariate linear regression models can be used to determine the effects of excitation mechanisms such as wave, wind, ice, motor power etc., on the vibration response of the vessel and the effect this has on human vibration comfort. Models can also be used to optimize the ships performance by changing operations with potential for structural fatigue and human discomfort.

2.6 Conclusion from the Literature Study

Full scale data provides valuable insight into the dynamic response of modern vessels operating in polar environments. The effect of vibration on human comfort is analysed by weighting the acceleration data using a filter based on equivalent comfort contours defined in BS ISO 2631-1. Investigations into human comfort on the S.A. Agulhas II to date have been case specific and have reported low vibration levels. A continuous measurement of human exposure to improve the measurement confidence is recommended. The vibration response of the structure is dependent on the boundary conditions, dynamic forces and associated modal parameters. Structural vibration investigations allow the prediction of structural

fatigue as a result of vibration. Further understanding of the structural dynamic responses can be gained through response only measurements using Operational Modal Analysis (OMA). This allows the determination of the natural frequencies, damping ratios and mode shapes of the structure. Multivariate statistical analyses (MSA) allow investigations into structure among the measured variables. MSA can also be used to develop multi-variable linear regression models in order to predict vibration response from a selected subset of predictor variables. This study seeks to contribute to the understanding of ships operating in both ice and open water.

Chapter 3

Full Scale Measurements

Full scale measurements were conducted on the 2013/2014 Antarctic voyage. The aim of these measurements is to determine the vibration response of the S.A. Agulhas II. This chapter presents the S.A Agulhas II as well as the measurement equipment and setup. This is followed by a description of the voyage, consortium measurement equipment and a graphical representation of the vibration data analyses contained in this thesis.

3.1 The S.A. Agulhas II

Full scale measurements were conducted on-board the PSRV S.A. Agulhas II, see Figure 3.1, which was built by STX Finland at the Rauma Shipyard and entered service in April 2012.

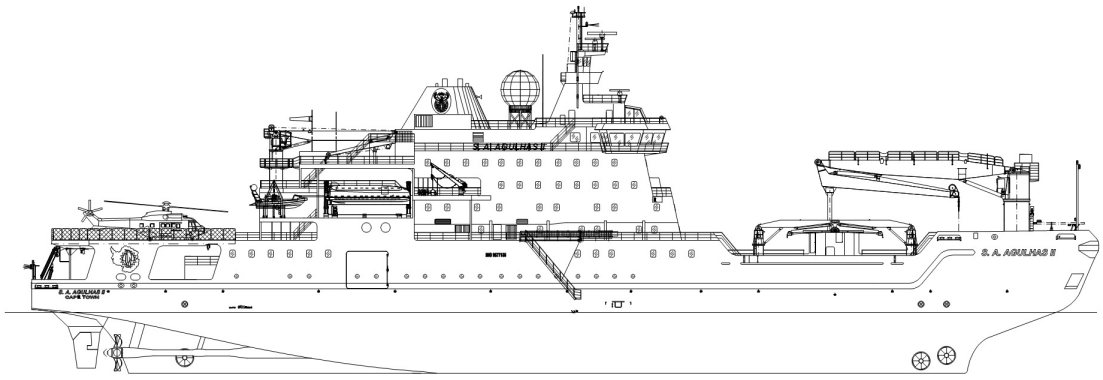

Figure 3.1: The S.A. Agulhas II.

The ship's main role is to provide logistical and research support for the South African National Antarctic Program (SANAP). The S.A. Agulhas II is designed to carry cargo, passengers, bunker oil, helicopter fuel and is also equipped with laboratories, a hydraulic A-frame, moon pool and drop keel to conduct scientific research in the Southern Ocean. The ships main dimensions are presented in Table 3.1.

Table 3.1: The main dimensions of the S.A. Agulhas II

Length, bpp	121,8 m
Beam	21,7 m
Draught, design	7,65 m
Deadweight at design displacement	5000 t
Installed power	4 × Wärtsilä 6L32 3000 kW
Propulsion	Diesel-electric 2 × 4500 kW
Speed, service	14 kn

3.2 Measurement Equipment

The data acquisition system (DAQ) and measurement equipment used is presented in Table 3.2.

Table 3.2: Measurement equipment

Equipment
1 x 16 channel, LMS SCADAS
1 x 12 channel, LMS SCADAS
1 x 8 channel, LMS SCADAS
9 x DC PCB accelerometers, 20,4 mV/(m/s^2)
9 x ICP PCB accelerometers, 10,2 mV/(m/s^2)
3 x Seismic PCB accelerometers, 1019,4 mV/(m/s^2)
1 x Triaxial PCB accelerometer, 10,2 mV/(m/s^2)
9 x DC signal conditioners
BNC and coaxial cables
LMS Test.Lab 11A Turbine Testing software

The LMS SCADAS were configured in a master-slave setup which allows simultaneous measurements controlled from one DAQ. The LMS SCADAS have a hardware low-pass anti-aliasing filter. Acceleration was measured at a sample frequency of 2048 Hz. LMS Test.Lab 11A Turbine Testing software was used to

control the DAQ's and enables continuous recording. DC signal conditioners were designed and built to supply 12 V DC power to the DC PCB accelerometers and to connect the output signal to the DAQ. Accelerometers were calibrated according to SABS standards by NMISA, and the calibration values can be found in Appendix B.

A measurement duration of 5 minutes was chosen which results in total of 22464 possible observations over the 78 day voyage. The duration was chosen for the following reasons:

1. It is thought to be representative of the measured physical phenomenon which change relatively slowly.
2. The confidence level for a lower limiting frequency of 0,5 Hz is greater than 90 %, assuming a random stationary signal (BS ISO 2631-1:1997, 1997).
3. It allows comparison with the 5 minute averaged hull loading data.

3.3 Measurement Setup

Nineteen vibration measurement channels were recorded on the hull structure and five on the superstructure as seen in Figure 3.2. The measurement equipment is shown in Figure 3.3. The measurement locations were chosen as follows:

- Measurements were conducted in the bow and stern to investigate the effect of hull slamming in open water and well as ice breaking and reversing during ice navigation.
- Measurements were conducted in the cargo hold and engine store room to determine the effect of global bending modes on the midship. Fatigue cracks had occurred prior to the current measurements in the cargo hold which is a further justification.
- Measurements were conducted in the bridge in order to investigate the effect of superstructure vibration on structural fatigue and human vibration discomfort.
- Vertical vibration (+Z) was measured on the port and starboard sides of the hull in order to investigate the vibration response caused by normal bending and torsional modes.
- Lateral vibration (+Y) was measured in the hull to determine the response of transverse bending.

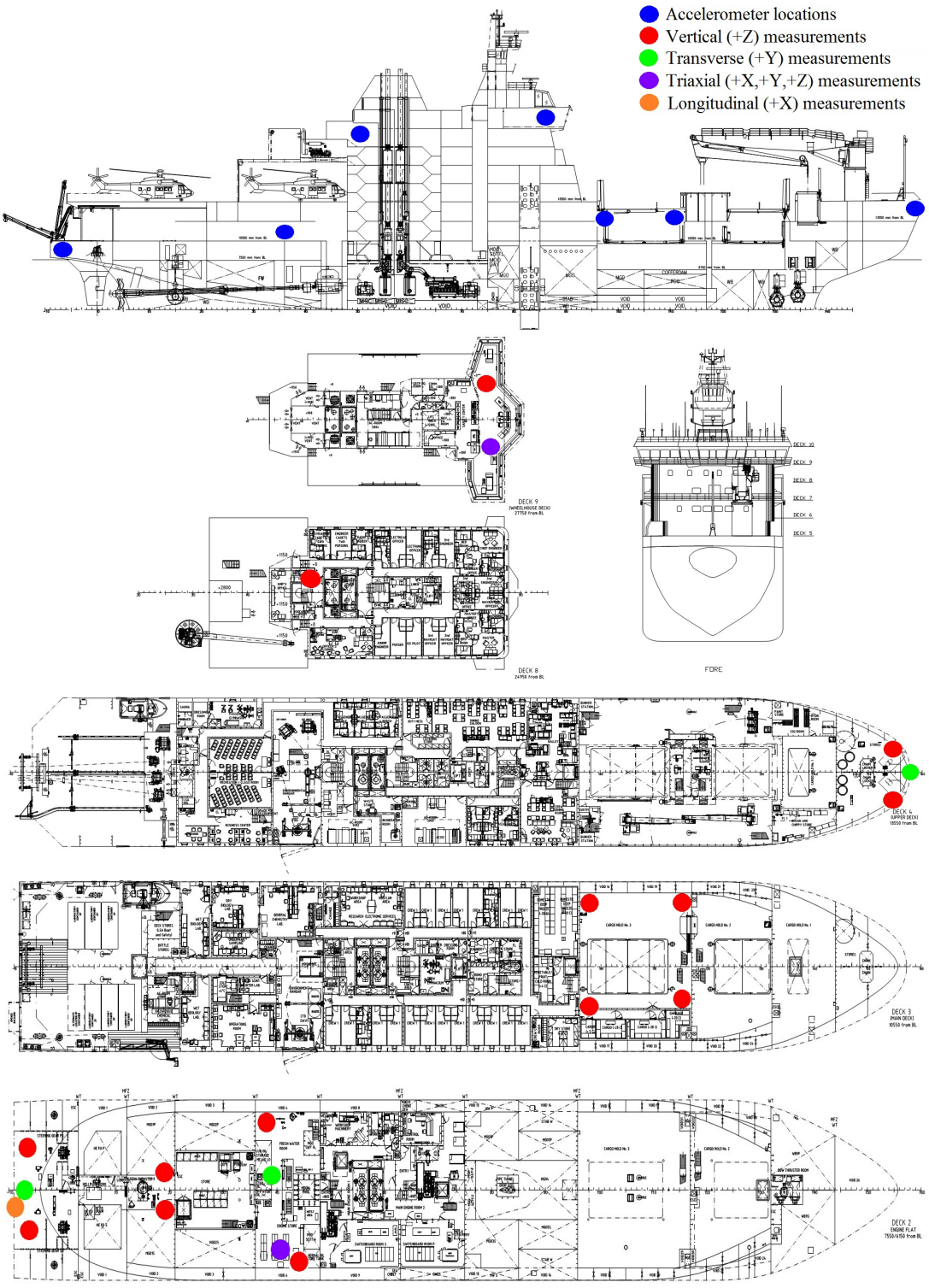

Figure 3.2: Measurement Locations.

- Longitudinal vibration (+X) was measured in the superstructure to investigate fore aft bending.
- Lateral vibration (+Y) was measured in the superstructure to investigate transverse bending and vertical vibration (+Z) was measured to investigate torsion.

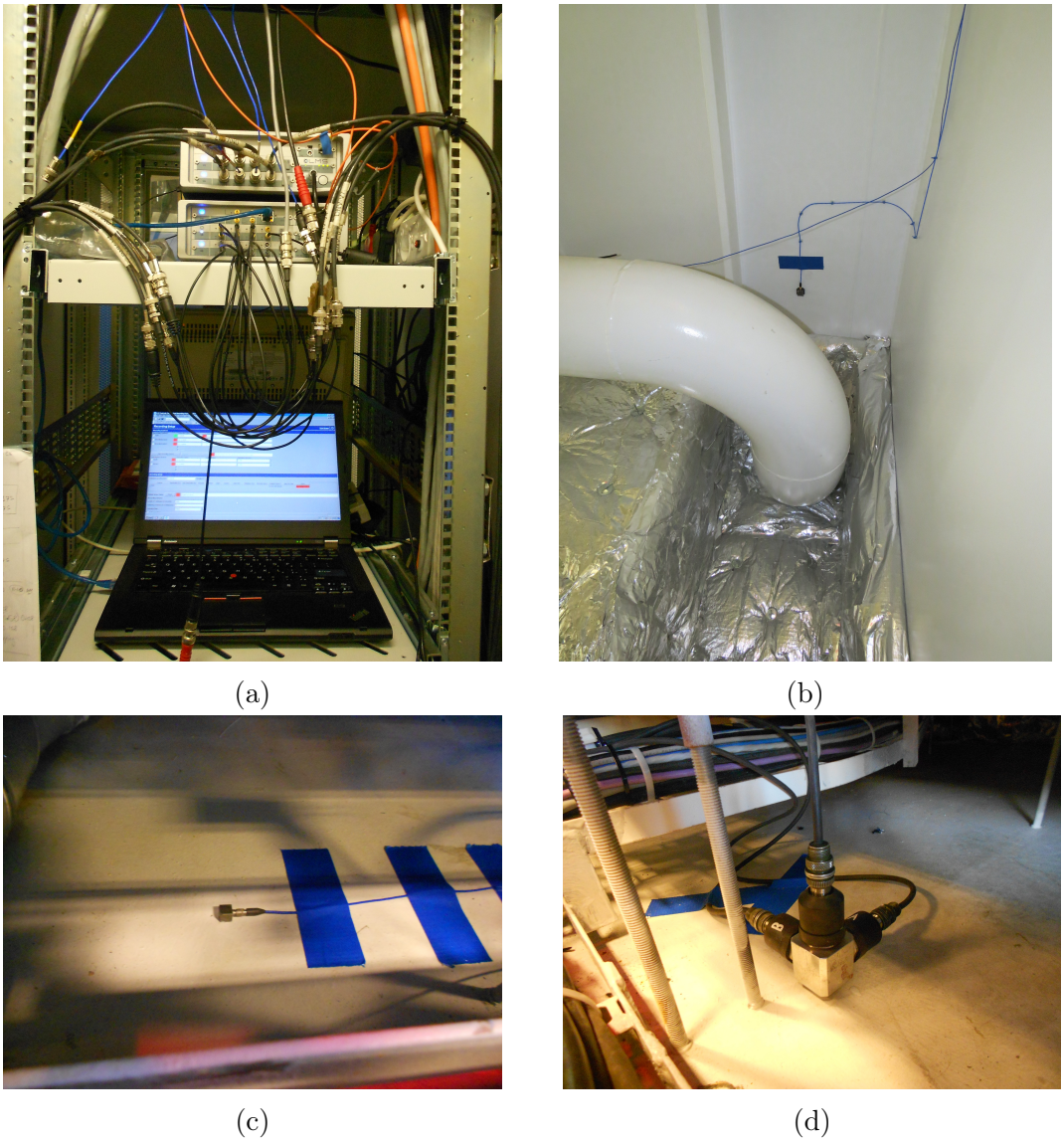

(a) (b)

(c) (d)

Figure 3.3: Measurement Equipment. a) LMS SCADAS and measurement laptop. b) DC accelerometer mounted to a deck-head longitudinal. c) ICP accelerometer mounted to a girder. d) Seismic accelerometers mounted in the bridge.

The measurement system was controlled by a single laptop mounted in the CMU measurement rack. A fibre optic cable was routed through water tight cable trays from the CMU to the steering gear room to enable synchronous measurements using the master-slave setup. Accelerometers were mounted to girders, transverse beams or longitudinal beams using super-glue. Rigid structural members were chosen in order to measure the global ship vibration response. BNC and co-axial cables were secured using saddles and cable ties as well as duct tape.

3.4 Description of the Voyage

The voyage started from Cape Town harbour on the 28*th* of November 2013 and lasted 78 days. Figure 3.4 shows the track of the S.A. Agulhas II and is followed by a short description of each leg.

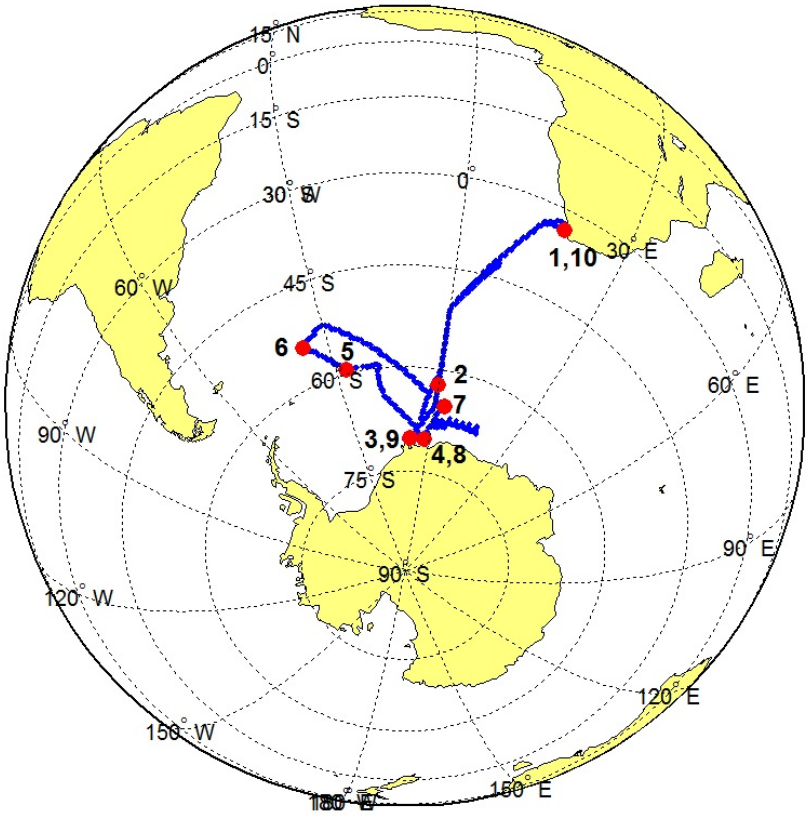

Figure 3.4: GPS data of the 2013/2014 voyage to Antarctica.

Table 3.3: Description of the voyage.

1	The first leg saw the S.A. Agulhas II depart from Cape Town harbour in a South Westerly direction on the Good Hope line, turning due South on the Greenwhich Meridian. Vibration measurements began on the 4th December 2013. Wave heights averaged 3,8 m with a maximum of 8 m.
2	The ship entered ice on the 7th December 2013. The ice began as pancake, brash and small ice floes. Floe ice became thicker and more concentrated as the ship moved deeper into the pack ice of the Weddell Sea. On the 9th December 2013 the ship encountered thick pack ice with large ice ridges, and became stuck (beset). Ramming techniques were used to break through thick ridges and ice floes. Large ridges and thick ice floes resulted in the ship being beset, often for several hours, and ramming numerous times over the next 13 days.
3	On the 22nd December 2013 the ship arrived at Atka Bay to begin offloading cargo for the German Neumayer Station III. In order to reach the ice shelf the ship first carved away the bay ice.
4	On the 24th December 2013 the ship departed for Penguin Bukta and arrived on 25th December 2013. The ship offloaded cargo and fuel at Penguin Bukta and remained pushed up against the ice shelf.
5	The ship departs on the 30th December 2013 for Southern Thule. Navigation progresses well through pack ice with occasional bergy bits. The ice pack begins to thin and open up, and the ship reaches Southern Thule on the 4th January 2014.
6	The ship departs on the 4th January 2014 for South Georgia. Shortly after departure the ship enters open water, with an average wave height of 4,3 m and a maximum of 7 m. The ship arrives at Grytviken Bay, South Georgia on the 6th January 2014.
7	The ship departs from South Georgia on the 6th January 2014 to conduct 13 days of whale research on the edge of the ice pack.
8	The ship enters the ice pack on the 23rd January 2014 and reaches Penguin Bukta on the 24th January 2014 to begin flying passengers back from SANAE IV base.
9	On the 26th January 2014 the ship departs for Atka Bukta and arrives on the 27th January 2014. The ship then carves bay ice until the 28th January 2014 to complete back loading.

Continued on next page

Table 3.3 – *Continued from previous page*

10	On the 31st January 2014 the ship sets sail for Cape Town. Ice navigation progresses well and the ship enters open water on the 1st February 2014. Scientific stations see the ship stop several times along the Good Hope line. The average wave height during the 11 day return voyage is 4 m with a maximum of 7 m. The ship arrives at St Helena bay on the 12th February 2014. After numerous safety drills the ship heads down South Africa's West Coast and enters Cape Town harbour on the 13th February 2014.

3.5 Consortium Measurement Equipment

The consortium measurement equipment used in this thesis is presented in Table 3.4. UTC time was used by all measurement systems throughout the voyage.

Table 3.4: Consortium measurement equipment

CMU (Central measurement Unit)
1. Strain data for hull loading.
2. Motor power, rudder position, propeller pitch.
SDS (Scientific Data System)
1. Longitude, Latitude.
2. GPS speed over ground.
3. Heading.
4. Wind speed and direction.
5. Air temperature.
Visual observations
1. Ice thickness, concentration and floe size.
2. Wave height and direction.
3. Draft.

3.6 Data Analysis

A graphical representation of the vibration analyses is presented in Figure 3.5 and the associated Matlab code can be found in Appendix C. Chapter 4 and 5 present the human vibration and structural vibration data analyses and results. Chapter 6 then uses the vibration data together with the consortium data to conduct multivariate statistical analyses. Operational Modal Analysis (OMA) is performed in Chapter 7 and provides insight into the structural dynamic response of the previous chapters.

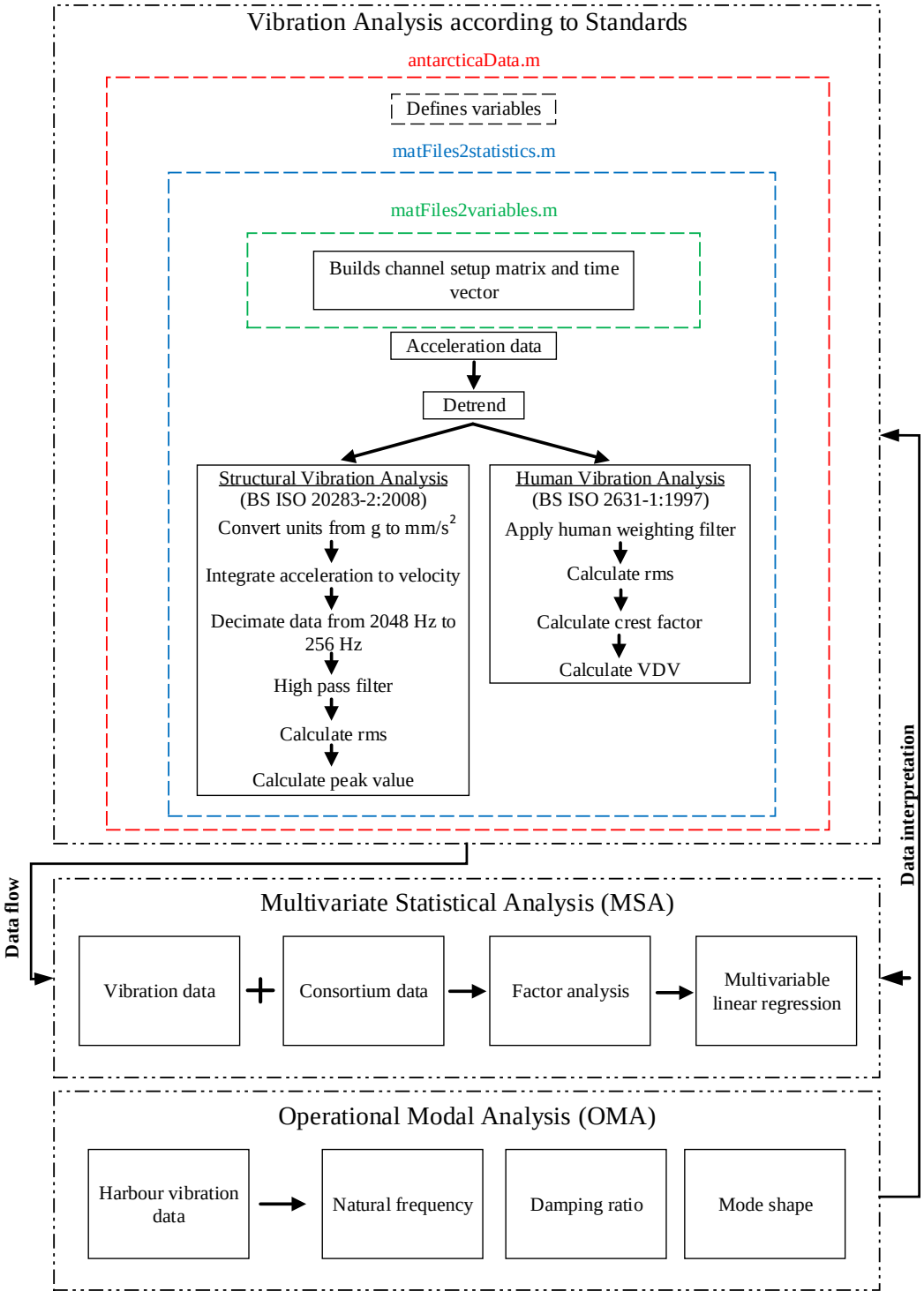

Figure 3.5: Graphical representation of vibration data analyses.

Chapter 4

Human Vibration Analysis

Whole body human vibration was measured on the bridge of the S.A. Agulhas II. The aim of the human vibration measurements is to determine whether the navigating officers of the vessel experience vibration discomfort which may lead to fatigue related accidents. Vibration was measured on the deck structure beneath the captain's chair in the vertical (+Z), lateral (+Y) and longitudinal (+X) directions. The accelerometers were mounted to a rigid aluminium block using threaded studs. The block was glued to the top of a junction between a longitudinal and transverse beam as seen in Figure 4.1. The following assumptions are made as part of the vibration analysis:

1. The measurement location provides an approximation between the vibration experienced by a navigating officer at the centre or starboard controls.
2. The carpet under the standing person's feet is compressed so as to be rigid.
3. The orientation of the standing person is forward facing, see Figure 2.3b.

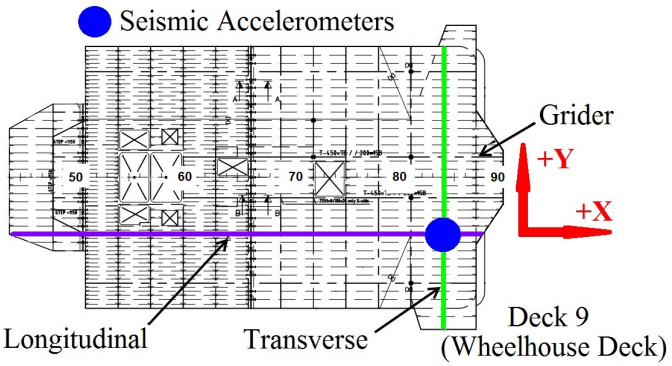

Figure 4.1: Structural steel layout of Deck 9 showing the accelerometer location.

4.1 Human Vibration Data Processing

Whole body human vibration data is post-processed according to BS ISO 2631-1. The data is human weighted in the time domain using the digital weighting filter developed by Rimell and Mansfield (2007). Time domain filters are more efficient than frequency domain filters as the data can be filtered without first computing the frequency spectrum. A modification was made to the time domain weighting filter algorithm by McMahon *et al.* (2013). Figure 4.2 presents the time domain filters compared in the frequency domain to the analytical filters found in BS ISO 2631-1. It can be seen that the digital filter approximates the analytical filter very accurately. Human vibration metrics are then calculated using the weighted data.

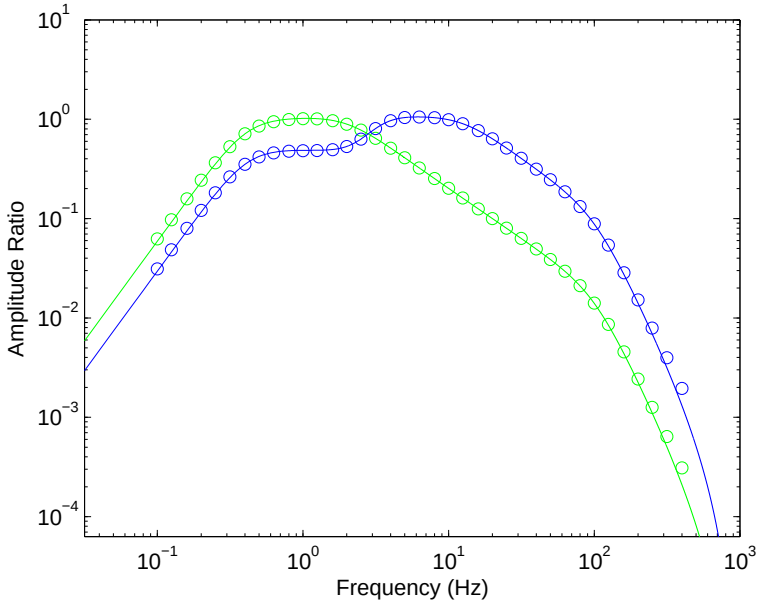

Figure 4.2: Human weighting filter. ◯ W_d filter as per BS ISO 2631-1, — W_d Filter as per Rimell and Mansfield (2007), ◯ W_k filter as per BS ISO 2631-1, — W_k Filter as per Rimell and Mansfield (2007).

4.2 Human Vibration Results

The results of the whole body human vibration measurements include the effects of vibration amplitude, direction and frequency on human comfort. Vibration amplitude is investigated using the rms acceleration, crest factor and VDV metrics. Total vibration values allow the determination of the combined vibration response of the 3 primary axes. The vibration frequency is also investigated using the PSD.

4.2.1 rms Acceleration

The human weighted rms acceleration values are presented in Figure 4.3. The vertical dashed lines indicate the events listed in the Description of the Voyage in Chapter 3. The crosses indicate the maximum rms values over the entire duration of the voyage, in the vertical, lateral and longitudinal directions.

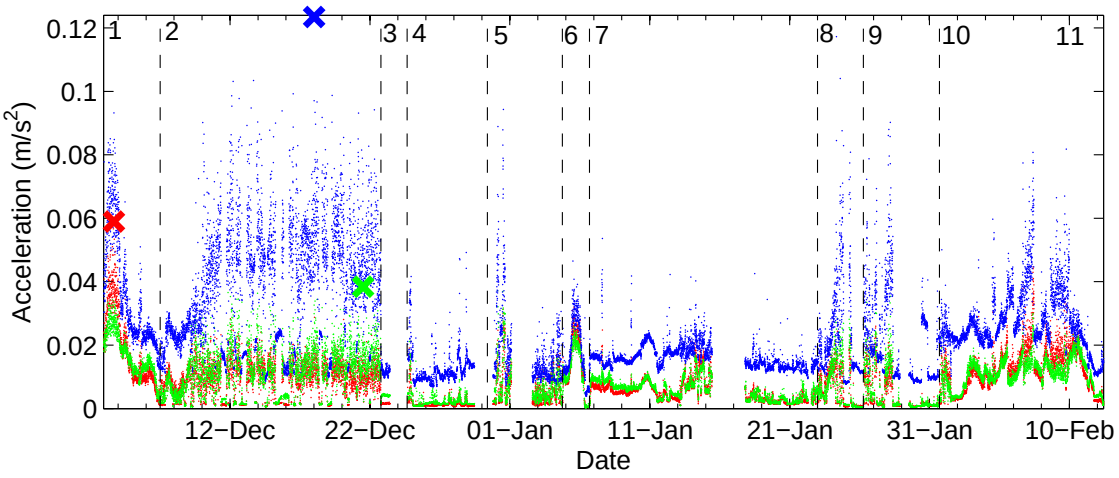

Figure 4.3: Human weighted rms acceleration values. • Longitudinal vibration (+X), • Lateral vibration (+Y),• Vertical vibration (+Z).

The following observations are made:

1. The maximum rms value is 0,124 m/s^2 in the vertical (+Z) direction during ice navigation.

2. Vibration in the vertical (+Z) direction is dominant, and is larger during ice then open water navigation.

3. The maximum rms value in the longitudinal (+X) direction is 0,059 m/s^2 and occurs in open water, while the maximum rms value in the lateral (+Y) direction is 0,038 m/s^2 and occurs in ice.

These results show that human vibration comfort is most effected by vibration in the vertical direction. Vibration in the vertical direction during ice navigation is also seen to have more of an effect on human comfort than that during open water navigation.

4.2.2 Crest Factors

The crest factors in Figure 4.4 indicate the impulsiveness of the vibration response. The horizontal line at a crest factor of 9 separates the impulsive and non-impulsive responses. 14 % of the longitudinal (+X), 24 % of the lateral (+Y) and 23 % of the vertical (+Z) crest factors exceed 9 and are therefore considered impulsive. The majority of the vibration data is therefore accurately represented by the rms values. The largest crest factors of 70, 62 and 45 in the vertical, longitudinal and lateral directions respectively occur during the same 5 minute measurement during ice navigation.

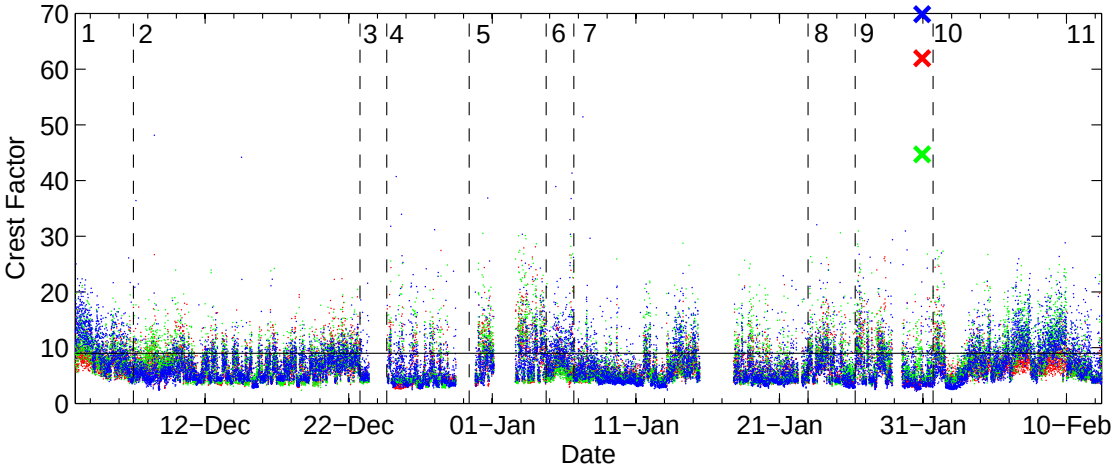

Figure 4.4: Crest factors. • Longitudinal vibration (+X), • Lateral vibration (+Y),• Vertical vibration (+Z).

4.2.3 Vibration Dose Value (VDV)

In order to evaluate the impulsive part of the vibration response the 5 minute VDV is calculated and plotted in Figure 4.5. The VDVs show a trend of higher vibration values in open water than in ice, indicating that open water navigation has a greater impact on human comfort than ice navigation. This is in contradiction to the rms acceleration findings, and is thought to be due to the better approximation of impulsive wave induced vibration by the VDV metric. The maximum VDV value of 1,07 $m/s^{1.75}$ occurs during ice navigation, and while this does not follow the general trend, it may be due to impulsive vibration during ice navigation.

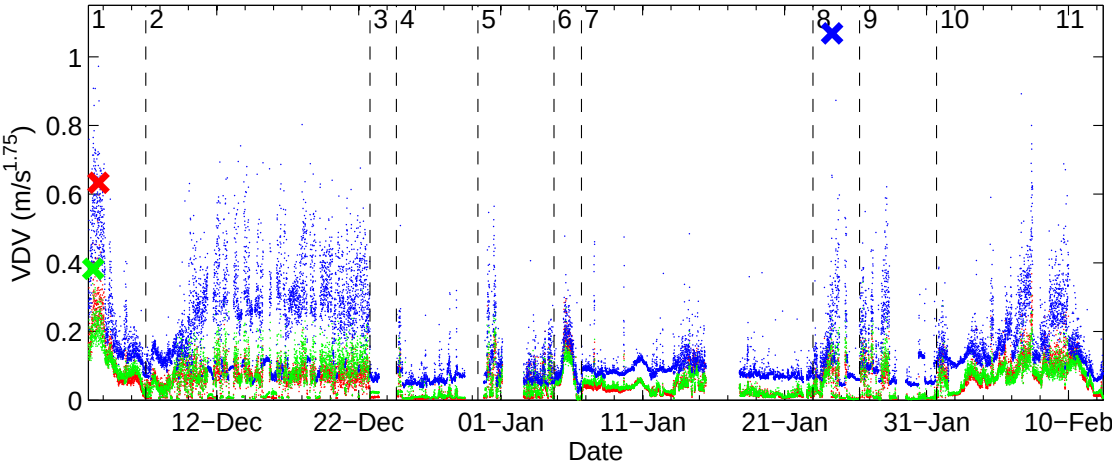

Figure 4.5: VDV. • Longitudinal vibration (+X), • Lateral vibration (+Y),• Vertical vibration (+Z).

4.2.4 Total Vibration Values

The vector sum of the vibration from orthogonal coordinates provides a metric which is indicative of the overall vibration at the vessel-occupant interface. Figure 4.6 shows the Point Vibration Total Value (PVTV), see Equation 2.2.4, as well as the Overall Vibration Dose Value (OVDV), see Equation 2.2.5.

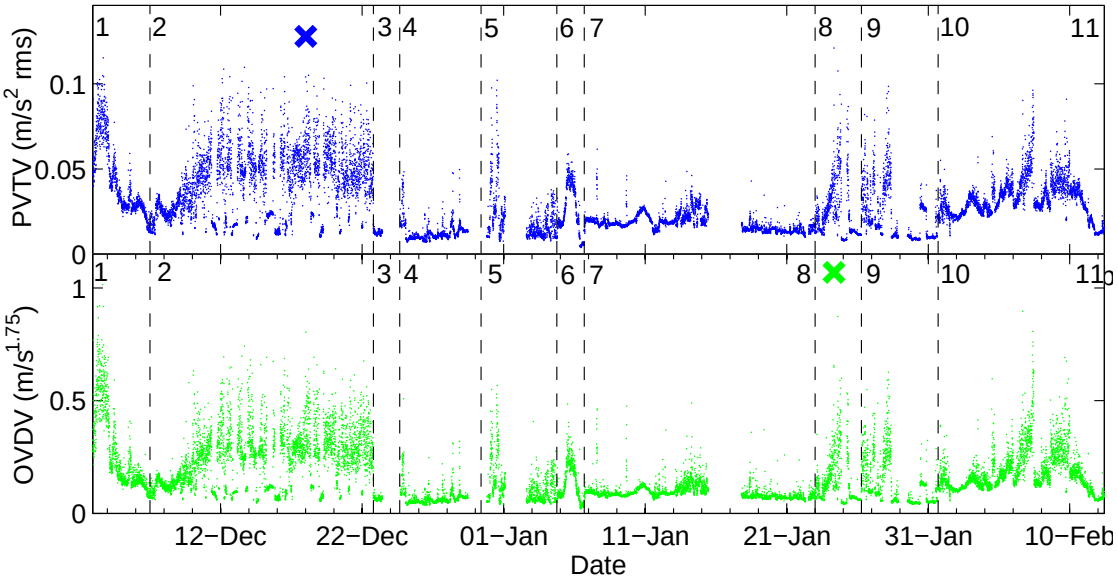

Figure 4.6: Vibration Total Values. • Point Vibration Total Value (PVTV), • Overall Vibration Dose Value (OVDV).

The maximum PVTV is 0,13 m/s^2 and the maximum OVDV is 1,1 m/s$^{1.75}$, both occurring during ice navigation. The maximum PVTV is below the approximate indication value provided by BS ISO 2631-1 of 0,315 m/s^2. The maximum measured vibration is therefore classified as not uncomfortable.

4.2.5 Power Spectral Density (PSD)

The frequency content of the acceleration signals is calculated using the power spectral density (PSD) to investigate the source of the measured vibration. The PSDs were calculated using Matlab's `pwelch.m` function with the following input parameters: Hanning window, 50 % overlap, block size of 2^{15} NFFT points, sample frequency of 2048 Hz. This results in a frequency resolution of 0,0625 Hz.

Figure 4.7 shows the PSDs of the un-weighted vibration signals in the left hand column and the human weighted vibration signals in the right hand column. This shows the actual measured vibration to which the occupants are exposed, how vibration is human filtered, and which frequencies have an effect on human comfort. The details of the PSD signals are presented in Table 4.1, and is followed by the key observations.

Table 4.1: PSD plot details.

A B Maximum rms Acceleration Ice Navigation 18 December 2013 00h22	C D Maximum Crest Factor Ice Navigation 30 January 2014 22h47
E F Maximum VDV Ice Navigation 24 December 2013 08h12	G H Maximum rms Acceleration Open Water Navigation 3 December 2013 16h52
I J Maximum VDV Open Water Navigation 3 December 2013 16h02	K L Maximum rms and VDV Anchored 6 December 2013 10h47

1. The majority of the frequency content of the bridge acceleration signals are concentrated below 20 Hz.

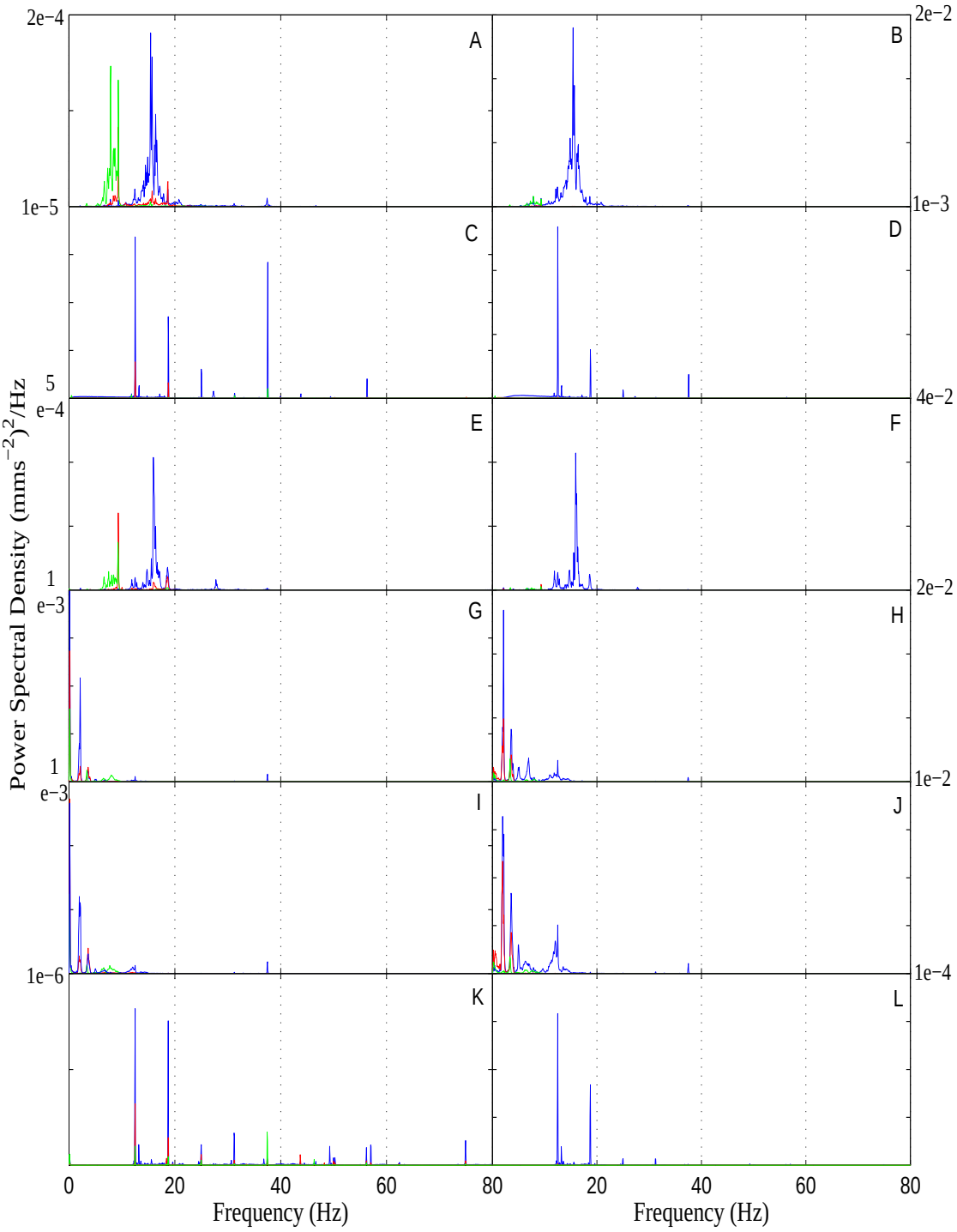

Figure 4.7: Power Spectral Density. • Longitudinal vibration (+X), • Lateral vibration (+Y),• Vertical vibration (+Z).

2. The frequency content of the maximum rms acceleration in ice (18th December 2013), and the maximum VDV in ice (24th January 2014) show similar distinct peaks in the vertical direction between 15 and 16 Hz. The source of this vibration is not yet apparent, but warrants investigations of structural modes in this frequency range.

3. Distinct peaks occur in the vertical direction between 1,9-2,2 Hz and 3,55-3,65 Hz in open water. These are identified as the 2-node and 3-node bending modes in Chapter 7

4. Peaks at 9,3 Hz in the lateral (+Y) and longitudinal (+X) directions during ice navigation are identified as the first blade pass frequency of the four bladed propeller rotating at 140 rpm, and are seen to be attenuated by the human weighting filter.

5. The frequency content of the maximum crest factor is similar to that when the ship is at anchor, with peaks at 12,5 Hz which can be attributed to the rotational speed of the engine at 750 rpm, 18,75 Hz which is the second blade pass frequency, and 37,56 Hz, which is the firing order of the six cylinder diesel engines.

6. The human weighting filter is seen to attenuate lateral (+Y) and longitudinal (+X) signals below 0,6 Hz and above 2 Hz. Furthermore this filter attenuates frequencies in the vertical (+Z) direction below 4 Hz and above 16 Hz.

7. The amplitude in the frequency range of the un-weighted signals is seen to be an order of magnitude larger in open water than in ice, and 3 orders of magnitude larger in open water than when anchored.

8. The amplitude in the frequency range of the weighted signals is seen to be the same order of magnitude in open water and ice, and 2 orders of magnitude larger than when anchored. The human weighting filter therefore attenuates vibration during open water navigation more than during ice navigation.

Chapter 5

Structural Vibration Analysis

Structural vibration was measured in the bow, stern, cargo hold, CMU and bridge. Measurements were recorded on main structural members such as girders, transverse beams and longitudinal beams in order to determine the global vibration response of the vessel. The measurement setup can be seen in Figure 3.2 and reflects the focus on the determination of global operational deflection shapes which were hypothesised to be normal and transverse bending and well as torsional modes.

5.1 Structural Vibration Data Processing

Structural vibration data is post-processed according to BS ISO 20283-2. A graphical representation of the data processing can be seen in Figure 3.5. The data is first converted from g to mm/s^2, and then integrated using the `trapz.m` function to mm/s. It is then decimated from 2048 Hz to 256 Hz using `decimate.m` which first low-pass filters the data with a cut-off frequency of 102,4 Hz before re-sampling. The signal is then high-pass filtered to remove vibration amplitude in the rigid body bandwidth. BS ISO 20283-2 specifies that data should be high-pass filtered above 2 Hz.

Two high-pass filters were designed in order to effectively attenuate low frequency vibration measured by the ICP and DC accelerometers respectively. The filters were designed using Matlab's Filter Design and Analysis Tool. A Chebyshev high-pass filter with an order N = 800, and a cut-off frequency $F_c = 1$ Hz was used to filter the ICP data. A higher order filter was required for the DC accelerometers which are able to measure low frequency vibration. A Chebyshev high-pass filter with an order N = 1400, and a cut-off frequency $F_c = 1.6$ Hz was used to filter the DC data. The resulting filters are shown in Figure 5.1.

The Chebyshev finite impulse response (FIR) filters were selected due to their sharp drop off and low ripple at 0 dB. The high filter order provides significant attenuation below the cut-off frequency. While higher filter orders are more computationally expensive, they do not effect the filter accuracy and it was decided that longer computational times was a necessary trade-off. Structural vibration metrics were subsequently calculated which include peak velocity values and frequency spectra.

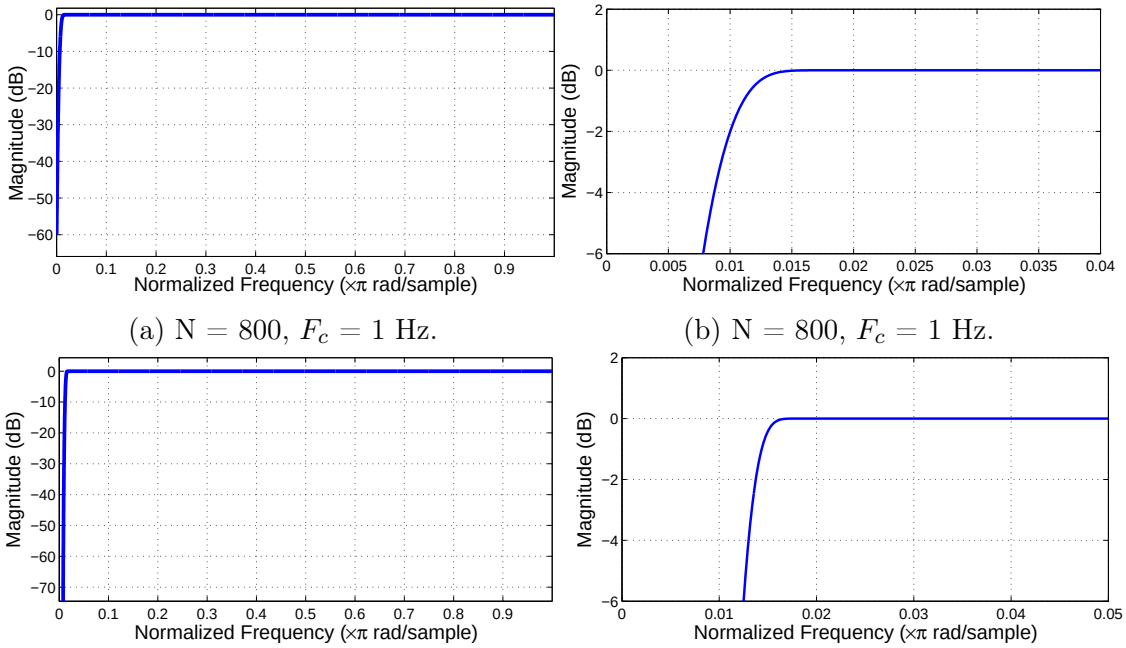

(a) N = 800, F_c = 1 Hz.

(b) N = 800, F_c = 1 Hz.

(c) N = 1400, F_c = 1.6 Hz.

(d) N = 1400, F_c = 1.6 Hz.

Figure 5.1: Chebyshev high-pass filters.

5.2 Structural Vibration Results

The results of the structural vibration measurements are presented and discussed below. Peak vibration velocity is plotted for the duration of the voyage and maximum values are investigated in the frequency domain and compared to structural vibration guidelines.

5.2.1 Peak Vibration Velocity

The peak vibration velocity values are presented in Figure 5.2 and 5.3. The vertical dashed lines indicate the events listed in the Description of the Voyage in Chapter 3. The crosses indicate the maximum peak vibration velocity values in the vertical, lateral and longitudinal directions. The following sensors are plotted in Figure 5.2 and 5.3: Steering Gear Stb X, Y and Z, Bow Centre Y and Stb Z, CMU Triax X, Y, Z, Cargo Hold Stb Z, Bridge Stb X, Y, Z.

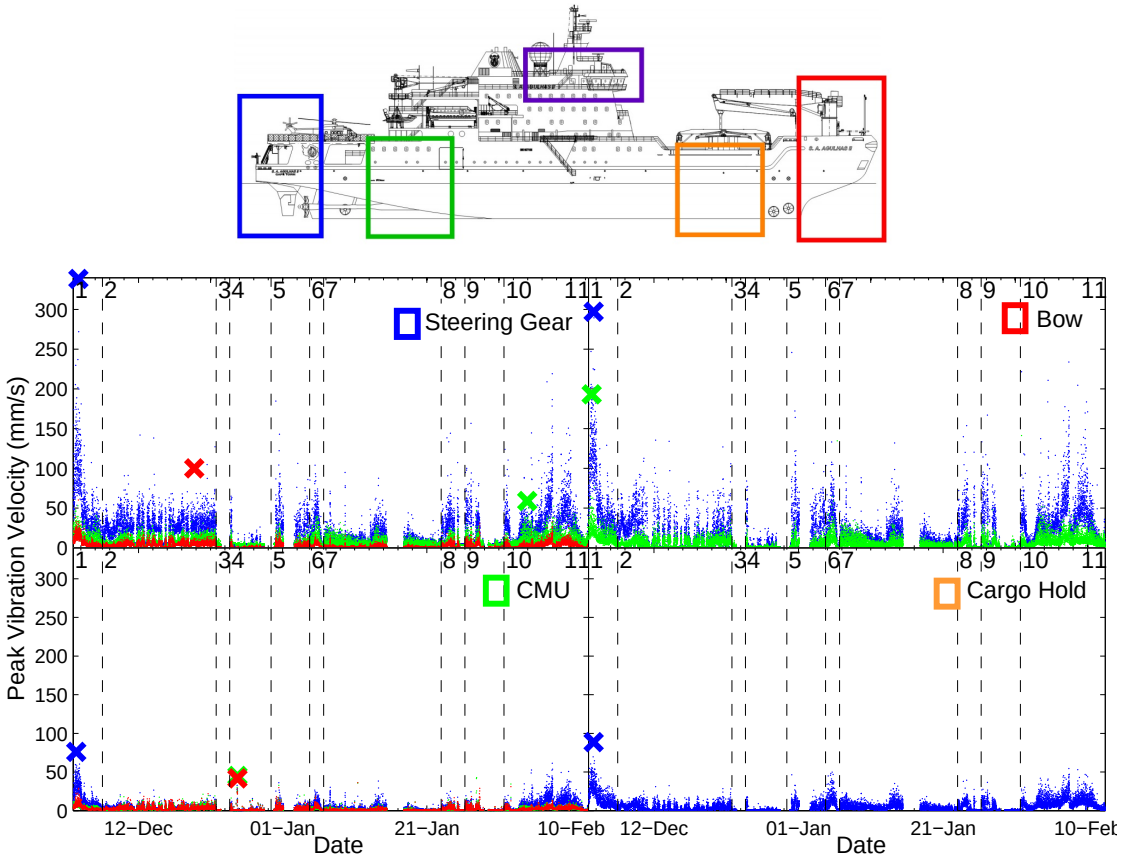

Figure 5.2: Structural vibration. • Longitudinal vibration (+X), • Lateral vibration (+Y),• Vertical vibration (+Z).

The following observations are made:

1. The largest peak vibration value is 338,35 mm/s in the vertical (+Z) direction in the stern of the vessel in open water.

2. The largest maximum values occur in open water in the vertical (+Z) direction at all the measurement locations.

3. Vibration amplitude is largest in the bow and stern, and decreases towards the middle of the vessel, increasing vertically towards the bridge.

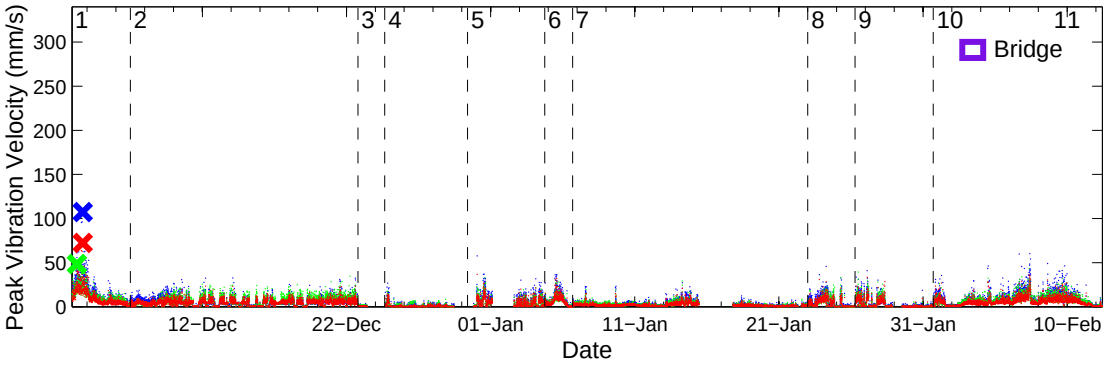

Figure 5.3: Structural vibration. • Longitudinal vibration (+X), • Lateral vibration (+Y),• Vertical vibration (+Z).

5.2.2 Frequency Spectra

The frequency spectra of the maximum peak values are presented in Figure 5.4. The PSDs are shown in the left hand column and the FFTs in the right hand column. The FFTs are compared to Germanischer Lloyd's (GL) guidelines for structural fatigue as a result of vibration. Two limit curves define the lower region in which vibration is unlikely to cause damage, the intermediate region where vibration may cause damage, and the upper region in which damage is probable.

The PSDs provide an accurate estimate of the frequency content of the random signals since they are based on the FFT of the autocorrelation function, which is a statistical indicator. The PSDs are calculated in Matlab using the following input parameters: Flattop window, 50 % overlap, block size of 4096 NFFT points, sample frequency of 256 Hz. This results in a frequency resolution of 0,0625 Hz. Two distinct peaks at 2,06 Hz and 3,88 Hz can be seen in the PSD plots at all the measurement locations.

The FFT plots are seen to contain peaks at the same frequencies. Results show that vibration in the stern of the vessel reaches amplitudes at which vibration may cause damage, and that vibration in the bow of the vessel reaches amplitudes at which damage is probable. These vibration amplitudes occur at 2,06 Hz in both locations. This is identified as the 2-node first bending mode of the vessel in Chapter 7. These findings highlight the need for further investigation into the

duration of possible fatigue exposure experienced by the vessel each year, and the effect this will have on its expected service life of 30 years. Other factors which also need to be investigated include the type of steel used in construction, the structural details in critical areas, the welding processes, the production methods and environmental conditions such as corrosion.

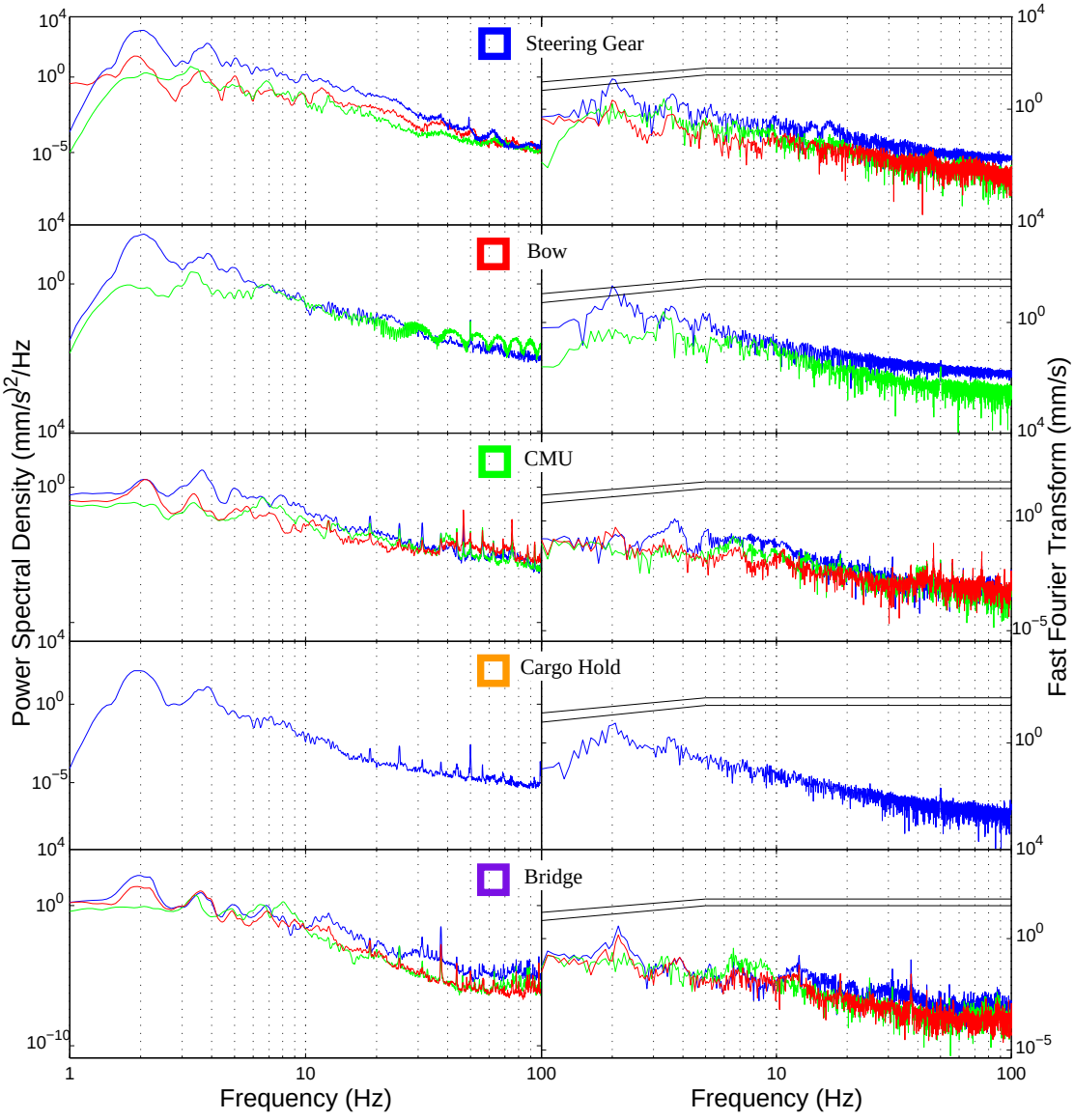

Figure 5.4: Structural vibration. • Longitudinal vibration (+X), • Lateral vibration (+Y),• Vertical vibration (+Z).

Chapter 6

Multivariate Statistical Analysis

Multivariate statistical analyses (MSA) are used to investigate the relationships between multiple predictor (independent) and response (dependent) variables. For the purpose of this work MSA is used to investigate the vibration response of the vessel as a function of several predictor variables. A summary of the predictor and response variables is provided in Figure 6.1.

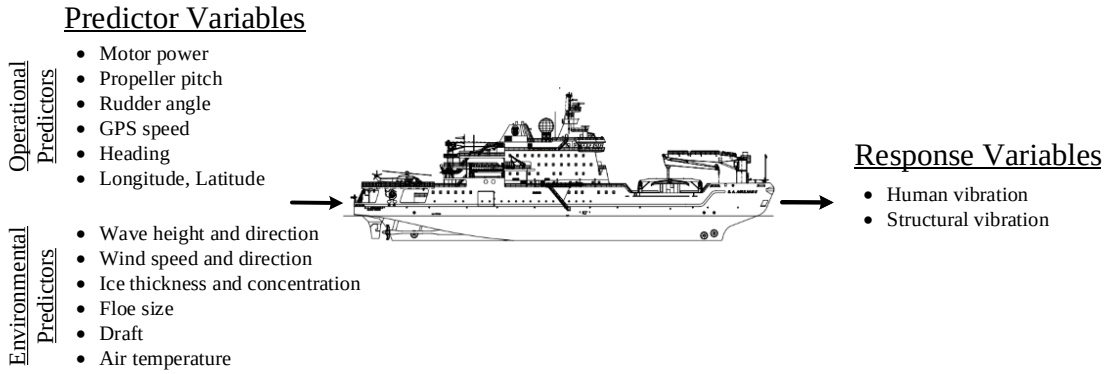

Figure 6.1: Multivariate statistical analysis variables.

Factor analysis is performed to reduce the number of variables into highly correlated orthogonal groupings called factors as well as to investigate possible structure among the variables. Multiple variable linear regression is used to investigate the linear dependence among response and predictor variables. The outcome of this work is the development of a mathematical model from which the vibration response can be predicted based on a smaller subset of operational and environmental parameters. A block diagram of the statistical analysis process is presented in Figure 6.2.

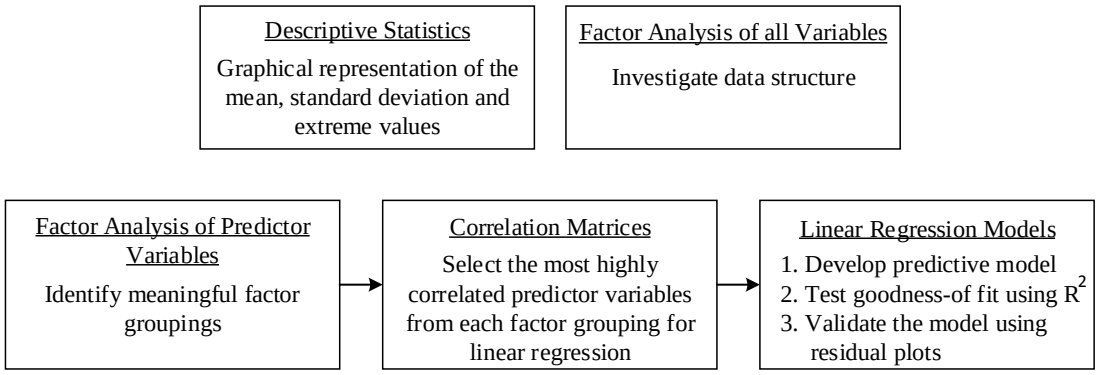

Figure 6.2: Block diagram of the multi-variable statistical analyses contained in this chapter.

6.1 MSA Data Processing

In order to perform multivariate statistical investigations, the data is post-processed to allow comparison of variables over the same 5 minute duration. The reason for the choice of this duration is explained in Chapter 3. Data sampled at lower frequencies such as the 10 minute ice observations and 4 hour wave observations are interpolated using the Matlab `spline.m` function. Data sampled at higher frequencies is reported using appropriate averaging metrics such as rms, peak or mean values. The metric associated with each measured variable is listed in Appendix D.

Due to the data being recorded by 4 different measurement systems namely LMS Test.Lab, the CMU, the SDS and visual observations, each system encountered its own errors and occasional downtime during the 78 day voyage. The data from each measurement system was therefore processed separately, and missing data was allocated a NAN (Not A Number) in Matlab. This is important for the comparison of data measured at the same time, as well as for missing values to count as no observation rather than zero which would cause incorrect results.

6.2 Descriptive Statistics

Figure 6.3 shows the mean, standard deviation, outlier and extreme structural vibration rms values for the entire duration of the voyage. The colours of the box and whisker plots indicate the measurement location and the name shows which are associated with open water and with ice. The following observations are made:

1. Vibration rms values in the +X, +Y and +Z directions decrease from the bow towards the centre of the ship. Increasing again towards the stern and as you move vertically to the bridge.

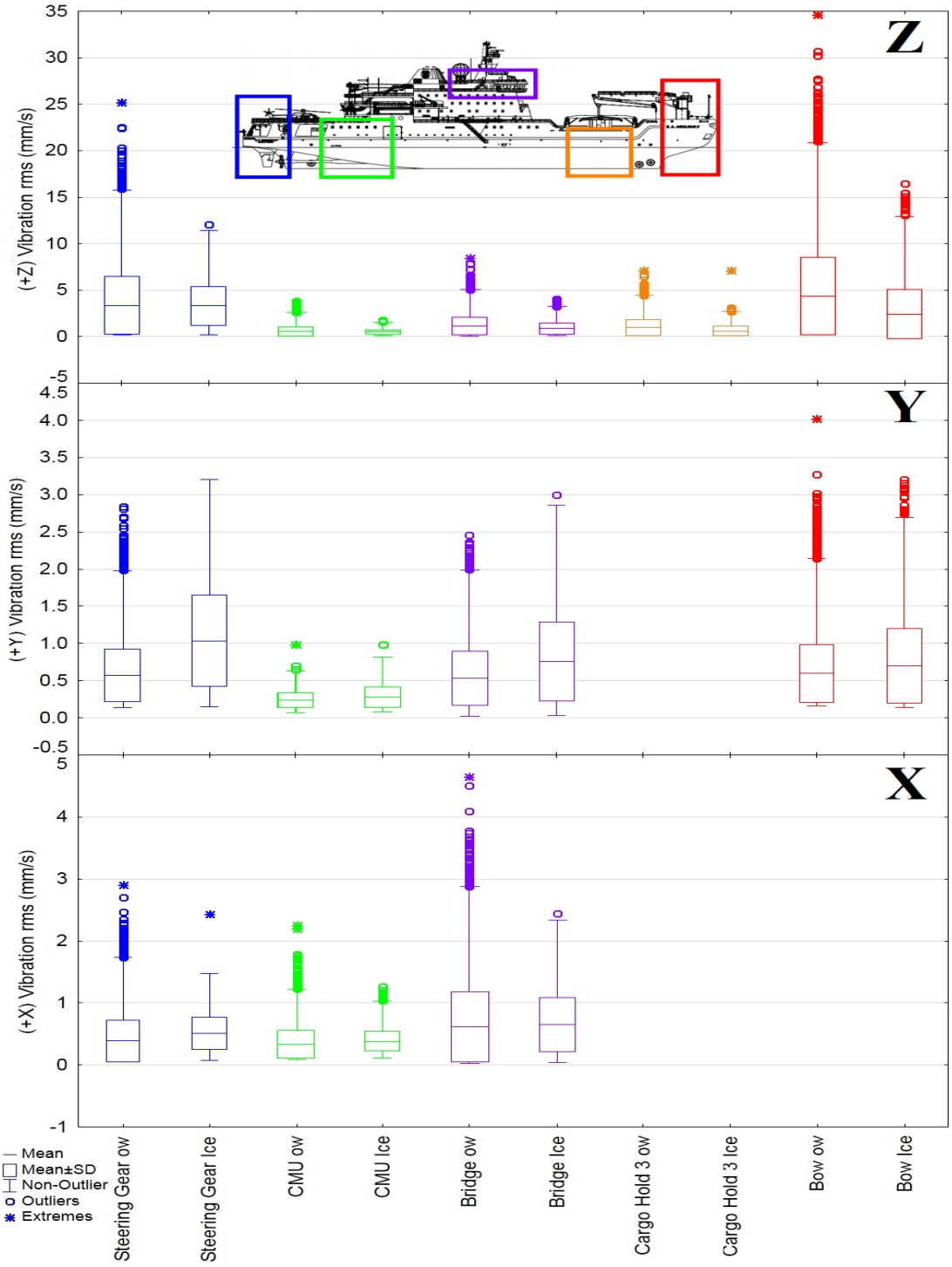

Figure 6.3: Box and whisker plot of rms structural vibration in the Vertical (+Z), lateral (+Y) and horizontal (+X) directions in open water and ice.

2. Mean and maximum values in the vertical +Z direction are larger in open water than in ice.

3. Mean values in the horizontal +X and transverse +Y directions are larger in ice than open water.

4. Maximum values in the horizontal +X direction are larger in open water than in ice. Maximum values in the transverse +Y direction are larger in ice than in open water except for measurements in the bow of the ship.

5. The magnitude of the average maximum and average mean vibration response in the vertical +Z direction is 4,6 and 3,4 times larger respectively than the horizontal +X and lateral +Y directions.

6. Maximum vibration magnitude in the vertical +Z direction in the bow and stern are 8,3 and 5,2 times larger than that in +X and +Y in open water and ice.

7. Mean and maximum values are larger in open water than in ice in the vertical +Z direction by a factor of 1,6. Mean and maximum vibration levels are similar in the +X and +Y directions in open water and ice.

6.3 Factor Analysis of all Variables

A factor analysis is first performed on all the measured variables. Table 6.1 presents the resulting Eigenvalues. The percentage total variance shows the contribution of each factor to the cumulative percentage of data explained. It can be seen that the first factor in open water accounts for 68 % of the data, while the first factor in ice explains 44 % of the data.

Table 6.1: Principle component Eigenvalue analysis of all variables in open water and in ice.

Open Water				Ice			
Val	Eigen value	% Total Variance	Cumulative %	Val	Eigen value	% Total Variance	Cumulative %
1	24.54	68.16	68.16	1	17.57	43.92	43.92
2	3.28	9.11	77.26	2	7.76	19.40	63.32
3	2.26	6.27	83.54	3	2.03	5.07	68.40
4	1.32	3.66	87.20	4	1.62	4.05	72.45
5	1.01	2.81	90.01	5	1.37	3.42	75.86
6	0.85	2.37	92.38	6	1.31	3.27	79.14

The scree plots in Figure 6.4 provide a graphical representation of the Eigenvalues and thus the relative importance of the factors. Cattell's scree test identifies the elbow at which point the gradient of the curve becomes less steep, and discards all factors after the one starting the elbow (Johnson and Wichern, 1988). Two factors would therefore be chosen for open water and three factors for ice. The most important criterion in determining the number of factors is whether these factors make sense. For this reason three factors were chosen for both ice and open water, and are explained below.

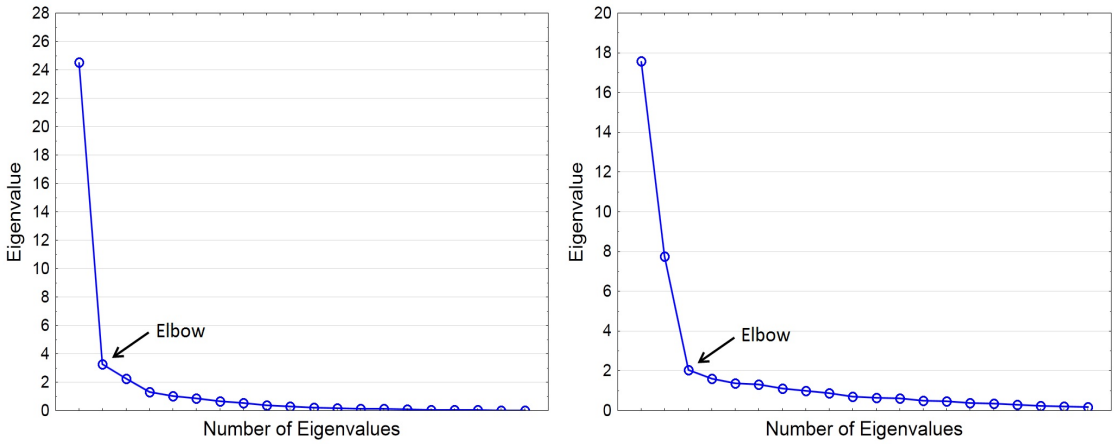

(a) Scree plot of Eigenvalues in open water. (b) Scree plot of Eigenvalues in ice.

Figure 6.4: Scree plots of the Eigenvalues for all variables.

6.3.1 Factor Analysis in Open Water

Table 6.2 shows the varimax normalised factor loadings in open water. Varimax is a data rotation scheme which maximizes the sum of the variance to reveal data structure. The data is normalised for statistical comparison across measurement units and the relative scale of variation. Each factor consists of variables which are highly correlated with each other, and highly orthogonal with the other factors. The "P" variables indicate vibration point values. The following structure is identified by each factor:

I **Vibration, wave height, wind speed relative, latitude and air temperature.** This grouping indicates that there is a strong relationship between wind and wave excitation and vibration response in open water. This also confirms the hypothesis that moving into windy latitudes such as the 'roaring forties' and 'raging fifties' results in higher wind speeds, which cause large wave heights, resulting in increased vibration response. Air temperature is also expected to be highly correlated with latitude.

Table 6.2: The varimax normalised factor loadings in open water.

Variable	Factor 1	Factor 2	Factor 3
P2 Stern Thruster Port(+Z)	0.9877	0.0395	0.0148
P6 CMU Port(-Z)	0.9720	-0.0479	0.1198
P7 Cargo Hold 3 Stb(-Z)	0.9927	0.0101	0.0385
P8 Cargo Hold 3 Port(-Z)	0.9926	0.0068	0.0400
P11 Bow Stb(+Z)	0.9909	0.0338	0.0398
P12 Bow Cent(+Y)	0.9487	0.1729	0.0708
P13 Bow Port(+Z)	0.9910	0.0335	0.0414
P15 Deck 8 Port(+Z)	0.9793	0.0569	0.1068
P16 Bridge Stb(+X)	0.9934	0.0351	0.0372
P17 Bridge Stb(+Y)	0.9547	0.2420	0.0964
P18 Bridge Stb(+Z)	0.9904	0.0457	0.0367
P19 Bridge Port(+Z)	0.9782	-0.0131	0.1112
P20 Cargo Hold 3 Port(+Z)	0.9899	0.0721	0.0439
P21 CMU Cent(+X)	0.9837	0.0408	0.0141
P22 CMU (+Y)	0.9009	0.3737	0.0542
P23 CMU Cent(+Z)	0.9782	-0.0225	0.1108
P33 Steering Gear Stb(+Z)	0.9932	0.0246	0.0423
P34 Steering Gear Stb(-Y)	0.9574	0.1733	0.0714
P35 Steering Gear Stb(+X)	0.9928	0.0028	0.0676
P36 Steering Gear Port(+Z)	0.9890	0.0288	0.0208
Port Propeller Motor Power	0.3730	0.8345	0.1836
Rudder Position Port	0.0263	-0.0527	-0.1777
Propeller Pitch Port	0.1777	0.8893	0.0979
Longitude	-0.3397	0.1190	-0.7105
Latitude	-0.6611	-0.3200	-0.0796
Air Temperature	0.6158	0.1622	0.0581
Wind Speed Relative	0.8574	0.2146	-0.0211
Wind Direction Relative	-0.2168	0.0673	-0.6158
Heading	0.3477	-0.0996	-0.6142
GPS Speed Over Ground	-0.1320	0.9338	0.0607
Wave height	0.7448	0.4249	-0.0629
Wave Direction Relative	0.1342	-0.3214	-0.6251
Draft Mid	0.2877	-0.0093	0.7953
P16 Bridge Stb(+X) HW	0.8716	0.3731	-0.0320
P17 Bridge Stb(+Y) HW	0.7597	0.5290	0.0763
P18 Bridge Stb(+Z) HW	0.8472	0.4273	0.0243

II **Port propeller motor power, propeller pitch port and GPS speed over ground.** This grouping represents the ship performance relationship between motor power, propeller pitch (related to thrust) and the speed of the ship.

III **Longitude, wind direction relative, heading, wave direction relative and draft.** This grouping shows the relationship between the wind direction and the wave direction, which in turn dictate the heading of the ship in open water. This is so as to avoid large pitching and rolling motions. Longitude and draft are thought to be related due to the easterly and westerly headings between loading and offloading cargo at Penguin and Atka Bukta.

The physical phenomena represented by the three factors are therefore:

I Forced structural dynamic excitation and response.

II Ship propulsion power.

III Ship heading.

The data structure revealed by the factor groupings indicate that vibration response in open water is caused by wave and wind excitation, and is influenced very little by ship propulsion power and heading relative to the swell direction.

6.3.2 Factor Analysis in Ice

Table 6.3 shows the varimax normalised factor loadings in ice. The "S" variables indicate ice loading on the hull. The following structure is identified by each factor:

I **Vibration in the fore of the ship, human weighted vibration in the bridge and ice loading in the bow.** This factor grouping shows that vibration in the bow and cargo hold 3 are highly correlated with ice loading in the bow. There is also a strong relationship between human weighted vibration in the bridge and vibration and ice loading in the bow.

II **Vibration in the middle and rear of the vessel, structural vibration in the bridge, port propeller motor power and propeller pitch port.** This grouping shows that vibration in the mid, rear and bridge of the vessel are highly correlated with the motor power and propeller pitch.

III **Longitude, latitude, GPS speed over ground, ice concentration and floe size.** This grouping indicates that the ice concentration and floe size increase the further south the ship travels, and the GPS speed over ground decreases as the ice increases.

Table 6.3: The varimax normalised factor loadings in ice.

Variable	Factor 1	Factor 2	Factor 3
P2 Stern Thruster Port(+Z)	0.9307	0.2763	-0.0972
P6 CMU Port(-Z)	0.3128	0.9050	0.0549
P7 Cargo Hold 3 Stb(-Z)	0.9635	0.1681	-0.1399
P8 Cargo Hold 3 Port(-Z)	0.9520	0.1643	-0.1338
P11 Bow Stb(+Z)	0.9630	0.1218	-0.1758
P12 Bow Cent(+Y)	0.7648	0.4875	-0.0588
P13 Bow Port(+Z)	0.9632	0.1217	-0.1750
P15 Deck 8 Port(+Z)	0.3877	0.8696	0.0680
P16 Bridge Stb(+X)	0.4195	0.8675	0.0172
P17 Bridge Stb(+Y)	0.2625	0.9054	0.0486
P18 Bridge Stb(+Z)	0.8820	0.4290	-0.0834
P19 Bridge Port(+Z)	0.2864	0.9061	0.1012
P20 Cargo Hold 3 Port(+Z)	0.8222	0.2347	0.0849
P21 CMU Cent(+X)	0.5482	0.7766	0.0977
P22 CMU (+Y)	-0.0186	0.8578	0.1719
P23 CMU Cent(+Z)	0.4721	0.8455	0.0002
P33 Steering Gear Stb(+Z)	0.4714	0.8281	-0.0080
P34 Steering Gear Stb(-Y)	0.1850	0.9614	0.1169
P35 Steering Gear Stb(+X)	0.1940	0.9310	0.1517
P36 Steering Gear Port(+Z)	0.4520	0.8437	-0.0121
S10 Bow	0.5936	0.2218	-0.0069
S12 Bow Shoulder	0.3420	0.2411	0.1688
S15 Stern Shoulder	0.2879	0.2801	0.1373
Port Propeller Motor Power	-0.0708	0.8025	0.1592
Rudder Position Port	-0.0776	0.0199	0.0373
Propeller Pitch Port	0.5159	-0.6529	-0.2717
Longitude	-0.3480	0.0506	-0.5804
Latitude	-0.0898	0.2886	0.7521
Air Temperature	-0.0272	0.0834	-0.3071
Wind Speed Relative	-0.3801	0.0198	0.0703
Wind Direction Relative	-0.1644	0.1197	0.1375
Heading	0.0864	-0.1951	-0.1397
GPS Speed Over Ground	0.4743	-0.2944	-0.6858
Ice Thickness	-0.2318	0.4250	0.4473
Ice Concentration	-0.1220	0.3736	0.7811
Floe Size	-0.1655	-0.0691	0.5533
Draft Mid	-0.2777	0.2953	0.5445
P16 Bridge Stb(+X) HW	0.8656	0.2801	-0.0883
P17 Bridge Stb(+Y) HW	0.8414	0.2715	-0.0927
P18 Bridge Stb(+Z) HW	0.8212	0.5316	-0.0645

The physical phenomena represented by the three factors in ice are:

I Ice excitation and vibration response in the bow and human weighted vibration response in the bridge.

II Propulsion power and vibration response in the stern, midship and bridge.

III Ice navigation performance.

The data structure in ice reveals that vibration response is caused by two different phenomenon, namely ice loading in the bow and the ship propulsion system. The effect of sea ice on navigation is also a factor.

6.4 Factor Analysis of Predictor Variables

A factor analysis of the predictor variables is then conducted in order to develop a multi-variable linear regression model of the vibration response on the S.A. Agulhas II. The Eigenvalue analysis of the predictor variables in Table 6.4 show that a smaller percentage of the data variation is explained by each factor, as compared to when all the variables are included. There is also no distinct elbow in the scree plots in Figure 6.5. Five factors were chosen as a result of their meaningful interpretation using engineering judgement, and explain 82 % of the variance in open water and 63 % in ice.

Table 6.4: Principle component Eigenvalue analysis of predictor variables in open water and in ice.

Open Water				Ice			
Val	Eigen value	% Total Variance	Cumulative %	Val	Eigen value	% Total Variance	Cumulative %
1	4.06	31.21	31.21	1	4.77	28.03	28.03
2	2.25	17.31	48.53	2	2.02	11.90	39.93
3	1.92	14.74	63.27	3	1.46	8.59	48.52
4	1.36	10.46	73.73	4	1.33	7.80	56.32
5	1.06	8.16	81.89	5	1.13	6.67	62.99
6	0.78	5.99	87.88	6	1.01	5.95	68.93

The principal component projection on the factor plane is presented in Figure 6.6, and provides a graphical illustration of the variables in each factor grouping. The tables of varimax normalised factor loadings are presented in Appendix D.

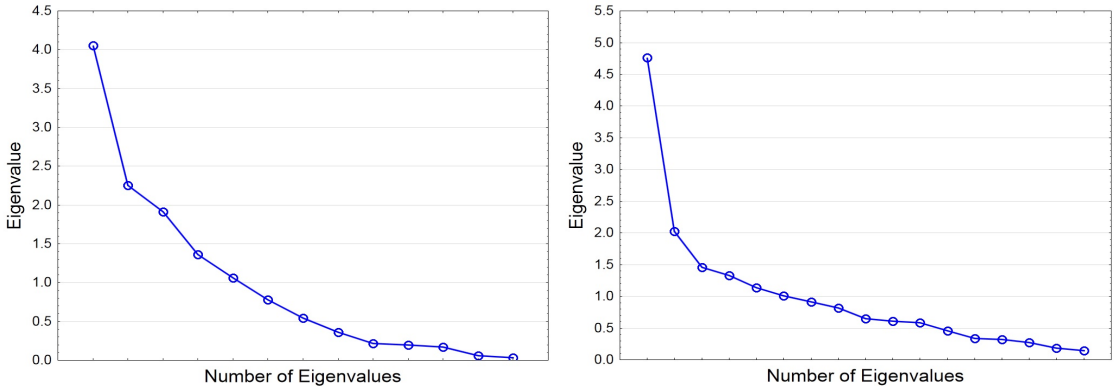

(a) Scree plot of Eigenvalues in open water. (b) Scree plot of Eigenvalues in ice.

Figure 6.5: Scree plots of Eigenvalues for predictor variables.

The identified phenomenon of each factor grouping are listed in Table 6.5. Meaningful factor groupings are chosen to contain causation variables, where the change in a given (second) variable is understood to be as a consequence of a change in the first variable (Johnson and Wichern, 1988). Casual relationships occur when two given variables change together, but not as a consequence of one another. These relationships are indicated in Table 6.5. Casual relationships cannot be left out of the analysis as one of the variables may still contain predictive power.

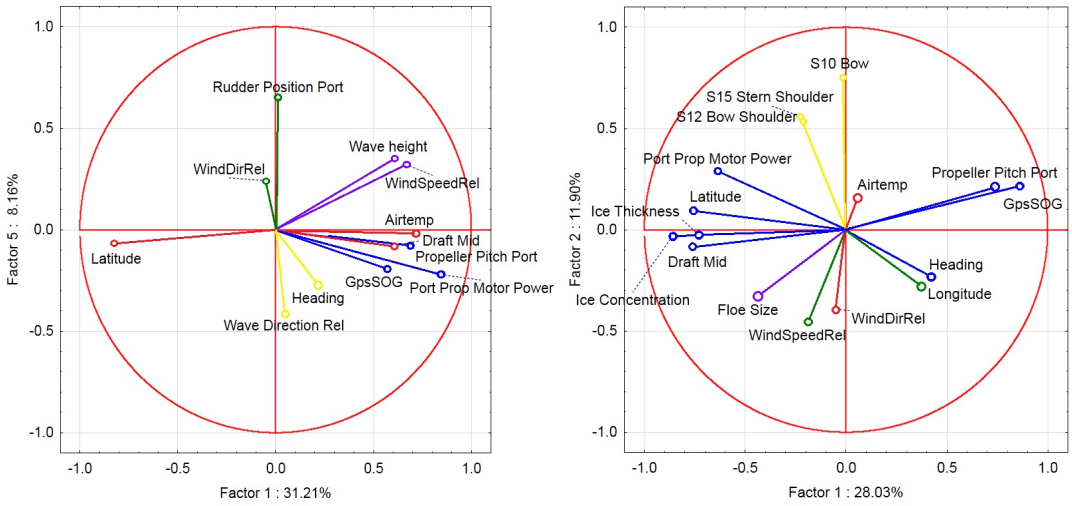

(a) Factor grouping in open water. (b) Factor groupings in ice.

Figure 6.6: Principal component projection of the variables on the factor plane.

Table 6.5: Identified phenomenon of the five factor groupings.

	Open Water		Ice
I	Ship Propulsion Power	I	Ship Propulsion Power and Ice Conditions
II	Ship Heading as a result of Wave Direction	II	Ice Loading on the Hull
III	Wind Direction and Rudder Position (Casual)	III	Longitude and Wind Speed (Casual)
IV	Draft as a result of Latitude	IV	Air Temperature and Wind Speed (Casual)
V	Wave Height as a result of Wind Speed	V	Floe Size

6.5 Correlation Matrices

The correlation coefficients provide an indication of the linear relationship between predictor variables and chosen response variables. The chosen response variables consist of structural vibration in the bow and stern, and human weighted vibration in the bridge. Table 6.6 and 6.7 present the correlation matrices of the response variables and the most highly correlated predictor variables from each factor grouping.

One variable per factor is chosen for the linear regression in order to provide an orthogonal representation of the physical phenomenon described by each factor. *S10 Bow* hull loading for example is the most highly correlated variable from Factor 2 with *P13 Bow Port(+Z)* vibration during ice navigation, and is therefore used in the multi-variable linear regression.

Table 6.6: Reduced correlation matrix in ice.

Variable	Bow		Steering Gear			Bridge		
	P13 Port(+Z)	P12 Cent(+Y)	P36 Port(+Z)	P34 Stb(-Y)	P35 Stb(+X)	P16 Stb(+X) HW	P17 Stb(+Y) HW	P18 Stb(+Z) HW
S10 Bow	0.55	0.63	0.38	0.32	0.28	0.67	0.64	0.57
S15 Stern Shoulder	0.25	0.43	0.28	0.34	0.29	0.36	0.37	0.34
Port Prop Motor Power	-0.01	0.31	0.64	0.78	0.72	0.21	0.24	0.37
Longitude	-0.22	-0.16	-0.17	-0.11	-0.16	-0.13	-0.10	-0.21
Wind Speed Rel.	-0.36	-0.26	-0.18	-0.06	-0.11	-0.31	-0.28	-0.29
Wind Dir Rel.	-0.13	-0.13	0.06	0.09	0.12	-0.15	-0.15	-0.06
Gps Speed	0.54	0.28	-0.02	-0.26	-0.28	0.34	0.36	0.27
Floe Size	-0.25	-0.18	-0.13	-0.02	0.01	-0.20	-0.19	-0.20

Table 6.7: Reduced correlation matrix in open water.

Variable	Bow		Steering Gear			Bridge		
	P13 Port(+Z)	P12 Cent(+Y)	P36 Port(+Z)	P34 Stb(-Y)	P35 Stb(+X)	P16 Stb(+X) HW	P17 Stb(+Y) HW	P18 Stb(+Z) HW
Port Prop Motor Power	0.40	0.51	0.38	0.52	0.39	0.63	0.74	0.69
Latitude	-0.64	-0.67	-0.65	-0.68	-0.65	-0.64	-0.68	-0.65
Wind Speed Rel.	0.85	0.81	0.85	0.82	0.83	0.85	0.81	0.84
Wind Direction Rel.	-0.23	-0.23	-0.20	-0.23	-0.24	-0.18	-0.19	-0.21
Heading	0.30	0.23	0.29	0.24	0.28	0.31	0.20	0.27
Wave height	0.73	0.76	0.74	0.77	0.71	0.82	0.85	0.83

6.6 Multi-Variable Linear Regression Models

The most highly correlated predictor variables from each factor grouping are then combined linearly to determine the best prediction of the response variables. The best subset technique is used which determines the best fitting model from all possible combinations of the predictor variables (Statistica, 2012).

Table 6.8 shows the R^2 values which determine the goodness-of-fit of the regression model. It can be seen that the open water models explain more of the variability of the response data than the ice models. The best response prediction in open water is for human weighted vibration in the bridge, where 84 % of the variation in the data is explained. The best response prediction in ice is in the steering gear room were 67 % of the variation in the data is explained.

Table 6.8: Coefficients of determination for regression analyses.

	Open Water	Ice
	Multiple R^2	Multiple R^2
P13 Bow Port(+Z)	0.76	0.54
P12 Bow Centre(+Y)	0.73	0.47
P36 Steering Gear Port(+Z)	0.77	0.54
P34 Steering Gear Stb(-Y)	0.75	0.67
P35 Steering Gear Stb(+X)	0.75	0.59
P16 Bridge Stb(+X) HW	0.82	0.52
P17 Bridge Stb(+Y) HW	0.83	0.49
P18 Bridge Stb(+Z) HW	0.84	0.45

Figure 6.7 shows the residual plots for the best and worst regression models in

open water and in ice. The residual plots provide a means of validating the R^2 values. It can be seen that the observed errors (residual) consist of a combination of deterministic and stochastic parts. Figure 6.7a shows a partial trend (deterministic) at lower predicted values and then becomes more random (stochastic). The worst open water residual plot consist of a large portion of deterministic values. The residual plots in ice appear more random than those in open water.

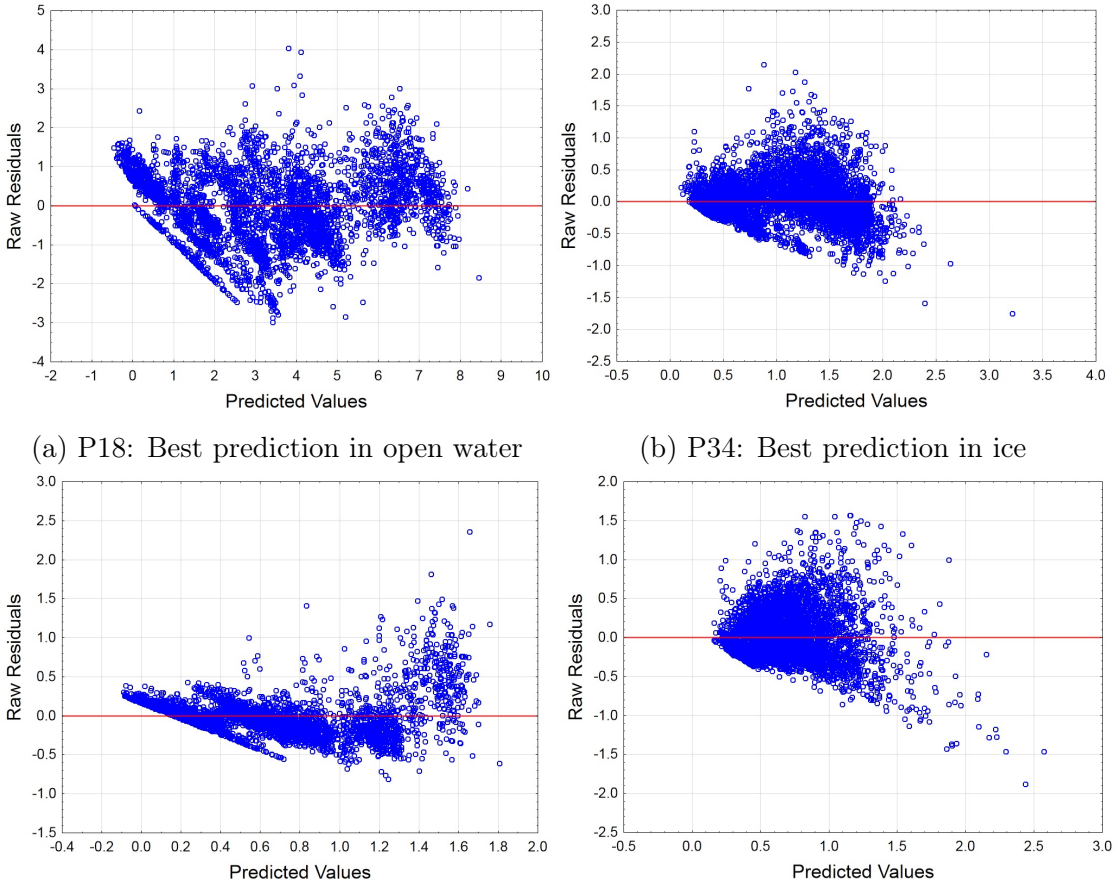

(a) P18: Best prediction in open water

(b) P34: Best prediction in ice

(c) P12: Worst prediction in open water

(d) P18: Worst prediction in ice

Figure 6.7: Predicted vs. Residual Values.

The deterministic part of the residual plots in open water mean that some of the models predictive power results from the error. This is not desirable as the idea is that the deterministic portion of the model is so good at explaining the response, that only the inherent randomness of any real-world phenomenon remains for the error terms (Frost, 2013). The reason for these deterministic parts in the residual could be due to (Frost, 2013):

1. Missing variables
2. The need for higher order terms (non-linear regression)
3. Missing interaction between variables already in the model

The residual plots are not entirely deterministic, which indicates that while improvements can be made, that the R^2 values can still be trusted.

6.6.1 Regression Model in Open Water

The linear regression model in open water is presented in Equation 6.6.1. The regression coefficients are presented in Table 6.9.

$$\boldsymbol{Y_n} = \boldsymbol{C_n} + \alpha \boldsymbol{X_1} + \beta \boldsymbol{X_2} + \gamma \boldsymbol{X_3} + \delta \boldsymbol{X_4} + \zeta \boldsymbol{X_5} + \eta \boldsymbol{X_6} \tag{6.6.1}$$

Table 6.9: Regression coefficients in open water.

	Bow		Steering Gear			Bridge		
	P13 Port(+Z) Y_1	P12 Cent(+Y) Y_2	P36 Port(+Z) Y_3	P34 Stb(-Y) Y_4	P35 Stb(+X) Y_5	P16 Stb(+X) HW Y_6	P17 Stb(+Y) HW Y_7	P18 Stb(+Z) HW Y_8
Intercept C	8.8236	1.1371	5.9295	1.0690	0.9025	2.7298	2.5711	1.7605
P.P. Motor Power α	-0.0006	0.0001	-0.0005	0.0000	-0.0001	0.0013	0.0016	0.0010
Latitude β	-0.0016	-0.0002	-0.0010	-0.0002	-0.0001	-0.0006	-0.0004	-0.0004
WindSpeedRel γ	0.5772	0.0470	0.3416	0.0424	0.0456	0.3430	0	0.2050
WindDirRel δ	-0.0052	-0.0004	-0.0023	-0.0003	-0.0005	-0.0007	-0.0010	-0.0008
Heading ζ	0.0045	0.0002	0.0020	0.0002	0.0003	0.0037	0.0011	0.0017
Wave height η	0	0	0	0	0	0	0.8668	0

The vibration response $\boldsymbol{Y_n}$ can then be predicted using the linear regression model coefficients $[C_n, \alpha, \beta, \gamma, \delta, \zeta, \eta]$ and measured or expected predictor values $\boldsymbol{X_{1-6}}$.

6.6.2 Regression Model in Ice

The linear regression model in ice is presented in Equation 6.6.2. The regression coefficients are presented in Table 6.10.

$$\boldsymbol{Y_n} = \boldsymbol{C_n} + \alpha \boldsymbol{X_1} + \beta \boldsymbol{X_2} + \gamma \boldsymbol{X_3} + \delta \boldsymbol{X_4} + \zeta \boldsymbol{X_5} + \eta \boldsymbol{X_6} + \theta \boldsymbol{X_7} + \phi \boldsymbol{X_8} \tag{6.6.2}$$

Table 6.10: Regression coefficients in ice.

	Bow		Steering Gear			Bridge		
	P13 Port(+Z) Y_1	P12 Cent(+Y) Y_2	P36 Port(+Z) Y_3	P34 Stb(-Y) Y_4	P35 Stb(+X) Y_5	P16 Stb(+X) HW Y_6	P17 Stb(+Y) HW Y_7	P18 Stb(+Z) HW Y_8
Intercept C	1.1337	0.4395	0.8307	0.2281	0.1940	0.4166	0.3939	0.4014
S10 Bow α	0.0087	0.0021	0.0029	0	0	0.0030	0.0033	0.0015
S15 Stern Shoulder β	0	0	0	0.0138	0.0041	0	0	0.0001
P.P. Motor Power γ	0	0.0001	0.0009	0.0004	0.0002	0	0	0
Longitude δ	0	0	0	0	0	0	0	0
WindSpeedRel ζ	-0.1064	-0.0129	-0.0563	-0.0143	-0.0089	-0.0210	-0.0182	-0.0151
WindDirRel η	0.0008	-0.0002	0.0014	0.0003	0.0002	0	0	0.0001
GpsSOG θ	0.2955	0	0	0	0	0.0363	0.0487	0
Floe Size ϕ	0.0000	0.0000	-0.0001	0.0000	0.0000	0	0.0000	0.0000

Figure 6.8 presents the regression plots of the best predicted vs observed vibration response for open water and ice. The rest of the plots of the predicted vs observed vibration response are presented in Appendix D.

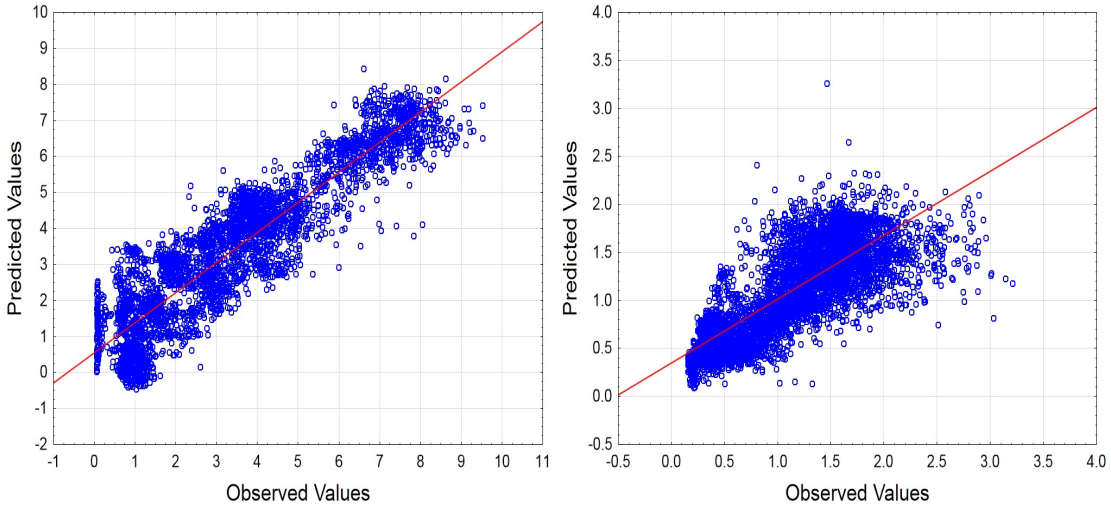

(a) P18: Best prediction in open water (b) P34: Best prediction in ice

Figure 6.8: Predicted vs. Observed Values.

Chapter 7

Operational Modal Analysis

Operational Modal Analysis (OMA) is used to investigate the global structural dynamic characteristics of the ship. The aim of OMA is to obtain the structure's modal parameters, namely the natural frequencies, damping ratios and unscaled mode shapes from response only measurements. These modal parameters will provide insight into the global dynamic response of the vessel, i.e. how the structure is bending and twisting. This information can then be used to further investigate:

1. Human comfort: By interrogating the frequency content of the measured response, amplitude contributions can be defined at discrete frequencies. These include those from structural excitation, rotating machinery and noise.

2. Excitation forces: Wave, ice and wind loading and their effects on the modal parameters can be identified.

3. Finite Element (FE) models: OMA can be used to validate and improve FE assumptions for future vessel design.

4. Operating and boundary conditions: Effects of different vessel operations on the modal parameters and the resulting fatigue life of the structure can be studied.

5. Structural health monitoring: OMA algorithms can monitor the normal migration of natural frequencies in order to identify irregularities resulting from collision or fatigue damage.

This chapter will deal with the measurement, identification and validation of modal parameters using two different OMA methods. Initial comparisons with the FE model of the S.A. Agulhas II will also be presented. Future work will involve excitation force identification, investigations into operating and boundary conditions and structural health monitoring.

7.1 Boundary Conditions

OMA was conducted on the S.A. Agulhas II while moored at East Pier in Cape Town harbour as shown in Figure 7.1a. Figure 7.1b shows the mooring conditions at the quayside. The ship is positioned against large rubber tyres hanging from the quayside using the bow and stern thrusters. Mooring lines are then attached to bollards (small concrete pillars) to secure the ship. Eight mooring lines are used in total with 2 head lines, 2 fore springs, 2 stern lines and 2 stern springs. A windlass and a capstan, mechanical devices consisting of an electric motor attached to a rotating drum, are then used to tension the fore and aft mooring lines respectively.

(a) Satellite image (Google). (b) Mooring conditions.

Figure 7.1: Location of the S.A. Agulhas II at East Pier in Cape Town harbour for Operational Modal Analysis.

7.2 Excitation

Figure 7.1a is a satellite image of East Pier where it can be seen that the ship is in an isolated mooring with possible small wave (ripple) excitation and wake excitation from other boats passing by. The ship is exposed to wave excitation on the port side and stern and possible reflected wave excitation at the bow. The starboard side is very isolated from any wave excitation as it lies against the quayside. OMA was performed during the following three conditions:

1. Main engines running during cargo operation.
2. Harbour generator running.
3. Shore power through a three phase connection.

7.3 Measurement Conditions

The 1 hour run chosen for this analysis was between 00h00 and 01h00 on the 28th of February 2014. The offloading of heavy cargo had been completed, and the ship had not been refuelled with polar diesel. The draft was 6,7 m fore, 6,8 m midship and 6,9 m aft.

The ship was on shore power and the wind had picked up during the night to 43 km/h. This measurement run was chosen due the lack of harmonic contamination from the engines and harbour generator as well as good wind and wave excitation.

7.4 Measurement Set-up

Figure 7.2 shows the measurement locations and directions used for the harbour OMA. Twenty three vibration measurement channels were recorded in total with eighteen on the hull structure and five on the superstructure.

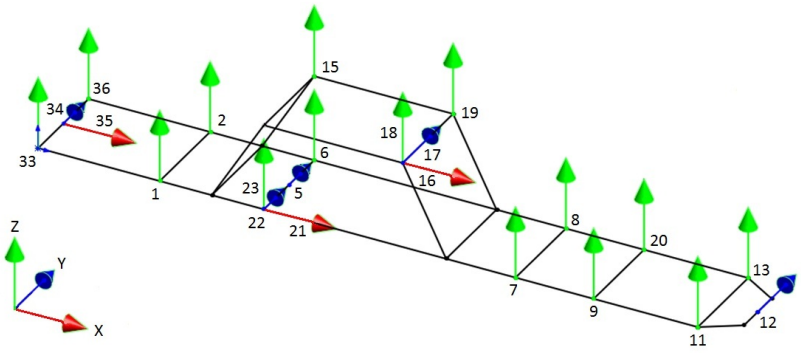

Figure 7.2: Measurement model indicating sensor location and measurement direction.

Vertical vibration (+Z) was measured on the port and starboard side of the ship hull at as close to equal increments as was physically possible. This was done in order to investigate the horizontal (x-y) plane for vertical bending and torsional modes. Lateral vibration was measured at three points along the hull to investigate the longitudinal vertical (x-z) plane for transverse bending modes. Longitudinal vibration (+X) in the hull is not considered in the present work.

Vibration measurements in the superstructure include longitudinal (+X) measurements to investigate fore-aft bending, lateral (+Y) measurements to investigate transverse bending and vertical (+Z) measurements to investigate torsion.

A measurement duration of an hour was selected based on the results from Rosenow (2007) in his PhD thesis, where he found that measurement durations of one hour or more were necessary to obtain stochastic excitation. The global modes are expected to lie below 10 Hz, but in order to improve the resolution of the data, a sample frequency of 128 Hz was chosen. It was decided that this could be down-sampled during post-processing if necessary.

7.5 Results

The results from the harbour vibration measurements are presented and discussed below. OMA is then conducted using the LMS Operational PolyMAX algorithm and compared to results by Prof Joerg Bienert at the University of Ingolstadt using the ARTeMIS CCSSI algorithm.

7.5.1 Acceleration Time History

The acceleration time histories of representative sensors are shown in Figure 7.3. Vertical (+Z) vibration measurements from five different locations, as well as lateral (+Y) and longitudinal (+X) vibration in the CMU and bridge respectively are presented together with their rms and maximum values.

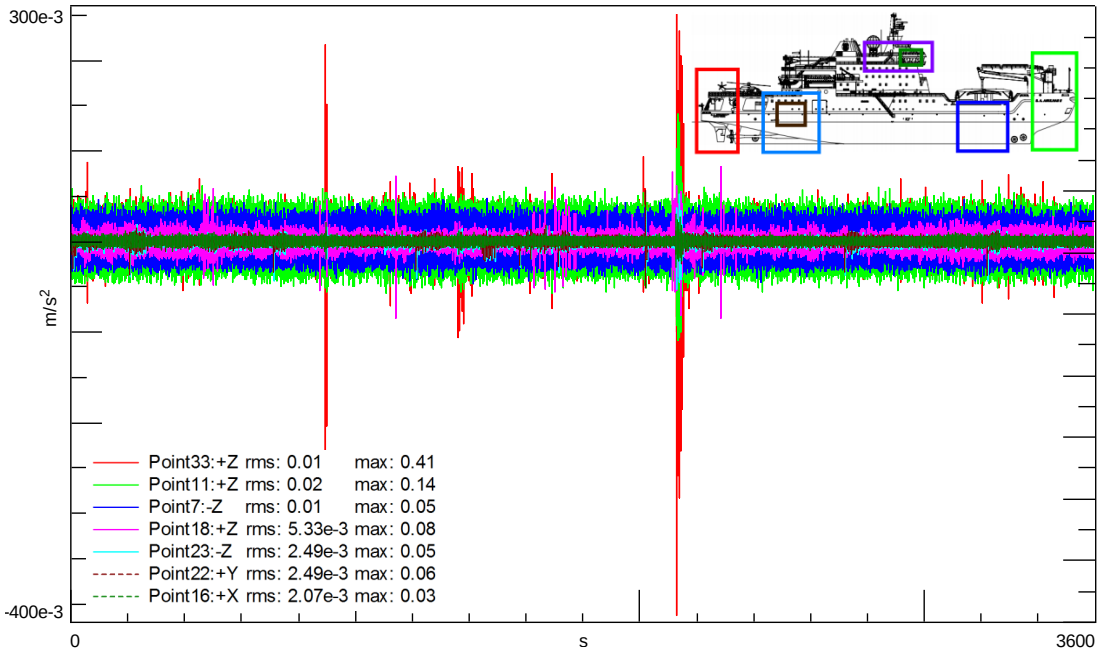

Figure 7.3: Acceleration time history with rms and maximum values during the 1 hour measurement run.

The peak vibration amplitudes are low with a maximum of 0,41 m/s^2 in the vertical (+Z) direction in the stern and a minimum of 0,03 m/s^2 in the longitudinal (+X) direction in the bridge. Rms values have a maximum of 0,02 m/s^2 in the vertical (+Z) direction in the bow and a minimum of 2,07 $\times$ 10^{-3} m/s^2 in the longitudinal (+X) direction in the bridge. The crest factors of the signals are presented in Table 7.1 and indicate an impulsive response.

Table 7.1: The mean values and crest factors of the time signals.

Signal	Crest Factor
Point33 (+Z)	41
Point11 (+Z)	7
Point7 (+Z)	5
Point18 (+Z)	15
Point23 (+Z)	20
Point22 (+Y)	24
Point16 (+X)	15

7.5.2 Power Spectral Density

The power spectral density (PSD) in Figure 7.4 shows how the signal power is distributed in the frequency domain. The PSD is calculated using the following parameters: peak amplitude mode, Hanning window, 50 % overlap and 2048 NFFT points resulting in a frequency resolution of 0,0625 Hz. The following observations are made:

1. There are distinct low frequency peaks at 1,9 Hz, 3,37 Hz and 4,66 Hz.
2. The amplitude of the frequency content under 5 Hz is largest in the bow, closely followed by that in the stern.
3. The amplitude in the frequency range between 5 Hz and 30 Hz is largest in the stern.
4. The frequency content in the vertical (+Z) direction in the bridge becomes dominant in the frequency range from 30 Hz to 36 Hz.
5. The lowest amplitude response occurs in the lateral (+Y) and longitudinal (+X) directions in the CMU and bridge respectively. Followed by vertical (+Z) vibration in the CMU.
6. There is a large peak at 50 Hz across all sensors from electrical noise.

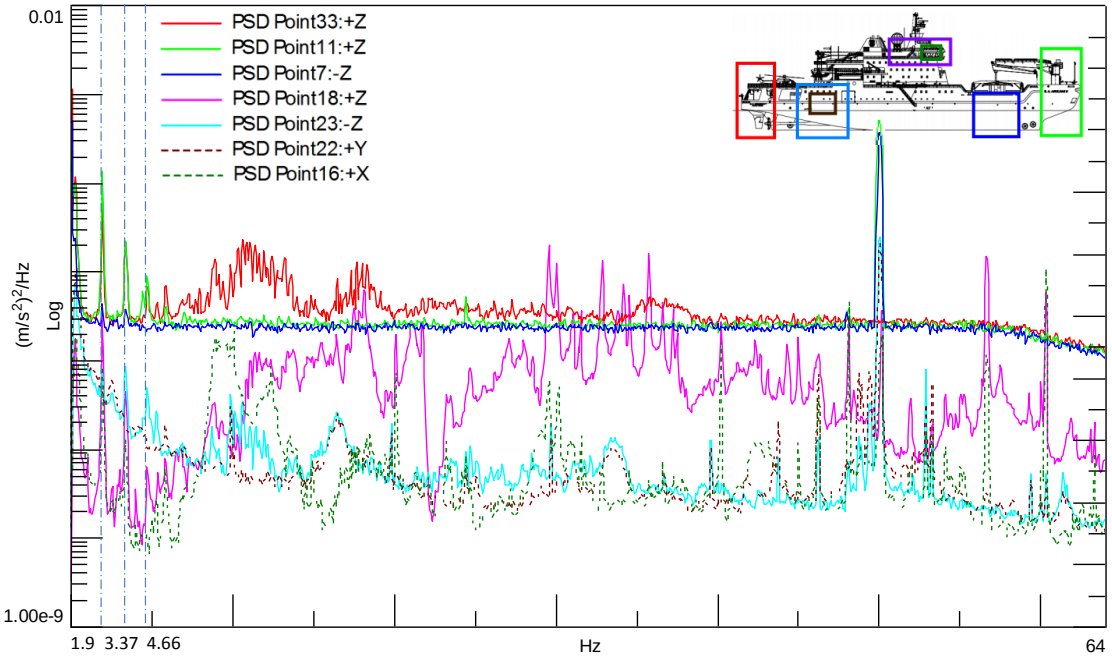

Figure 7.4: Power Spectral Density (PSD) of the time signals.

7.5.3 Crosspower Spectrum

The crosspower spectrum calculates the Fourier transform of the cross correlation function (LMS, 2000). The cross correlation function is a measure of the similarity of two signals as a function of a time lag. The crosspower spectrum can therefore be used to investigate the input output relationship, in the frequency domain, between a selected reference (input) signal and measured (output) signal.

Vertical vibration at Point 11 in the bow is selected as the reference as this resulted in a clear stabilization diagram, see Section 7.5.4. Figure 7.5 and 7.6 show the crosspower spectra between sensors in the vertical (+Z) direction to 64 Hz and 6 Hz respectively. The following observations are made:

1. Three distinct peaks occur at 1,94 Hz, 3,37 Hz and 4,69 Hz. This confirms the similarity between the signal peaks observed in the PSDs.

2. The amplitude at the resonant peaks is largest for the crosspowers between Point 33 (Stern) and Point 11 (bow). This indicates a strong relationship between the frequency content in the bow and stern.

3. It is important to note that the selected reference sensor does not account for all the input excitation. The reference sensor can then move in or out

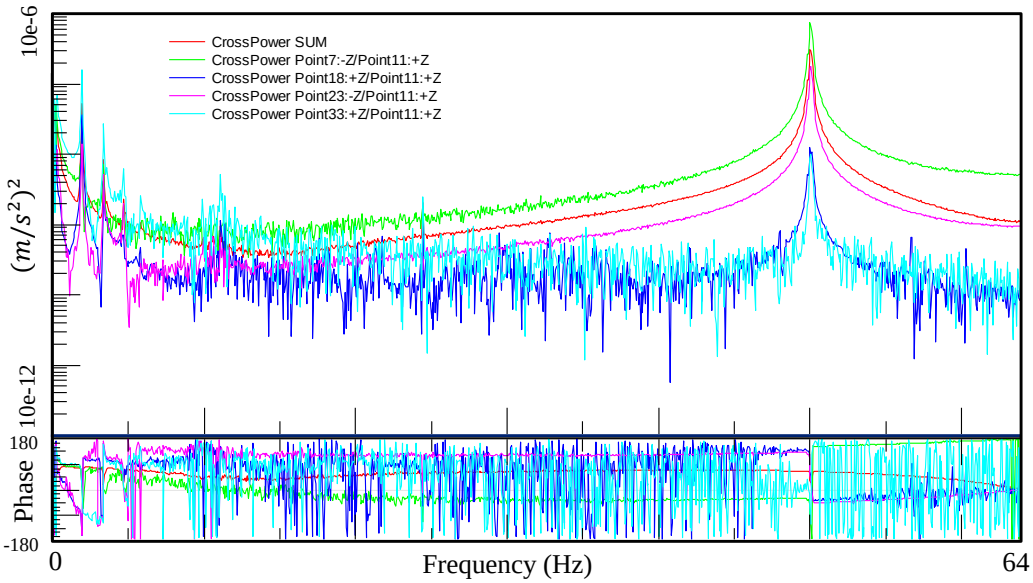

Figure 7.5: Crosspower spectra with Point 11 as reference to 64 Hz.

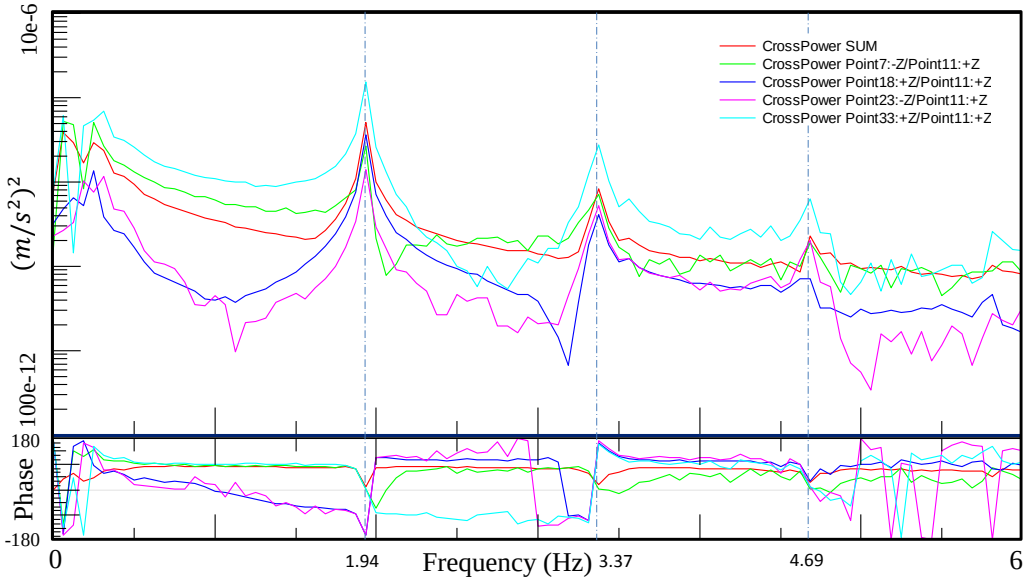

Figure 7.6: Crosspower spectra with Point 11 as reference to 6 Hz.

of phase with the true excitation. The physical phenomenon of 90° phase at resonance therefore does not apply to cross power spectra between system responses.

4. The phase is seen to shift from positive to negative, or visa versa around the first three resonant peaks.

5. Crosspower spectra between vertical (+Z), transverse (+Y) and longitudinal (+X) sensors are omitted as they do not provide insight into the current modal parameter investigations.

7.5.4 Stabilization Diagrams

An Eigenvalue analysis is used to plot the stabilization diagram from which the modal parameters can be estimated. Poles are fitted to the data for a certain mathematical model with n first order DOF along the horizontal axis. The increasing model order plotted along the vertical axis allow the identification of modes, and the discrimination of physical and spurious modes, from vertical alignments of stable poles. Figure 7.7 shows the stabilization diagram produced by the LMS Operational PolyMAX frequency domain algorithm.

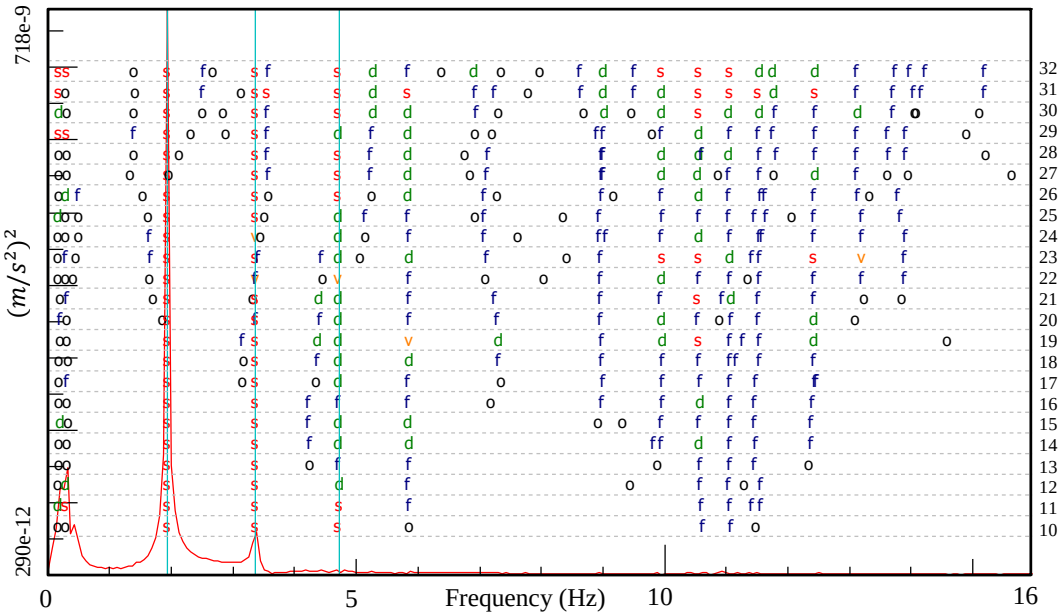

Figure 7.7: Operational PolyMAX stabilization diagram. (s) Stable pole with high confidence, (v) Some confidence in the Eigenvector, (d) Some confidence in damping, (f) Some confidence in the Eigenvalue, (o) Unstable pole.

Stable poles with high confidence are seen to align at 1,94 Hz and 3,37 Hz indicating stable physical modes. A third less stable pole at 4,72 Hz is also selected. Poles at higher frequencies were investigated but did not provide clear results. While it is expected that more modes do exist in this frequency range, the current measurements are unable to clearly separate physical modes from non-physical noise modes.

The stabilization diagram from the ARTeMIS CCSSI time domain algorithm is presented in Figure 7.8. Three stable poles are identified at 1,93 Hz, 3,36 Hz and 4,67 Hz. The CCSSI stabilization diagram is clearer than that produced by Operational PolyMAX. The third mode is also identified with high confidence in CCSSI.

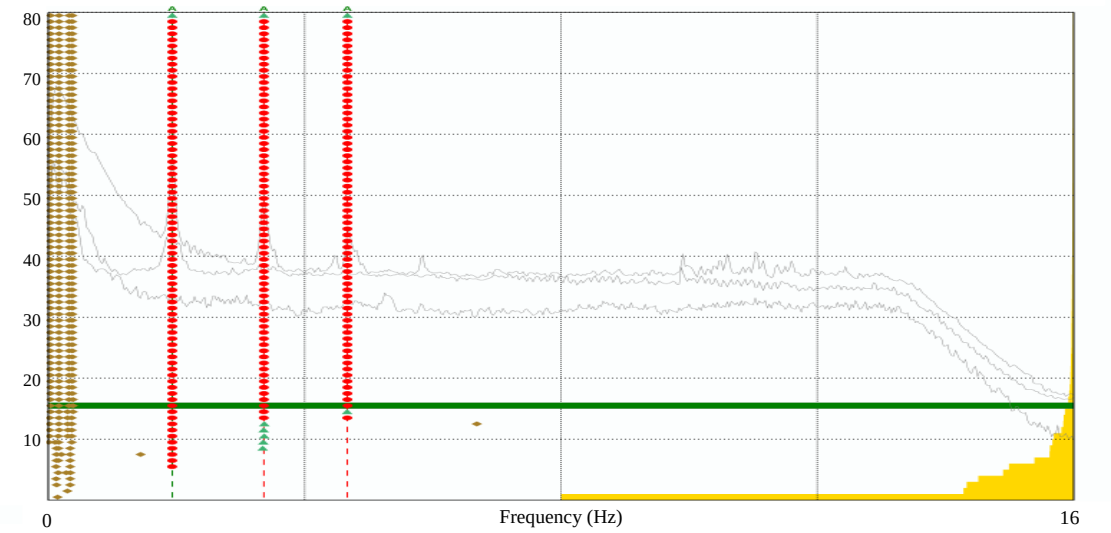

Figure 7.8: CCSSI stabilization diagram of estimated state space models. ● Stable mode, ▲ Unstable mode, ♦ Noise mode (Joerg Bienert).

The natural frequencies and damping ratios of the three selected modes using Operational PolyMAX and CCSSI as well as the percentage difference between the two estimates are presented in Table 7.2. CCSSI and Operational PolyMAX agree to within 1,2 % on the natural frequencies. The damping estimates however show less agreement, especially for mode 3 which differ by 59 %. The damping percentage for all three selected modes is small due to the high stiffness of the structure which is reinforced for ice navigation.

Table 7.2: A Comparison of natural frequencies and damping ratio estimates using Operational PolyMAX and ARTeMIS CCSSI as well as their percentage difference.

	Frequency (Hz)			Damping (%)		
Mode	PolyMAX	CCSSI	Diff (%)	PolyMAX	CCSSI	Diff (%)
1	1.935	1.934	0.052	0.651	0.571	-12.289
2	3.367	3.363	0.119	0.969	1.075	10.939
3	4.721	4.667	1.157	1.512	2.406	59.127

7.5.5 Mode Shapes

The operational mode shapes of the three selected poles are presented alongside the FE model prediction of STX Finland in Figure 7.9. The modes are identified as the 2-node (first), 3-node (second) and 4-node (third) normal bending modes of the structure. Due to the fairly symmetrical geometry of the structure, the three modes show little complex mixing of modes, i.e. modes comprised of a combination of bending and torsion.

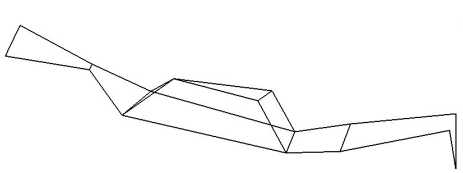

(a) f = 1,94 Hz, 2-node vertical bending.

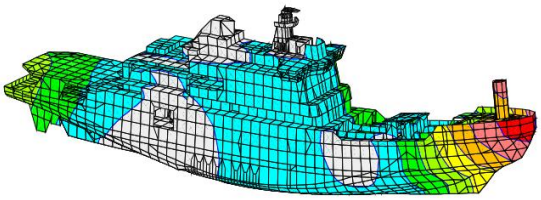

(b) f = 2,60 Hz, 2-node vertical bending.

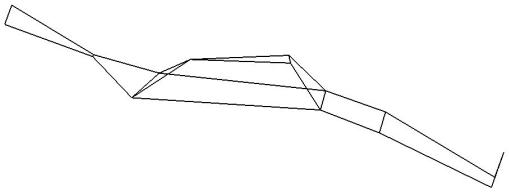

(c) f = 3,37 Hz, 3-node vertical bending

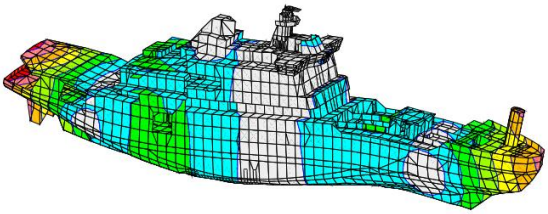

(d) f = 4,28 Hz, 3-node vertical bending

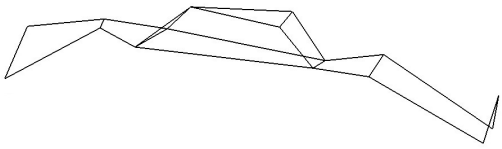

(e) f = 4,72 Hz, 4-node vertical bending

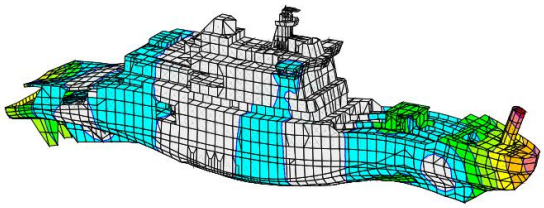

(f) f = 5,63 Hz, 4-node vertical bending

Figure 7.9: Mode shapes for the first three vertical bending modes. OMA models generated using LMS are on the left, and FE models developed by STX Finland are on the right.

The FE model shows the nominal vectors, which are relative mode shapes and do not have physical dimensions. The surrounding water has been taken into account by the addition of mass to the mass matrix connected to the wet surface of the shell. The method is based on green functions of pressure distribution, and

describes the case when the vessel is located in deep water (Luosma, 2013). The total mass of the model corresponds to the displacement with a draught of 7,7 m, and loading condition STR-2 which is fully loaded at departure.

The analytical FE natural frequencies are larger than the measured OMA natural frequencies by 34 %, 27 % and 19 % respectively. The FE model draught of 7,7 m is 0,9 m deeper than the 6,8 m draught during OMA measurements. The effect of adding mass in the form of cargo and fuel is however expected to further decrease the measured OMA natural frequencies, due to the relationship between the natural frequency (ω_n), mass (m) and stiffness (k) matrices:

$$\omega_n = \sqrt{\frac{k}{m}} \tag{7.5.1}$$

This implies that the stiffness of the elements used in the FE model may be inaccurate. The effects of greater hull surface area exposed to water and the mooring boundary conditions on the natural frequencies and damping also need to be further investigated.

The absence of torsional modes from the OMA is thought to be due to the structure not being physically excited to measurable amplitudes in a torsional manner by waves and wind in the harbour mooring. While the absence of transverse bending modes from the OMA is thought to be due to a combination of low measurement resolution in the transverse (+Y) direction as well as possible low transverse structural excitation. The use of more sensors and larger structural excitation is recommended for future research. Isometric and side views of the operational mode shapes have been included in Appendix E.

7.5.6 Modal Assurance Criterion (MAC) Matrix

The modal assurance criterion (MAC) is a statistical indicator that is most sensitive to large differences and relatively insensitive to small differences in the mode shapes (Pastor *et al.*, 2012). The MAC matrix therefore provides a quantitative comparison between mode shapes.

Mode shapes are expected to be independent of one another and comprised of orthogonal vectors. The MAC matrix for the three modes identified using Operational PolyMAX is presented in Figure 7.10. Mode pair 1-2 as well as 2-3 have low MAC values and are therefore decoupled. Mode pair 1-3 show a 69 % correlation. This is due to the physical similarity between the 1st and 3rd bending mode shapes. MAC matrix results by Orlowitz and Brandt (2014) show similar

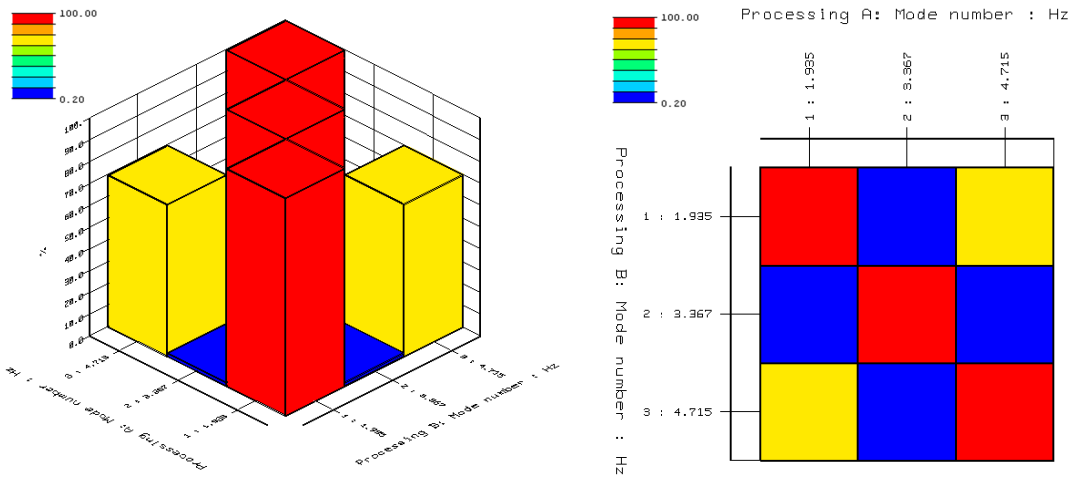

(a) Isometric view. (b) Top view.

Figure 7.10: MAC matrix.

correlations between the 1st and 3rd bending modes. The MAC value is expected to decrease for non diagonal pairs as the number of measurement locations along the hull structure increase.

The ARTeMIS CCSSI MAC matrix show similar results to LMS Operational PolyMAX and is presented in Appendix E. It is important to note that the MAC matrix can only indicate consistency and is not a validity check to identify spurious modes (Orlowitz and Brandt, 2014). A cross MAC matrix can be computed to determine the statistical similarity between the different algorithms as well as between OMA and FE results, and is proposed for future research.

7.5.7 Complexity Plots

The modes are validated by plotting the components of the Eigenvectors in the complex plane. The resulting complexity plots for the three identified modes are presented in Figure 7.11 a, b and c, with the real values on the x-axis and imaginary values on the y-axis. The complexity plots show that all the DOF are nearly in phase within each mode. This means that the Eigenvectors reach their respective maximums and minimums at the same time, and that there is little complex mixing of modes. This confirms the proportional damping model approximation for lightly damped structures which expects real valued mode shapes (Rainieri and Fabbrocino, 2014).

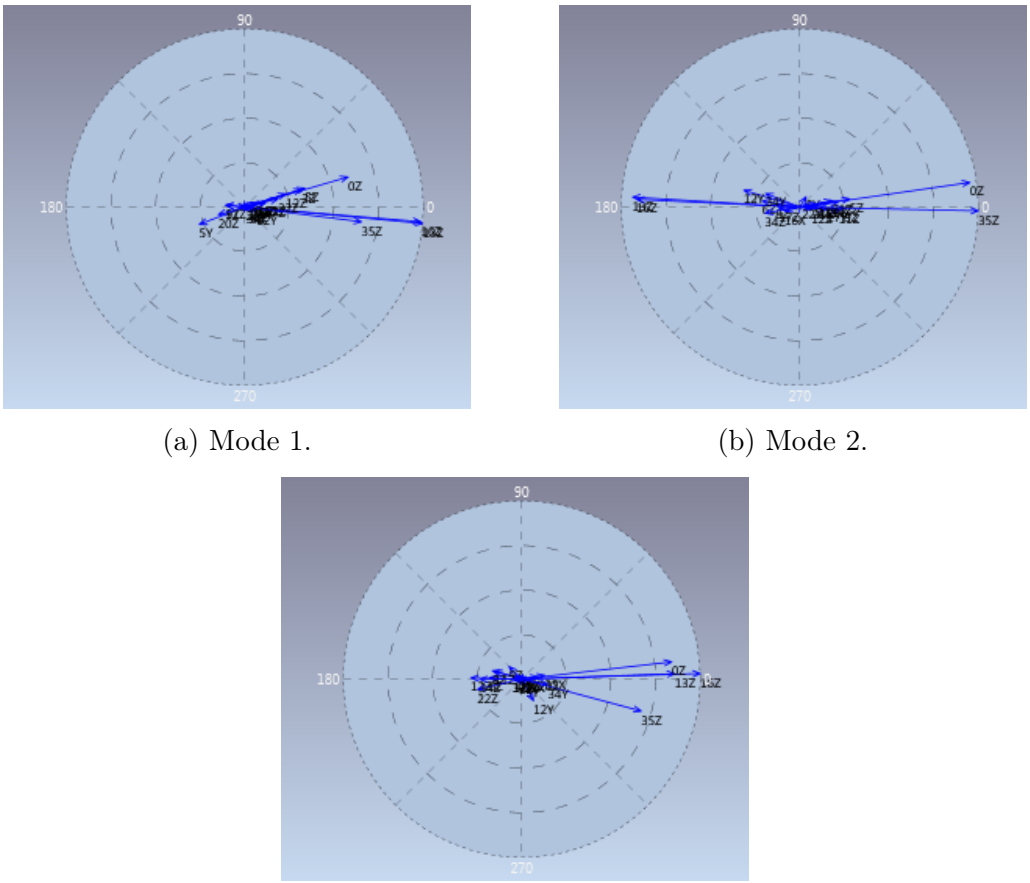

(a) Mode 1.

(b) Mode 2.

(c) Mode 3.

Figure 7.11: Complexity plots using ARTeMIS CCSSI (Joerg Bienert).

Chapter 8

Conclusion

The S.A. Agulhas II plays a key role in the South African National Antarctic Program, and is relied upon for logistical and research support. The safe operation of the vessel is a primary concern for the ship owner and operator as well as the crew and scientists on board. This thesis presents a vibration response analysis of the S.A. Agulhas II in Antarctica and the Southern Ocean to determine the effects of vibration on human comfort and the structural dynamic response.

Full scale measurements were conducted during a 78 day voyage from Cape Town to Antarctica during 2013/2014. An experimental setup of 20 accelerometers distributed across the hull and superstructure measured vibration continuously and simultaneously. Vibration measurements were performed to investigate the effects of vibration on human comfort and structural fatigue. This analysis formed part of a consortium of research which aims to create a scientific basis for the design of future ice-going vessels. Consortium data is used in a multivariate statistical analysis to investigate the effects of predictor variables on ship vibration response. Operational Modal Analysis (OMA) is also performed to investigate the structural dynamic characteristics of the vessel.

Vibration in the bridge of the vessel is found to have little effect on human comfort and is classified as not uncomfortable according to BS ISO 2631-1. The crest factors indicate that rms is an appropriate metric for more than 76 % of the measured vibration. The VDV does however show a trend of higher values during impulsive open water navigation. While this is beneficial for a vibration metric, the lack of VDV comfort limit values in standards as well as VDV measurements on other ships for comparison, remain a limiting factor. Despite low human vibration levels, complaints of vibration discomfort on board highlight the complexity of the subject, and the observations that there is no simple approach to the evaluation and prevention of human vibration discomfort.

The structure of the vessel is found to be most effected by vertical vibration during open water navigation, with a maximum peak velocity of 338,35 mm/s in 8 m swells. Vibration levels are larger in the bow and stern, decreasing towards the centre of the vessel and increasing again as you move up to the bridge. The source of the measured vibration is identified in the frequency domain. Vibration during ice navigation is dominated by the first blade pass frequency at 9,3 Hz in the lateral and longitudinal directions, as well as by an unknown peak between 15 and 16 Hz in the vertical direction. Distinct peaks at 1,9 Hz and 3,6 Hz during open water navigation are identified as the 2-node and 3-node vertical bending modes of the vessel. Vibration of the diesel engines rotating at 750 rpm can be seen at 12,5 Hz, and from the firing order of the six cylinders at 37,5 Hz.

Structural fatigue as a result of vibration is found to reach the level where damage is possible in the stern and were damage is probable in the bow according to Germanischer Lloyd's ship vibration guidelines. The vibration levels with potential to cause fatigue damage were measured in 8 m swells during open water navigation. This calls for further research into the effects of the duration at these exposures, materials of construction, structural details in the effected areas, welding processes and environmental conditions. The occurrence of fatigue cracks on the ship hull in the cargo hold prior to these measurements provide further justification for research into structural health monitoring and damage detection.

Multivariate statistical analyses are performed to investigate the relationships between multiple predictor and response variables. Physical phenomena are identified from the data structure revealed by factor analysis. During open water navigation wind speed relative, wave height and vibration response group together in a factor identified as *forced structural dynamic excitation and response*. The propulsion power and heading relative to the wave direction are seen to group in orthogonal factors and are therefore considered to have less influence on vibration response. During ice navigation the vibration response separates into two factors. *Vibration response in the bow and hull loading* group together and *vibration response in the stern, midship and bridge group with propulsion power*. Navigating with all four engines running during ice mode is therefore seen to have a significant effect on the vibration response in the stern and superstructure.

A factor analysis of the predictor variables is used to develop a multi-variable linear regression model for predicting vibration response. Five factors are selected and the most highly correlated predictor variables from each factor grouping are used in the model. This provides an orthogonal representation of the measured

physical phenomenon. The resulting regression models provided better vibration prediction in open water than in ice. The best prediction of the vibration response in open water is 84 % for human weighted vibration in the bridge, while the best prediction during ice navigation is 67 % for structural vibration in the steering gear room. The models are validated using residual plots which indicate that some of the predictive power during open water navigation results from the error, but that in general the residual term is random. This indicates that the correlation values (R^2) are trustworthy.

The envisioned uses of the developed prediction models are the mitigation of undesirable vibration responses and the prediction of vibration response for future vessel designs. Undesirable vibration can be mitigated by understanding how different variables combine to result in certain vibration responses, examples include the effect of changing course in open water to mitigate excessive lateral vibration. Predictive vibration response models can be used during the conceptual design stages to determine the effects of expected operating conditions on structural or human vibration.

Operational Modal Analysis (OMA) is used to investigate the structural dynamic characteristics of the vessel. The LMS Operational PolyMAX frequency domain and ARTeMIS CCSSI time domain OMA techniques are used to estimate the modal parameters. Three stable modes are identified at 1,94 Hz, 3,37 Hz and 4,72 Hz and show agreement to within 1,2 % by both Operational PolyMAX and CCSSI. The damping estimates show less agreement, especially for mode 3 which differs by 59 %. The three modes are identified as the 2-node (first), 3-node (second) and 4-node (third) normal bending modes. The MAC confirms three unique modes, with cross coupling between mode pair 1-3 due to the geometrical similarities. The complexity plots reveal real valued mode shapes which confirm the proportional damping model approximation for lightly damped structures and thus validate the results.

The natural frequencies predicted by the FE model are greater than those measured using OMA by 34 %, 27 % and 19 % respectively. The FE calculations are based on a vessel draught of 7,7 m which is deeper than the 6,8 m draught during OMA testing. The effect of adding mass to the structure is however expected to further reduce the OMA natural frequencies. This implies that the stiffness of the elements used in the FE model may be inaccurate. Further investigation into the effect of boundary and operation conditions is recommended for further insight into the modal parameters.

Vibration analyses provide valuable insight into the dynamic response of large ship structures. The challenge and opportunity is to now use this insight together with modern technology to develop a vessel monitoring system, which is able to detect fatigue or collision damage and warn the crew before catastrophic failure. In this way the research does not only provide benefits to the academic and shipping communities, but also to those living and working on PSRVs.

Chapter 9

Recommendations

Full scale data provides a valuable source of information for understanding the dynamic response of a vessel. Due to the unpredictable Antarctic and Southern Ocean environments in which the vessel operates, a number of full scale data sets are required in order to improve the confidence in the data analyses. The amount of measurable phenomena together with the diversity of operating conditions provide various opportunities for further research.

Despite current state-of-the-art ship designs, humans are still ultimately responsible for their safe operation. Investigations into the effect of vibration duration on human fatigue of the officers who work two four hour shifts each day, and live and work in the same environment for months at a time is therefore recommended. Further investigation into the use of the VDV metric to replace the rms metric for both impulsive and non-impulsive responses is also recommended, especially if the vessel is exposed to slamming during normal operation.

Validation of the current multi-variable linear regression model based on the upcoming 2014/2015 Antarctic voyage measurements is recommended. The 2014/2015 data should also be combined with the 2013/2014 data to update the regression coefficients and hopefully improve the model prediction. Improvements to the multi-variable linear regression models may also be achieved by using non-linear statistical analyses, including further predictor variables and testing different analysis techniques.

Boundary conditions imposed on polar supply and research vessels range from various sea states in open water to various ice thickness's, concentrations and ice bending and compressive strengths. Investigations into the effect of these boundary conditions on the ship's structural dynamic characteristics is therefore recommended. Further investigations into OMA during normal vessel operation to

determine the effect of various ship loadings and operating conditions on the modal parameters is also recommended. An area of particular concern is the stern slamming phenomenon experienced during voyages in rough seas to Marion Island. This should be investigated using OMA to determine how the structure is responding, and how to attenuate harmful vibration.

The potential exists for the development of an OMA solver which is optimised to solve the modal parameters of large ship structures operating in ice and open water. Such an algorithm can then be used to develop a low cost autonomous structural health monitoring system. This will require testing low cost MEMS acceleration sensors and configuring a system to measure and monitor the natural frequencies of the structure during normal operation. Eigenvalue tracking techniques will need to be developed to track the normal migration of modes. The navigating officers and engineers can then be warned if abnormal changes in the natural frequencies occur which could be as a result of collision or fatigue damage. This will provide large benefits to the Department of Environmental Affairs (DEA) who own the S.A. Agulhas II as well as provide further safety for the crew and scientists on-board the vessel.

List of References

Aenlle, M.L., Brincker, R. and Canteli, A.F. (2009). Some Methods to Determine Scaled Mode Shapes in Natural Input Modal Analysis. In: *IMAC-XXIII*. Orlando, Florida USA.

Alfred Wegener Institute, A.W.I. (2014). About the German National Antarctic Program. Available at: `https://www.comnap.aq/Members/AWI/SitePages/Home.aspx`

Annis, C. (2014). Central Limit Theorem. Available at: `https://www.statisticalengineering.com/central_limit_theorem.htm`

Asmussen, I., Menzel, W. and Mumm, H. (2001). Ship Vibration. Tech. Rep., GL Technology, Germanischer Lloyd, Hamburg.

BBC (2014). Captain James Cook (1728 - 1779). Available at: `https://www.bbc.co.uk/history/historic_figures/cook_captain_james.shtml`

Bekker, A. (2013). Whole-Body Vibration Comfort on the Bridge of the S.A. Agulhas II Polar Supply and Research Vessel During Ice-Breaking. In: *48 th United Kingdom Conference on Human Responses to Vibration*. Ascot, England.

Belov, I.M. and Spiridonov, N.N. (2012). Features of Ship Vibration in Ice Operation Conditions. In: *Twenty-second (2012) International Offshore and Polar Engineering Conference*, vol. 4, pp. 1223–1228. Rhodes, Greece.

Bridges, R., Zhang, S., Pavic, M., Tong, J., Kavanagh, S. and Fitzsimmons, P. (2013). Ice Load Monitoring Systems, Shiprightsea Event Analysis Procedure for ice. In: *22nd International Conference on Port and Ocean Engineering under Arctic Conditions*. Espoo, Finland.

Brincker, R. and Andersen, P. (2003). A Way of Getting Scaled Mode Shapes in Output Only Modal Testing. In: *IMAC XXI*. Kissemmee (FL), USA.

BS ISO 20283-2:2008 (2008). *Mechanical Vibration - Measurement of Vibration on Ships - Part 2: Measurement of Structural Vibration*. International Organization for Standardization (ISO).

BS ISO 2631-1:1997, E. (1997). *Mechanical Vibration and Shock - Evaluation of human exposure to whole-body vibration Part 1: General Requirements*. BSI Standards Publication.

COMNAP (2014). COMNAP Member National Antarctic Programs.
Available at: `https://www.comnap.aq/Members/SitePages/Home.aspx`

Coppotelli, G., Dessi, D. and Rimondi, R. (2008). Output-Only Analysis for Modal Parameter Estimation of an Elastically Scaled Ship. *Ship Research*, vol. 52, pp. 45–56.

Dinham-Peren, T.A. and Dand, I.W. (2010). THE NEED FOR FULL SCALE MEASUREMENTS. In: *William Froude Conference: Advances in Theoretical and Applied Hydrodynamics - Past And Future*, November. Portsmouth, UK.

Döhler, M., Andersen, P. and Mevel, L. (2012). Operational Modal Analysis using a Fast Stochastic Subspace Identification Method. In: *30th IMAC*, pp. 1–7. Springer, Jacksonville, Florida USA.

Encyclopeadia Britannica (2014). Roald Amundsen.
Available at: `https://www.britannica.com/EBchecked/topic/21974/Roald-Amundsen`

Ewins, D.J. (1984). *Modal Testing: Theory and Practice*. Research Studies Press LTD., Letchworth, Hertfordshire, England.

Fiennes, R. (2004). *Captain Scott*. Hodder and Stoughton, London.

Filcek, P. (2006). Ship Vibration and Noise. July.

Frost, J. (2013). Regression Analysis: How Do I Interpret R-squared and Assess the Goodness-of-Fit?
Available at: `https://www.blog.minitab.com/blog/adventures-in-statistics/regression-analysi`

Goursat, M., Dohler, M., Mevel, L. and Andersen, P. (2010). Crystal Clear SSI for Operational Modal Analysis of Aerospace Vehicles. In: *IMAC-XXVIII*. Springer, Jacksonville, Florida USA.

Griffin, M. (1990). *Handbook of Human Vibration*. Elsevier Academic Press, London.

Inman, D.J. (2014). *Engineering Vibration*. Fourth edi edn. Pearson, Essex, England.

ISO 6954:2000, E. (2000). *Mechanical Vibration - Guidelines for the measurement, reporting and evaluation of vibration with regard to habitability on passenger and merchant ships*, vol. 2000. International Organization for Standardization (ISO).

Janssens, K., Kollar, Z., Peeters, B., Pauwels, S. and Van derAuweraer, H. (2014). Order-based resonance identification using operational PolyMAX. In: *LMS Online*, 1.

Johnson, R.A. and Wichern, D.W. (1988). *Applied Multivariate Statistical Analsysis*. 2nd edn. Prentice Hall, Englewood Cliffs, New Jersey.

Khatibi, M.M., Ashory, M.R. and Albooyeh, A.R. (2009). Determination of scaled mode shapes in response only modal analysis. In: *IMAC-XXVII*. Orlando, Florida USA.

Kujala, P. (2011). Full-scale measurements on board NB1369 PSRV. Tech. Rep., Aalto University, School of Engineering, Marine Technology, Helsinki, Finland.

Lagerbom, C.H. (2014). America, Antarctica and The American Polar Society. Available at: `https://www.americanpolar.org/polar-compendium/aps-history/`

Lansing, A. (2007). *Endurance - Shackleton's Incredible Voyage*. Basic Books, New York, United States of America.

LMS (2000). Theory and Background. Available at: `https://www.read.pudn.com/downloads71/ebook/257215/Complete theory.pdf`

Lubbad, R., Raaij, E.V. and Eik, K.J. (2013). Oden Arctic Technology Research Cruise 2012. In: *22nd International Conference on Port and Ocean Engineering under Arctic Conditions*, vol. 2012. Espoo, Finland.

Luosma, J. (2013). S.A. Agulhas II FE-Model.

McMahon, K., Soal, K., Lehtiranta, J., Kulovesi, J., Boulle, B. and Gildenhuys, F. (2013). Frequency Weighting Time Domain.

Mills, W.J. (2003). *Exploring Polar Frontiers: A Historical Encyclopedia, Volume 1*. ABC-CLIO, Santa Barbara, California.

Nyseth, H.v., Frederking, R. and Sand, B.r. (2013). Evaluation of Global Ice Load Impacts Based on Real-Time Monitoring of Ship Motions. In: *22nd International Conference on Port and Ocean Engineering Under Arctic Conditions (POAC'13)*. Espoo, Finland.

Orlowitz, E. and Brandt, A. (2014). Modal test results of a ship under operational conditions. In: *IMAC XXXIII Conference and Exposition on Structural Dynamics*. Orlando, Florida.

Parloo, E., Verboven, P., Guillaume, P. and Van Overmeire, M. (2002 September). Sensitivity-Based Operational Mode Shape Normalisation. *Mechanical Systems and Signal Processing*, vol. 16, no. 5, pp. 757–767. ISSN 08883270.

Pastor, M., Binda, M. and Harčarik, T. (2012 January). Modal Assurance Criterion. *Procedia Engineering*, vol. 48, pp. 543–548. ISSN 18777058.

Preston, A. (2013). The quest to find Ernest Shackleton's lost ship Endurance that disappeared beneath the ice of the Antarctic nearly a century ago. Available at: `https://www.dailymail.co.uk/home/moslive/article-2256577/Ernest-Shackletons-E`

Rainieri, C. and Fabbrocino, G. (2014). *Operational Modal Analysis of Civil Engineering Structures*. Springer, New York.

Rimell, A.N. and Mansfield, N.J. (2007 August). Design of digital filters for frequency weightings required for risk assessments of workers exposed to vibration. *Industrial health*, vol. 45, no. 4, pp. 512–9. ISSN 0019-8366.

Rosenow, S.-E. (2007). *Identification of the dynamic behaviour of marine construction structures*. Ph.D. thesis, Universität Rostock.

Soal, K. and Bekker, A. (2013). Whole-Body Vibration Comfort on the S.A. Agulhas II Polar Supply and Research Vessel During a Voyage to Antarctica. In: *48th United Kingdom Conference on Human Responses to Vibration*, September, pp. 16–18. Sunningdale Park, Ascot, SL5 0QE, England.

Statistica (2012). Best-Subset and Stepwise GDA ANCOVA with Deployment. Available at: `https://www.documentation.statsoft.com/STATISTICAHelp.aspx?path=DM/Nodes/GDAA`

Structural Vibration Solutions (). Technical Review No. 1. Available at: `https://www.svibs.com/solutions/Technical_Reviews/Review_1_2012.aspx`

Suhr, D.D. (1994). Principal Component Analysis vs. Exploratory Factor Analysis. In: *SUGI 30 Statistics and Data Analysis*, pp. 1–11. Philadelphia, Pennsylvania.

Suominen, M., Karhunen, J., Bekker, A., Kujala, P., Elo, M., van Bock und Polach, R., Enlund, H. and Saarinen, S. (2013). Full-Scale Measurements on board PSRV S.A. Agulhas II in the Baltic Sea. In: *22nd International Conference on Port and Ocean Engineering under Arctic Conditions*. Espoo, Finland.

Temple, D. and Collette, M. (2012). Multi-Objective Hull Form Optimization to Compare Build Cost and Lifetime Fuel Consumption. In: *IMDC 2012. 11th International Marine Design Conference Volume 2*. Glasgow, Scotland.

Tryfos, P. (1997). Chapter 14: Factor Analysis. York University, Toronto, Canada. Available at: `www.yorku.ca/ptryfos/f1400.pdf`

Wagner, J., Binkowski, E. and Bronsart, R. (2014). Scenario based optimizaton of a container vessel with respect to its projected operating conditions. *Naval Architecture and Ocean Engineering*.

Ward, P. (2001). Cool Antarctica - Fabien (Thaddeus) Gottleib von Bellingshausen. Available at: `https://www.coolantarctica.com/Antarctica fact file/History/antarctic_whos_who_mirnyi_vostok_bellinghausen.htm`

Weisstein, E.W. (2014). Multivariate Normal Distribution. From Mathworld - A Wolfram Web Resource.
Available at: `https://www.mathworld.wolfram.com/MultivariateNormalDistribution.html`

Zhang, L., Brincker, R. and Andersen, P. (2005). An Overview of Operational Modal Analysis : Major Development and Issues. In: *Proceedings of the 1st International Operational Modal Analysis Conference (IOMAC)*, 1. Copenhagen, Denmark.

Appendices

Appendix A

Conference Paper

WHOLE-BODY VIBRATION COMFORT ON THE S.A. AGULHAS II POLAR SUPPLY AND RESEARCH VESSEL DURING A VOYAGE TO ANTARCTICA

Keith Soal, Anriëtte Bekker
Sound and Vibration Research Group
Department of Mechatronic and Mechanical Engineering
University of Stellenbosch
Stellenbosch, 7600
South Africa

Abstract

Ice-going ships are renowned for being uncomfortable to travel in when breaking through thick ice due to constant vibration and jarring. In order to efficiently break through ice, these vessels have thick, rounded keels with no protuberances for stability which can lead to heavy rolling even in light seas. There is a lack of scientific research that reports on the dynamic comfort of passengers and crew on-board ice-going ships. To this end full scale vibration comfort measurements were conducted on-board the polar supply and research vessel the S.A. Agulhas II during a 76 day voyage from Cape Town to Antarctica. Measurements were performed to adhere to ISO 2631-1 and ISO 6954:2000.Vibration levels were compared to the comfort class notation of the Norwegian classification society Det Norske Veritas. The most severe vibration levels were recorded when ramming, in pack ice. This research aims to contribute field data towards the development of a scientific basis for the design of ice-going ships.

1. Introduction

Ships operating in polar environments are exposed to extreme conditions, and encounter a number of excitation mechanisms. These excitation mechanisms include waves, ice, machinery and propellers, with each creating different local and global dynamic responses.

In order to efficiently break through ice, polar vessels have thick rounded keels with no protuberances for stability which can lead to heavy rolling even in light seas (Kujala, 2011). These dynamic responses can result in vibration propagating through the ship structure, which may exacerbate structural fatigue, damage equipment as well as impair the well-being, efficiency and health of people on-board (Asmussen *et al.*, 2001). Since Polar Regions, and the Antarctic in specific, are so remote, passengers, scientists and crew often spend months on-board, living and working in this dynamic environment. The habitability of polar vessels is therefore an important design consideration in order to prevent human fatigue which could result in the damage of equipment, cargo, the ship structure and possible loss of life.

Full scale measurements of ice-going ships have played an important role in understanding the dynamic responses of various excitation mechanisms (Nyseth *et al.*, 2013). Measurements are compared to relevant standards such as ISO 6954:2000, ISO 2631-1 and Det Norske Veritas (DNV) Comfort Class notation, which provide guidelines for evaluating the habitability on-board ships. Current habitability standards are however becoming out-dated, and have been found to contain inconsistencies (Asmussen *et al.*, 2001, Biot and De Lorenzo, 2007, Savreux *et al.*, 2007). There is current development of Polar Class Rules, based on the International Association of Classification Societies (IACS) Unified Requirements for Polar Ships. These aim to create an international standard

Presented at the 48th United Kingdom Conference on Human Responses to Vibration, held at Sunningdale Park, Ascot, SL5 0QE, England, 16 - 18 September 2013.

based on well-defined and transparent research. The current lack of high quality data has been cited as one of the most important factors limiting further understanding of dynamic ship excitations.

The University of Stellenbosch had the opportunity to be involved in a consortium conducting full scale measurements on-board the Polar Supply and Research Vessel (PSRV) the S.A. Agulhas II. The consortium members include Aker Arctic, STX Finland, DNV, Rolls-Royce, Wärtsilä, The Department of Environmental Affairs, of South Africa, Smit Vessel management Services, Aalto University and the University of Oulu. The project aim is to create a scientific basis for the design of ice-going ships with regards to ship hull, propulsion, power requirement and comfort for passengers and crew on-board.

The objective of the Sound and Vibration Research Group at the University of Stellenbosch was to perform full scale vibration comfort measurements. Measurements were performed to adhere to ISO standards, as well as DNV comfort class notation. Investigations were also conducted to determine the excitation mechanism and the associated vibration levels.

2. Background

2.1 Ship Vibration

The dynamic interaction of a ship's structure with oscillatory forces causes vibration. The excitation sources responsible for these oscillatory forces include waves, ice, machinery and propellers. In order to reduce the effect of these vibrations, the natural frequency of the ship and its various structures must not coincide with the excitation frequencies experienced during normal operation.

Ship vibrations can be classified as global vibrations, vibrations of substructures and local vibrations. Global vibrations deal with the dynamic response of large ship structures such as the hull in the frequency range from about 0.5 to 10 Hz (Asmussen *et al.*, 2001). Vibration of substructures account for the vibration of large subsystems such as the deckhouses, masts, engine systems and shaft lines. Local vibration includes vibration of plate fields, stiffeners and panels as a result of global or substructure vibration.

2.2 Standards for Assessment

Standards provide guidelines for evaluating the habitability of different areas on a ship. Existing standards are aimed solely at ensuring comfort and well-being.

ISO 6954

International standard ISO 6954:1984 was the first standard developed for the evaluation of human exposure to vibrations on-board ships. The standard considered peak amplitude values at discrete frequencies as an indication of vibration severity. Weaknesses included a maximum repetitive value (MRV) which was not clearly defined (ISSC Committee II.2, 2006), and no distinction given for different living areas.

In 2000 the ISO 6954:2000 became applicable to both merchant ships and passenger ships. The overall shipboard vibration is evaluated in terms of an overall frequency-weighted root mean square (r.m.s.) value, in the frequency range from 1 Hz to 80 Hz. Clear distinction is also made between

living areas and vibration levels vary with specified areas. The highest value obtained, without preferential direction, is used for the habitability evaluation. The guidelines for habitability are presented in Table 1, and areas are classified as A) passenger cabins, B) crew accommodation and C) working areas.

Table 1 - Overall frequency-weighted r.m.s. values from 1 Hz to 80 Hz given as guidelines for the habitability of different areas on a ship

	Area Classification		
	A mm/s	B mm/s	C mm/s
Values above which adverse comments are probable	4	6	8
Values below which adverse comments are not probable	2	3	4
NOTE The zone between upper and lower values reflects the shipboard vibration environment commonly experienced and accepted.			

DNV Comfort Class

Det Norske Veritas 2003 Comfort Class Rules specify vibration limits in mm/s peak for single frequency components between 5 and 100 Hz. Specifications are also defined in terms of data acquisition and post-processing as well as test conditions and reporting.

3. The S.A. Agulhas II

Full scale measurements were conducted on-board the PSRV S.A. Agulhas II which was built by STX Finland at the Rauma Shipyard and entered service in April 2012. The ship will support the South African National Antarctic (SANAE IV) base on the Antarctic continent carrying cargo, passengers, bunker oil and helicopter fuel. She is also equipped with laboratories to conduct scientific research in the Southern Ocean. The ship was built to Polar Ice Class PC 5 and was classified by DNV with a comfort class notation of COMF-V(2)C(2). The main dimensions of the S.A. Agulhas II are listed in Table 2.

Table 2 - The main dimensions of the S.A. Agulhas II

Length, bpp	121.8 m
Beam	21.7 m
Draught, design	7.65 m
Deadweight at design displacement	5000 t
Speed, service	14 kn

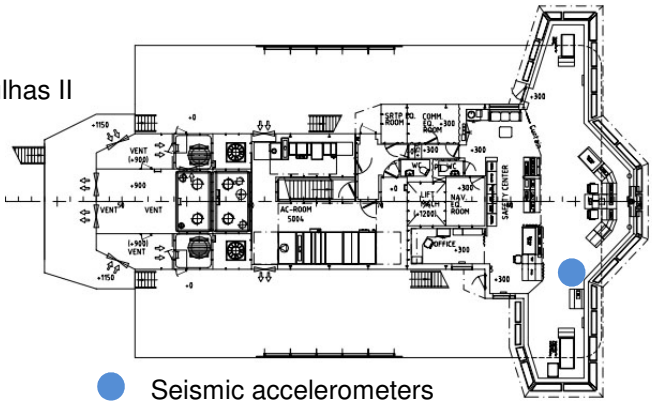

Figure 1 – Location of seismic accelerometers on the Bridge

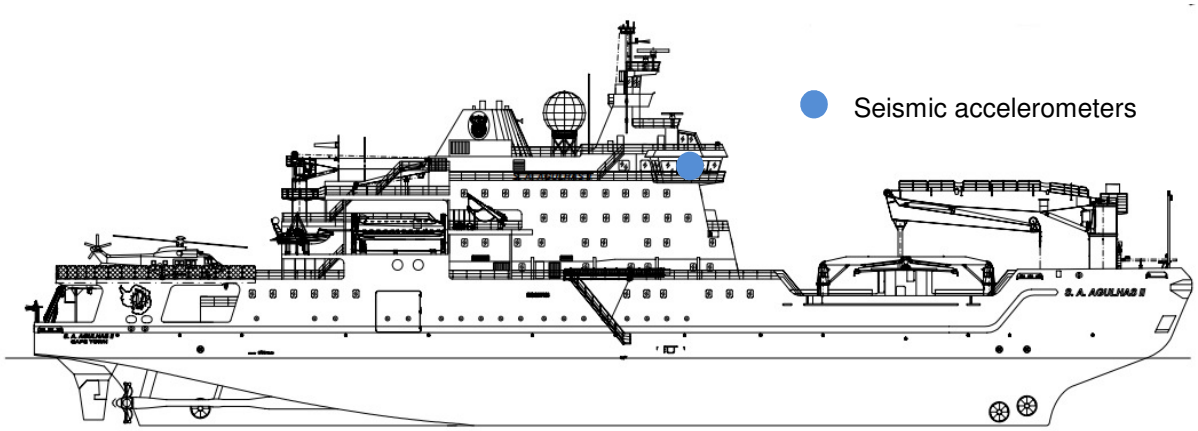

Figure 2 - Location of the seismic accelerometers

4. Instrumentation of the Vessel

Vibration comfort measurements were performed on the floor, at the base of the Captain's chair in the bridge (see Figure 1 and 2). Translational acceleration was measured in the longitudinal (+X), lateral (+Y) and vertical (+Z) directions using 10 000 mV/g seismic accelerometers. The area around the Captain's chair was cordoned off during measurements to prevent contamination from officers and crew walking past sensors. Recordings were made at a sample rate of 160 Hz using LMS Test.Lab 10A Signature Testing, and an LMS SCADAS data acquisition system. Signature testing enables continuous recording and a duration of 73 s was used for all results reported in this article.

As part of the research consortium, the ship's hull and shaft line were instrumented with strain gauges in order to determine the ice-induced loading. Stereo cameras were used to determine ice thickness, and visual observations of ice thickness and concentration were made throughout the voyage. Whole body vibration comfort measurements were conducted on the Captain's chair on the seat, backrest and footrest. Sound and vibration measurements were made on Deck 3 in the Electronics Laboratory as well as on Deck 2 in the Engine Room. Ice samples were also collected and tested for bending and compressive strength during the voyage. All measurements were synchronised to UTC time and navigational data as well as weather data were recorded throughout the voyage.

This article will only present vibration results measured on the floor in the Bridge. Correlations between human vibration comfort and the prevailing ice conditions, as well as their loading on the hull and the shaft line will still be investigated.

5. Post Processing

Post processing was performed using both LMS software and Matlab. The acceleration time signals were first integrated to velocity time signals in LMS. The data was then converted into the frequency domain in LMS, using the Fast Fourier Transform (FFT) with averaged FFT settings consisting of a linear spectrum format, a flattop window, a block size of 1024 and 50% overlap. Two sets of averaged FFT's were generated, one using peak amplitude scaling as required by DNV's Comfort Class notation, and the other using r.m.s. amplitude scaling as required by ISO 6954:2000.

The averaged FFT's with r.m.s. amplitude scaling were then band limited into one-third-octave bands using LMS. A Matlab script then weighted the filtered data according to ISO 2631-2 for the purpose of analysis according to ISO 6954. The overall frequency-weighted r.m.s. value was then calculated according to the following equation

$$v_w = \sqrt{\sum_i \left(W_{v_i} v_i\right)^2} \quad [1]$$

Where the i-th W_v value is the weighting factor for velocity, to be applied to the measured r.m.s. velocity in mm/s calculated in the i-th one-third-octave band. The Matlab script then computed the maximum, mean and standard deviation of the measured frequency-weighted r.m.s. values, as well as maximum vibration amplitude in mm/s for single frequency components as specified by DNV.

6. Vessel Operation during Measurements

Measurements were performed during ice navigation in the Weddell Sea. The Weddell Sea is characterised by relatively cold ocean water with compact sea ice and large areas of ice cover which remain during the summer (Onstott, 2004). Ice which survives one or more summer melts is known as second year or multiyear ice, and is generally fresher and therefore mechanically stronger than first year ice. Multiyear ice is also usually thicker, having undergone numerous cycles of growth and melt (Haas, 2013).

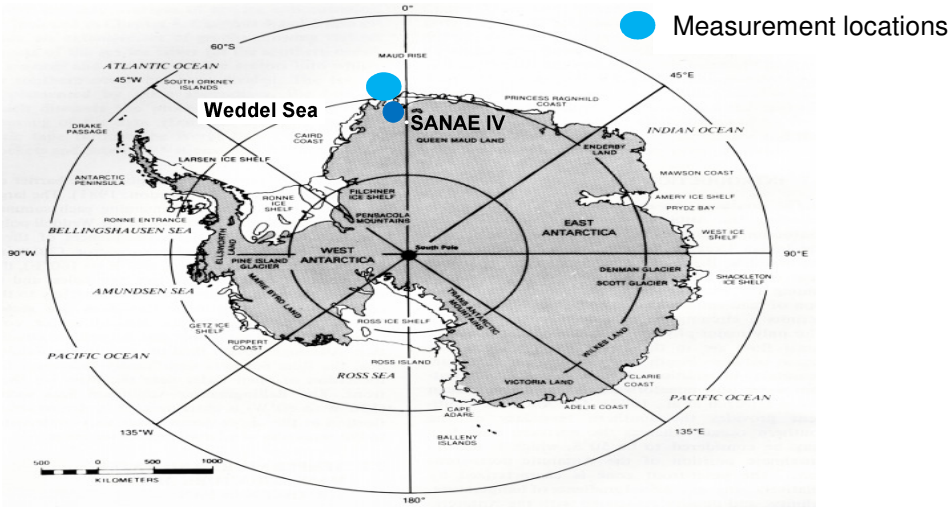

Figure 3 - Map of Antarctica and the Southern Ocean

Ice navigation is further categorized into the three groups which resulted in the highest vibration levels namely: pack ice, carving and ramming. Pack ice is consolidated, and consists mainly of floes which vary from a few metres in diameter to a several kilometres in diameter. Carving refers to navigation through the coastal zone which is attached to the ice shelf. Ramming refers to operations conducted in pack ice when the vessel encountered ice in excess of 1.5 m, which required numerous rams to penetrate. The dates and GPS locations, as well as the visual observations of average ice thickness, average ice concentration and average floe size are presented in Table 3. The location of ice navigation is shown in Figure 3.

Table 3 – Ice measurement locations and visual observations

	Date	GPS Coordinates		Average Ice Thickness (cm)	Average Ice Concentration (%)	Average Floe Size Diameter (m)
		S	W			
Pack Ice	13-01-13	69^0 32.1’	01^0 32.7’	100 - 120	80 - 90	20 - 100
	14-01-13	68^0 59.9’	00^0 30.7’	20-60	20-30	<2
	28-01-13	69^0 56.9’	08^0 29.8’	40 - 80	40 - 70	<20
	31-01-13	70^0 12.1’	05^0 22.8’	40 - 160	60 - 100	2 - 100
Carving	30-01-13	70^0 33.5’	08^0 03.1’	80-100	100	Level Ice
Ramming	03-02-13	70^0 13.6’	05^0 28.4’	120-160	100	20 - 100
	04-02-13	70^0 13.7’	05^0 30.0’	100 - 160	100	20 - 100

7. Measurement Results

Ice loading on the ship hull is very stochastic in nature. The resulting acceleration time signal shown in Figure 4 measured during ice breaking through pack ice is indicative of this stochastic loading mechanism. Dominant lateral (+Y) vibration peaks can also be seen and were prevalent throughout ice navigation.

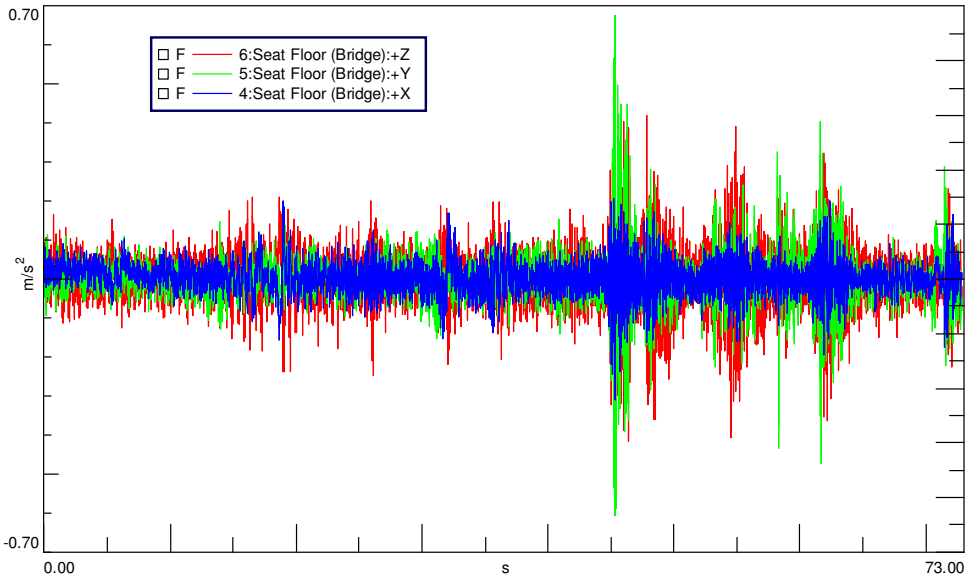

Figure 4 - Acceleration time signal measured in pack ice

The crest factors for the un-weighted acceleration time signals are presented in Table 4. Crest factors in ice range from 5 to 10 which provide an indication of the impulsive ice loading. Crest factors in open water are around 3. ISO 2631-1:1997 specifies a crest factor limit of 9 for using r.m.s as an indicator of human comfort however this applies to data which has been frequency weighted. It is noted by Griffin (1990) that measurements are frequently reported without crest factors, but that it is highly desirable to provide some quantitative description of the way the vibration varied about the reported r.m.s. value.

Table 4 - Crest factors of ice and open water navigation

		Crest Factor		
		X	Y	Z
Pack Ice	Run 1262	7.59	**9.85**	7.99
Carving	Run 1233	6.39	6.76	5.79
Ramming	Run 1321	5.31	5.44	5.63
Engines	Run 1402	3.42	3.83	2.82
Open Water - Rough Weather	Run 1542	3.18	3.12	3.66
Open Water - Calm Weather	Run 30	3.32	3.48	0.34

The results of the overall frequency-weighted vibration values are presented in Table 5. The number of runs in each category was selected to represent the excitation mechanism while conditions remained relatively constant. The maximum r.m.s value of 2.35 mm/s was recorded in the lateral (+Y) direction during ramming, with an average ice thickness of 120 – 160 cm. Large maximum and average r.m.s. values in the lateral (+Y) direction were recorded for pack ice, carving and ramming.

These high lateral velocities are due to lateral ice impacts as well as ice impacts on the propeller blades. Ice navigation in the Antarctic involves following leads in the ice, which require constant port and starboard manoeuvring. These manoeuvres create lateral ice deflections of the ship's hull. Glancing impacts with large ice floes are also capable of changing the heading of the ship, and cause lateral impacts on the ship's bow. Turning in ice may also expose the propellers which creates more propeller induced ice loading.

Table 5 - Overall frequency-weighted r.m.s. values for ice and open water navigation

	Maximum r.m.s. values (mm/s)			Average r.m.s. values (mm/s)			Standard Deviation (mm/s)		
	X	Y	Z	X	Y	Z	X	Y	Z
Pack Ice 83 Runs	0.786	**1.552**	1.059	0.336	0.496	**0.564**	0.134	0.237	0.168
Carving 37 Runs	**1.991**	1.975	1.235	0.993	**1.079**	0.834	0.458	0.494	0.234
Ramming 41 Runs	1.881	**2.348**	1.189	0.608	**0.948**	0.699	0.443	0.541	0.212
Engines 10 Runs	0.045	0.057	**0.237**	0.042	0.055	**0.229**	0.002	0.002	0.004
Open Water - Rough Weather 21 Runs	0.725	0.747	**1.334**	0.420	0.446	**0.653**	0.188	0.138	0.280
Open Water - Calm Weather 10 Runs	0.199	0.328	**0.499**	0.177	0.296	**0.479**	0.014	0.019	0.020

The large standard deviations during ice navigation are indicative of the stochastic ice loading mechanism. During ice navigation the S.A. Agulhas II operates in Ice Mode, which allows maximum power from all four diesel engines to drive the two electric motors turning the propeller shafts. This increased engine power adds to the vertical (+Z) vibration measured during ice breaking.

The maximum r.m.s. value in ice exceeds the maximum r.m.s. value in open water during rough weather by a factor of 1.76 and in calm weather by a factor of 4.7. Vibration levels during carving and ramming in the longitudinal (+X) and lateral (+Y) directions exceed the vibration levels in open water during rough weather by a factor of between 2.5 and 3.1.

The largest maximum and average r.m.s. values for open water occur in the vertical (+Z) direction. This is as a result of the waves impacting the bow (bow slamming) as the ship moves in and out of phase with the swell. The dominant engine vibration is also in the vertical (+Z) direction as expected.

Frequency Analysis

Averaged frequency spectra with r.m.s. amplitude scaling are plotted in Figure 5 to investigate the frequency content of the different excitation mechanisms.

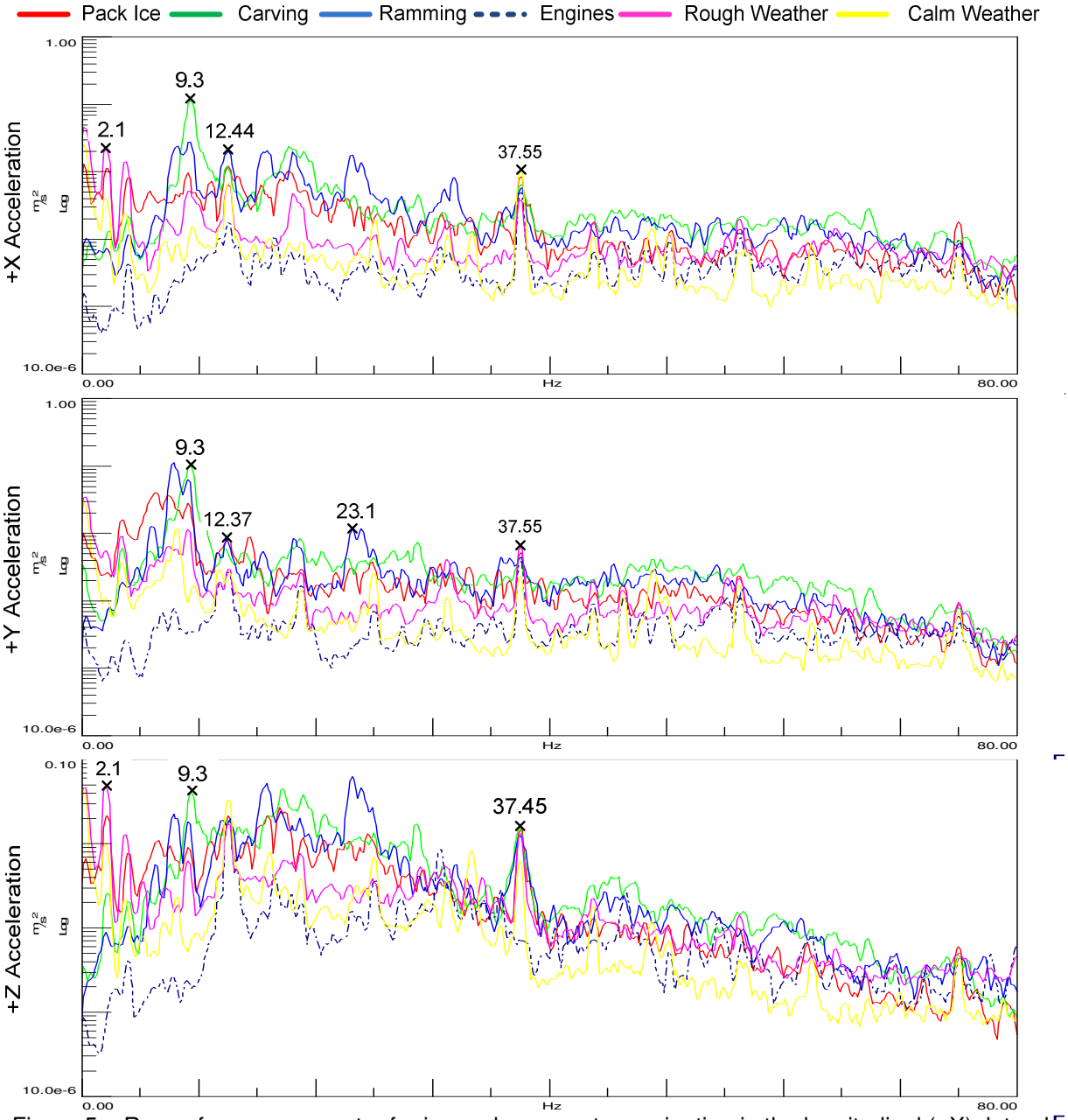

Figure 5 – R.m.s. frequency spectra for ice and open water navigation in the longitudinal (+X), lateral (+Y) and vertical (+Z) directions plotted on a log scale.

From the averaged frequency spectra it can be seen that there is a lot of frequency content in the lateral (+Y) direction between roughly 6 Hz and 9.5 Hz for all ice navigation. During ice navigation the propeller shaft rotates at 140 r.p.m. which generates vibration at 2.3 Hz, with a blade-pass frequency of the four bladed propeller at 9.3 Hz. This propeller vibration is transmitted to the bridge in the lateral (+Y) direction during all ice navigation and is also transmitted in the longitudinal (+X) direction during carving.

The majority of the frequency content between 12 Hz and 35 Hz for all excitation mechanisms is in the vertical (+Z) direction. By comparison to the frequency spectrum of the engines alone, this spectrum is seen to be as a result of the engine excitation, which increases in amplitude when in Ice Mode. The vibration of the firing order of the six cylinder diesel engines can be seen throughout all frequency spectra at 37.45 Hz. The rotational speed of 750 r.p.m. of the diesel engines can also be seen by the recurring peak at 12.44 Hz.

The spectra also reveal that the majority of the frequency content lies below 30 Hz. The amplitude of the frequency content below 25 Hz for ice navigation is significantly higher than that during open water in rough weather. Open water navigation in rough weather is dominated by frequency content bellow 4 Hz and has a peak at 2.1 Hz. This matches the first bending mode of the ship which occurs at 2.09 Hz, as reported by STX Finland's modal analysis (STX Europe, 2010).

Analysis According to ISO 6954:2000

The habitability in the Bridge was evaluated at the base of the Captain's chair according to the overall frequency-weighted r.m.s velocity limits given as guidelines in ISO 6954:2000. The highest frequency-weighted r.m.s value 0f 2.35 mm/s in the lateral (+Y) direction measured during ramming (Table 5) is below the 4 mm/s lower limit. Adverse comments during all ice and open water navigation are therefore not probable.

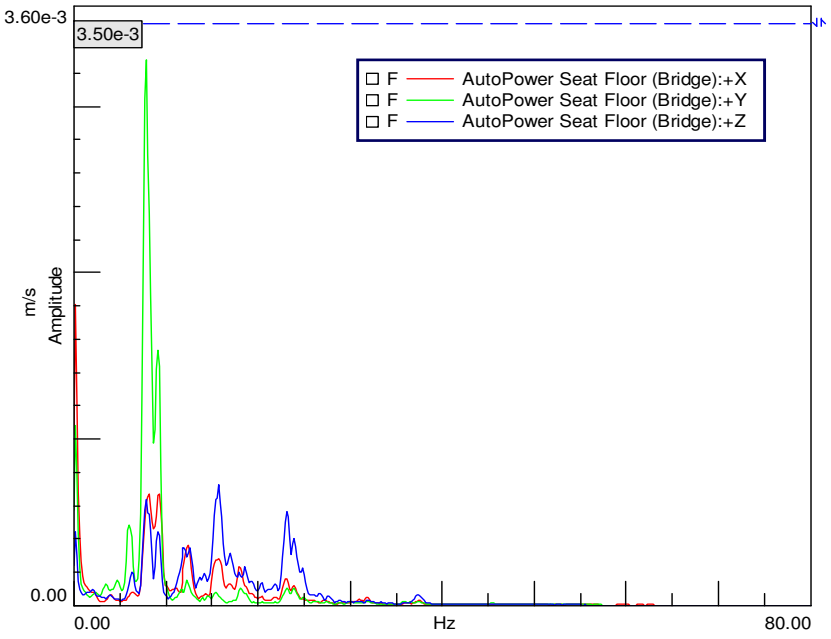

Figure 5 – Peak FFT of longitudinal (+X), lateral (+Y) and vertical (+Z) vibration measured during ramming

Analysis According to DNV Comfort Class

The largest vibration velocity peak for single frequencies components between 5 and 100 Hz was 3.3 mm/s measured in the lateral (+Y) direction during ramming. This is below the constant velocity limit of 3.5 mm/s for the navigation Bridge on cargo ships as seen in Figure 6.

8. Discussion

The maximum vibration levels measured in the bridge for all the excitation mechanisms were below the habitability limits of both the ISO 6954:2000 and the DNV Comfort Class notation. Vibration conditions experienced on the Bridge are in the zone in which adverse comments are not probable.

The consequence of low vibration levels on the Bridge is low response feedback from the vessel. Full scale measurements conducted by Heggelund *et al*. (2010) assessed fatigue damage accumulation on an LNG carrier. The highest fatigue damage was obtained in rough seas, sailing into or with the swell. It was found that speed reduction in rough seas acted to reduce fatigue damage below that predicted at constant service speed (ISSC Committee II.2, 2006).

Seamanship as applied through weather routing avoidance, voluntary and involuntary speed reduction, and changes in heading relative to the swell direction is revealed in literature to be an important factor acting to mitigate wave induced vibrations (ISSC Committee II.2, 2006). Further investigation into the effects of seamanship and ice navigation on ice induced vibration is proposed by the authors and will be the topic of subsequent research. The justification and further development of a real time monitoring system, such as the integrated decision support system proposed by Nyseth *et al*. (2013) for polar vessels operating in the Antarctic will also be investigated. Improving safety by understanding the response feedback of the vessel, and allowing the officers to make decisions based on real time data is the ultimate goal.

9. Conclusions

Full scale data provides a valuable source of information in understanding the dynamic responses of a vessel. Measurements performed on the S.A. Agulhas II in Antarctica allow investigation into the effects of excitation mechanisms such as waves, ice, machinery and propellers and how this relates to human comfort.

Measurements performed in ice revealed the stochastic and impulsive nature of ice loading. Lateral (+Y) vibration was dominant during ice navigation, and the maximum r.m.s value of 2.35 mm/s was recorded in the lateral (+Y) direction during ramming. The reason for these lateral vibrations in ice is due to glancing lateral ice impacts as well as ice induced loading on the propellers. Maximum vibration amplitudes measured during ice navigation was also found to exceed open water navigation in rough weather by a factor of 1.76 and in calm weather by a factor of 4.7.

Frequency analysis further investigated the causes of vibration during ice and open water navigation. The blade pass frequency of the four blade propeller at 9.3 Hz was found to transmit vibration in the lateral direction during ice navigation. Significant vibration amplitude in the lateral direction was observed in this bandwidth during carving and ramming. The vibration generated by the engines firing

order was also identified at 37.45 Hz in all frequency spectra. Open water spectra were dominated by low frequency content below 4 Hz. A peak occurred at 2.1 Hz which matches the first bending mode of the ship.

Whole-body vibration comfort measurements conducted on the Bridge of the S.A. Agulhas II in Antarctica revealed low vibration levels at which adverse comments are not probable. These full scale measurements aim to contribute scientific data to further the understanding of dynamic ship interactions. Further investigation into human response to measured vibration amplitude and frequency will provide insight into the feedback response of the vessel. The effect of seamanship and ice navigation on ice induced vibration can then be determined, and will allow polar vessels to operate more efficiently and safely.

10. Acknowledgements

The authors would like to thank The Department of Environmental Affairs, South Africa and the S.A. Agulhas II represented by Captain Syndercombe for their hospitality and allowing us to perform measurement on their ship. Furthermore we would like to thank all the other project partners namely STX Finland, Aalto University, the University of Oulu, Aker Arctic, Rolls-Royce, DNV and Wärtsilä. We would also like to thank the National Research Foundation and Department of Science and Technology under the South African National Antarctic Programme for project funding.

11. References

Asmussen I, Menzel W, Mumm H (2001) Ship Vibration. Germanischer Lloyd Technology, Hamburg.

Biot M, De Lorenzo F (2007) Noise and Vibrations on Board Cruise Ships: Are New Standards Effective? 2nd International Conference on Marine Research and Transportation ICMRT '07, June 28-30, Ischia (Naples), Italy.

Det Norske Veritas (2003) Comfort Class. Rules for Classification of Ships, Special Service and Type Additional Class, Høvik, Norway.

Griffin MJ (1990) Handbook of Human Vibration. Elsevier Academic Press, London.

Haas C (2013) Arctic Sea Ice – Where are we Headed? Proceedings of the 22nd International Conference on Port and Ocean Engineering under Arctic Conditions, Espoo, Finland.

British Standards Institution and International Organization for Standardization (1997) Mechanical vibration and shock - evaluation of human exposure to whole-body vibration - Part 1: General requirements, International Standard, BS ISO 2631-1.

International Organization for Standardization (2000) Mechanical vibration and shock – Guidelines for the measurement, reporting and evaluation of vibration with regard to habitability on passenger and merchant ships, ISO 6954:2000(E).

International Ship and Offshore Structures Congress (2012) ISSC Report of Technical Comitee II.2: Dynamic Response. Proceeding of the 18th International Ship and Offshore Structures Congress. Schiffbautechnische Gesellschaft, Hamburg.

Kujala P (2011) Full-scale measurements onboard NB1369 PSRV. Aalto University, School of Engineering, Marine Technology, 18th October 2011, Helsinki, Finland.

Nyseth H, Frederking R, Sand B (2013) Evaluation of Global Ice Load Impacts Based on Real-Time Monitoring of Ship Motions. Proceedings of the 22nd International Conference on Port and Ocean Engineering under Arctic Conditions, Espoo, Finland.

Onstott RG (2004) Chapter 19. Antarctic Sea Ice and Icebergs. Synthetic aperture Radar Marine User's Manual. Washington, DC.

Savreux K, Crouzet S, Andreau C (2007) Overview of Comfort Criteria for Vibration Assessment Proposed by ISO 6954 and Different Classification Societies.

STX Europe (2010) NB-1369: Natural Modes. FINNSAP. Oslo, Norway.

Appendix B

Accelerometer Calibration Values

Table B.1: Accelerometer calibration values and dates.

Point	Type	Model No	SN	Calibration ($mV/m/s^2$)	Date Calibrated
1	ICP	333B32	49500	10.31	31/10/2012
2	ICP	333B32	49498	10.25	31/10/2012
3	DC	3711B1110G	LW6310	20.17	14/9/2012
5	ICP	333B32	50900	10.43	31/10/2012
6	DC	3711B1110G	LW6301	20.25	14/9/2012
7	DC	3711B1110G	LW6302	20.24	14/9/2012
8	DC	3711B1110G	LW6304	20.22	14/9/2012
9	ICP	333B32	49496	9.7	31/10/2012
11	DC	3711B1110G	LW6308	20.20	14/9/2012
12	DC	3711B1110G	LW6300	20.33	14/9/2012
13	DC	3711B1110G	LW6309	20.00	14/9/2012
15	ICP	333B32	49493	9.96	31/10/2012
16	Seismic	393B12	23820	1098	21/11/2013
17	Seismic	393B12	12298	1088	21/11/2013
18	Seismic	393B12	12299	1074	21/11/2013
19	ICP	333B32	49495	10.05	31/10/2012
20	ICP	333B32	49501	10.44	31/10/2012
21	Tri -axial	356B40	26977	10.52	21/11/2013
22	Tri -axial	356B40	26977	10.64	21/11/2013
23	Tri -axial	356B40	26977	10.55	21/11/2013
26	DC	3711B1110G	LW6300	20.33	14/9/2012
33	DC	3711B1110G	LW6305	20.14	14/9/2012
34	DC	3711B1110G	LW6303	20.21	14/9/2012
35	ICP	333B32	49502	10.36	31/10/2012
36	ICP	333B32	49499	10.32	31/10/2012

Appendix C

Matlab Code

```
% antarcticaData2014.m
% Antarctica 2014
% Updated 14/05/2014
clear all
clc

tic
fs = 2048;          % Sample frequency in Hz
dfs = 256;          % Decimated sample frequency in Hz
fileTime = 300;     % recording duration in s
rmsTime = 300;      % rms averaging time
g = 9.81;           % Gravity
numChannels = 31;   % Number of Channels

% Save current working directory
workDir = pwd;

[dataRms,peakAcceleration,driftMatrix,timeVector] = matFiles2statistics(
    fs,fileTime,rmsTime,workDir,g,numChannels,dfs);
toc
```

```
% matFiles2statistics.m
% Antarctica 2014
% Structural Vibration

function [dataRms,peakAcceleration,driftMatrix,timeVector] =
    matFiles2statistics(fs,fileTime,rmsTime,workDir,g,numChannels,dfs)

%Folder directory on external hard drive
folderDir(1,:) = 'E:\Antarctica 2013-2014\LMS Data\20131203_230740_Run';
cutLengthVec(1) = 286720;
folderDir(2,:) = 'E:\Antarctica 2013-2014\LMS Data\20131208_093858_Run';
cutLengthVec(2) = 126976;
folderDir(3,:) = 'E:\Antarctica 2013-2014\LMS Data\20131210_162541_Run';
cutLengthVec(3) = 528385;
folderDir(4,:) = 'E:\Antarctica 2013-2014\LMS Data\20131225_163129_Run';
cutLengthVec(4) = 430081;
folderDir(5,:) = 'E:\Antarctica 2013-2014\LMS Data\20131231_191553_Run';
cutLengthVec(5) = 505857;
folderDir(6,:) = 'E:\Antarctica 2013-2014\LMS Data\20140103_143027_Run';
```

```
cutLengthVec(6) = 559105;
folderDir(7,:) = 'E:\Antarctica 2013-2014\LMS Data\20140115_132922_Run';
cutLengthVec(7) = 77824;
folderDir(8,:) = 'E:\Antarctica 2013-2014\LMS Data\20140118_192742_Run';
cutLengthVec(8) = 282624;
folderDir(9,:) = 'E:\Antarctica 2013-2014\LMS Data\20140123_131129_Run';
cutLengthVec(9) = 432129;
folderDir(10,:) = 'E:\Antarctica 2013-2014\LMS Data\20140130_124824_Run';
cutLengthVec(10) = 194560;
folderDir(11,:) = 'E:\Antarctica 2013-2014\LMS Data\20140201_160904_Run';
cutLengthVec(11) = 114688;

directory = folderDir;
sdir=size(directory);
count=0;

for i=1:sdir(1)

        % Chooses the correct channel setup from matFiles2variables due
            to lms
        % harware adjustments during the voyage
        if i==1
                channelSetup=1;
        elseif i==2
                channelSetup=2;
        else
                channelSetup=3;
        end

        % Change current working directory
        cd(directory(i,:))
        filePostfix='.mat';
        dataPath='.';

        % List the files in the directory
        d=dir(dataPath);
        db={};
        ind=1;

        % Select .mat files only
        for n=1:length(d)
                if length(d(n).name)>3 && strcmp(d(n).name(end-3:end),
                    filePostfix)
                        db{ind}=d(n).name;
                        ind=ind+1;
                end
        end

        nx=length(db);

        for t=1:nx-1
                %% Build data matrix and time vector

                cd(workDir)
                [dataMatA,timeStartA,timeEndA] = matFiles2variables(
                    channelSetup,directory,i,fileTime,t);
        cd(workDir)
        [dataMatB,timeStartB,timeEndB] = matFiles2variables(channelSetup,
```

```
            directory,i,fileTime,t+1);
74              dataMatC = [dataMatA ; dataMatB];
75          cutLength = cutLengthVec(i);
76          dataMat = dataMatC(cutLength+1:cutLength+614400,:);
77          clear dataMatA; clear dataMatB; clear dataMatC;
78
79          timeA = linspace(timeStartA,timeEndA,614400);
80          timeB = linspace(timeStartB,timeEndB,614400);
81          totalTime = [timeA timeB];
82          timeStart = totalTime(cutLength+1);
83          timeEnd = totalTime(cutLength+614400);
84          clear totalTime; clear timeA;clear TimeB
85
86          %% Drift Calculation
87          driftMat(t,:) = mean(dataMat);
88
89                  %% Zero DC offset
90          dataOffset = detrend(dataMat,'constant');
91          clear dataMat;
92
93                  %% Integrate to velocity in (mm/s)
94                  dataDouble = (double(dataOffset))*g*1000;  % Convert to (
                        mm/s^2)
95          dataSize = size(dataDouble);
96          for w = 1:dataSize(2)
97              dataIntegrate(:,w) = cumtrapz(dataDouble(:,w))./fs;
98          end
99          clear dataDouble; clear dataOffset;
100
101         %% Decimate data to 256Hz with low pass filter
102                 R = fs/dfs; % Resamples at 1/R times the original length
103                 for e = 1:dataSize(2)
104             data(:,e) = decimate(dataIntegrate(:,e),R);
105         end
106                 clear dataIntegrate;
107         %% High pass filter
108         cd(workDir)
109         Hd1 = hpFilterCheby800;          % Call Chebyshev filter Fc=1,
                Order=800
110         Hd2 = hpFilterCheby1400Fc16;     % Call Chebyshev filter Fc=1.6,
                Order=1400
111
112         icpIndex = [1 2 4 8 13 14 15 16 17 18 19 20 21 30 31]; % Index
                ICP channels
113         dcIndex = [3 5 6 7 9 10 11 28 29];                     % Index DC
                 channels
114         icpMatrix = data(:,icpIndex);    % Build ICP matrix
115         dcMatrix = data(:,dcIndex);      % Build DC matrix
116
117         hp1 = filter(Hd1,icpMatrix);     % High pass filter ICP matrix
118         hp2 = filter(Hd2,dcMatrix);      % High pass filter DC matrix
119
120         i1=hp1(:,1);     % Point1 ICP stern thruster Stb(+Z)
121         i2=hp1(:,2);     % Point2 ICP stern thruster Port(+Z)
122         i3=hp2(:,1);     % Point3 DC central measurement Stb(-Z)
123         i4=hp1(:,3);     % Point5 ICP central measurement Centre(+Y)
124         i5=hp2(:,2);     % Point6 DC central measurement Port(-Z)
125         i6=hp2(:,3);     % Point7 DC cargo hold 3 Stb(-Z)
```

```
126         i7=hp2(:,4);     % Point8 DC cargo hold 3 Port(-Z)
127         i8=hp1(:,4);     % Point9 ICP cargo hold 3 Stb(+Z)
128         i9=hp2(:,5);     % Point11 DC bow Stb(+Z)
129         i10=hp2(:,6);    % Point12 DC bow Centre(+Y)
130         i11=hp2(:,7);    % Point13 DC bow Port(+Z)
131         i12=hp1(:,5);    % Point15 ICP deck 8 Port(+Z)
132         i13=hp1(:,6);    % Point16 ICP bridge Stb(+X)
133         i14=hp1(:,7);    % Point17 ICP bridge Stb(+Y)
134         i15=hp1(:,8);    % Point18 ICP bridge Stb(+Z)
135         i16=hp1(:,9);    % Point19 ICP bridge Port(+Z)
136         i17=hp1(:,10);   % Point20 ICP cargo hold 3 Port(+Z)
137         i18=hp1(:,11);   % Point21 ICP central measurement Centre(+X)
138         i19=hp1(:,12);   % Point22 ICP central measurement Centre(+Y)
139         i20=hp1(:,13);   % Point23 ICP central measurement Centre(+Z)
140         i21=hp2(:,8);    % Point33 DC starboard steering gear Stb(+Z)
141         i22=hp2(:,9);    % Point34 DC starboard steering gear Stb(-Y)
142         i23=hp1(:,14);   % Point35 ICP starboard steering gear Stb(+X)
143         i24=hp1(:,15);   % Point36 ICP port steering gear Port(+Z)
144         hp = [i1 i2 i3 i4 i5 i6 i7 i8 i9 i10 i11 i12 i13 i14 i15 i16 i17
                i18 i19 i20 i21 i22 i23 i24]; % Compile full vibration data
                matrix
145         clear i1;clear i2;clear i3;clear i4;clear i5;clear i6;clear i7;
                clear i8;clear i9;clear i10;clear i11;clear i12;clear i13;
                clear i14;clear i15;clear i16;clear i17;clear i18;clear i19;
                clear i20;clear i21;clear i22;clear i23;clear i24;
146         clear hp1; clear hp2;clear Hd1;clear Hd2; clear dcMatrix; clear
                icpMatrix
147
148 %% Save filtered data
149         cd('C:\Users\15632555\Desktop\Masters\Keith_Soal_Masters_Thesis\
                figs\Standards\Structural Vibration\PSD\bridge')
150         A1 = datestr(timeStart,'yyyymmdd');
151         [y,m,d,h,mi,s] = datevec(timeStart);
152         if round(s)-s > 0
153             mi = mi+1;
154         end
155         h = num2str(h);
156         mi = num2str(mi);
157         sample = strcat(A1,h,mi);
158         save(sample,'hp')
159         % Change current working directory
160         cd(directory(i,:))
161         filePostfix='.mat';
162         dataPath='.';
163         clear y; clear m; clear d; clear h; clear mi; clear s;clear
                sample; clear A1
164
165                 %% Variable rms calculator (mm/s)
166                 for h = 1:fileTime/rmsTime
167
168                         vect = (h-1)*(fs/R)*rmsTime+1:(h)*(fs/R)*rmsTime;
169                         varRms(t,:) = (((trapz(hp(vect,:).^2)./dfs)./
                                rmsTime).^0.5);
170
171         end
172
173         %% Peak Acceleration (mm/s)
174         peakAcc(t,:) = max(abs(hp));
```

```
175
176                 %% Create time vector
177                 timeVec(t,1)=(timeStart+timeEnd)/2;
178                 disp(datestr(timeStart))
179
180         end
181
182         % Build data matrix
183         dataRms(1+count:count+nx-1,:)=varRms;
184     peakAcceleration(1+count:count+nx-1,:)=peakAcc;
185     driftMatrix(1+count:count+nx-1,:)=driftMat;
186         timeVector(1+count:count+nx-1,1)=timeVec;
187
188     clear dataIntegrate
189     clear data
190     clear hp
191
192     %% Incremental file saving
193     fileName = ['A';'B';'C';'D';'E';'F';'G';'H';'I';'J';'K'];
194     save(fileName(i),'varRms','peakAcc','timeVec')
195         clear varRms
196     clear peakAcc
197     clear driftMat
198         clear timeVec
199         count=count+(nx-1);
200         clear nx;
201
202 end
203
204 end
```

```
1  % matFiles2statistics.m
2  % Antarctica 2014
3  % Human Vibration
4
5  function [dataRmsA,dataVDVA,peakAccelerationA,timeVector] =
       matFiles2statistics(fs,fileTime,rmsTime,workDir,g,numChannels)
6
7  % % Folder directory on external hard drive
8  folderDir(1,:) = 'E:\Antarctica 2013-2014\LMS Data\20131203_230740_Run';
9  cutLengthVec(1) = 286720;
10 folderDir(2,:) = 'E:\Antarctica 2013-2014\LMS Data\20131208_093858_Run';
11 cutLengthVec(2) = 126976;
12 folderDir(3,:) = 'E:\Antarctica 2013-2014\LMS Data\20131210_162541_Run';
13 cutLengthVec(3) = 528385;
14 folderDir(4,:) = 'E:\Antarctica 2013-2014\LMS Data\20131225_163129_Run';
15 cutLengthVec(4) = 430081;
16 folderDir(5,:) = 'E:\Antarctica 2013-2014\LMS Data\20131231_191553_Run';
17 cutLengthVec(5) = 505857;
18 folderDir(6,:) = 'E:\Antarctica 2013-2014\LMS Data\20140103_143027_Run';
19 cutLengthVec(6) = 559105;
20 folderDir(7,:) = 'E:\Antarctica 2013-2014\LMS Data\20140115_132922_Run';
21 cutLengthVec(7) = 77824;
22 folderDir(8,:) = 'E:\Antarctica 2013-2014\LMS Data\20140118_192742_Run';
23 cutLengthVec(8) = 282624;
24 folderDir(9,:) = 'E:\Antarctica 2013-2014\LMS Data\20140123_131129_Run';
25 cutLengthVec(9) = 432129;
26 folderDir(10,:) = 'E:\Antarctica 2013-2014\LMS Data\20140130_124824_Run';
```

```
27 cutLengthVec(10) = 194560;
28 folderDir(11,:) = 'E:\Antarctica 2013-2014\LMS Data\20140201_160904_Run';
29 cutLengthVec(11) = 114688;
30
31 directory = folderDir;
32 sdir=size(directory);
33 count=0;
34
35 for i=1:sdir(1)
36
37     % Chooses the correct channel setup from matFiles2variables due to
       lms
38         % harware adjustments during the voyage
39         if i==1
40                 channelSetup=1;
41         elseif i==2
42                 channelSetup=2;
43         else
44                 channelSetup=3;
45         end
46
47         % Change current working directory
48         cd(directory(i,:))
49         filePostfix='.mat';
50         dataPath='.';
51
52         % List the files in the directory
53         d=dir(dataPath);
54         db={};
55         ind=1;
56
57         % Select .mat files only
58         for n=1:length(d)
59                 if length(d(n).name)>3 && strcmp(d(n).name(end-3:end),
                    filePostfix)
60                     db{ind}=d(n).name;
61                     ind=ind+1;
62                 end
63         end
64
65         nx=length(db);
66
67         for t=1:nx-1
68                 %% Build data matrix and time vector
69                 cd(workDir)
70                 [dataMatA,timeStartA,timeEndA] = matFiles2variables(
                        channelSetup,directory,i,fileTime,t);
71         cd(workDir)
72         [dataMatB,timeStartB,timeEndB] = matFiles2variables(channelSetup,
               directory,i,fileTime,t+1);
73                 dataMatC = [dataMatA ; dataMatB];
74         cutLength = cutLengthVec(i); % 286720;
75         dataMat_old = dataMatC(cutLength+1:cutLength+614400,:);
76         dataMat = dataMat_old(:,[13 14 15 16 17 19 20 21]);
77         clear dataMatA; clear dataMatB; clear dataMatC;clear dataMat_old
78
79         timeA = linspace(timeStartA,timeEndA,614400);
80         timeB = linspace(timeStartB,timeEndB,614400);
```

```
81          totalTime = [timeA timeB];
82          timeStart = totalTime(cutLength+1);
83          timeEnd = totalTime(cutLength+614400);
84          clear totalTime; clear timeA;clear TimeB
85
86                  %% Zero DC offset
87          dataOffset = detrend(dataMat,'constant');
88                  clear dataMat
89
90          %% Acceleration
91          dataMatA = double(dataOffset)*g;
92
93          %% Human Weight Data in Acceleration
94          cd(workDir)
95          [A13, exa] = FrequencyWeightingTimeDomain(dataMatA(:,1), fs, '
                Wk_IS');
96          [A14, eya] = FrequencyWeightingTimeDomain(dataMatA(:,2), fs, '
                Wd_IS');
97          [A15, eza] = FrequencyWeightingTimeDomain(dataMatA(:,3), fs, '
                Wd_IS');
98          [A16, exa] = FrequencyWeightingTimeDomain(dataMatA(:,4), fs, '
                Wk_IS');
99          [A17, eya] = FrequencyWeightingTimeDomain(dataMatA(:,5), fs, '
                Wk_IS');
100         [A18, eza] = FrequencyWeightingTimeDomain(dataMatA(:,6), fs, '
                Wd_IS');
101         [A19, exa] = FrequencyWeightingTimeDomain(dataMatA(:,7), fs, '
                Wd_IS');
102         [A20, eya] = FrequencyWeightingTimeDomain(dataMatA(:,8), fs, '
                Wk_IS');
103
104         Data_A = [A13 A14 A15 A16 A17 A18 A19 A20];
105              clear dataMatA;clear A13;clear A14;clear A15;clear A16;clear
                    A17;clear A18;clear A19;clear A20;clear Y;clear Z;clear ex
                    ;clear ey;clear ez;
106
107         %% Variable rms calculator (mm/s)
108                 for h = 1:fileTime/rmsTime
109
110                         vect = (h-1)*(fs)*rmsTime+1:(h)*(fs)*rmsTime;
111                         varRmsA(t,:) = (((trapz(Data_A(vect,:).^2)./fs)./
                                rmsTime).^0.5);
112
113         end
114
115                 %% VDV
116                 for j = 1:fileTime/rmsTime
117
118                         vect = (j-1)*(fs)*rmsTime+1:(j)*(fs)*rmsTime;
119                         VDVA(t,:) = ((trapz(Data_A(vect,:).^4)./fs)
                                .^0.25);
120
121         end
122
123 %% Peak Acceleration (mm/s)
124         peakAccA(t,:) = max(abs(Data_A));
125
126                 %% Create time vector
```

```
                timeVec(t,1)=(timeStart+timeEnd)/2;
                disp(datestr(timeStart))

        end
        % Build data matrix
        dataRmsA(1+count:count+nx-1,:)=varRmsA;
    dataVDVA(1+count:count+nx-1,:)=VDVA;
    peakAccelerationA(1+count:count+nx-1,:)=peakAccA;
        timeVector(1+count:count+nx-1,1)=timeVec;

    clear dataIntegrate;clear data;clear Data_A;clear varRmsA;clear VDVA;
        clear peakAccA;clear driftMat;clear timeVec
        count=count+(nx-1);
        clear nx;

end

end
```

```
% Antarctica 2014
% Function reads matlab files, builds the channel setup matrix and time
% vector
function [dataMat,timeStart,timeEnd] = matFiles2variables(channelSetup,
    directory,i,fileTime,t)

% Change current working directory
cd(directory(i,:))

% Logic operator allows the function to run without inputs
filePostfix='.mat';
dataPath='.';

% List the files in the directory
d=dir(dataPath);
db={};
ind=1;

% Select .mat files only
for i=1:length(d)
        if length(d(i).name)>3 && strcmp(d(i).name(end-3:end),
            filePostfix)
                db{ind}=d(i).name;
                ind=ind+1;
        end
end

nx=length(db);
data = open(db{t});

% Create time vector
datemat = data.n_Point1__Z.function_record.
    TL_export_properties_annotation.absolute_time;
dateCorrection = 1;
timeStart = datenum(datemat,'yyyy-mm-dd HH:MM:SS');
timeEnd = (timeStart + fileTime/60/60/24.000130177250274);

%% Channel setup 1 Start:2013 12 03 (31 Channels)
if channelSetup == 1
```

```
37          % Stern thruster
38          Point1 = data.n_Point1__Z.y_values.values';
39          Point2 = data.n_Point2__Z.y_values.values';
40          % Central measurement unit
41          Point3 = data.n_Point3__Z.y_values.values';
42          Point5 = data.n_Point5__Y.y_values.values';
43          Point6 = data.n_Point6__Z.y_values.values';
44          % Cargo hold 3
45          Point7 = data.n_Point7__Z.y_values.values';
46          Point8 = data.n0_Point8__Z.y_values.values';
47          Point9 = data.n1_Point9__Z.y_values.values';
48          % Bow
49          Point11 = data.n3_Point11__Z.y_values.values';
50          Point12 = data.n4_Point12__Y.y_values.values';
51          Point13 = data.n5_Point13__Z.y_values.values';
52          % Dummy Channel
53          Point14 = zeros(length(Point1),1);
54          % Superstructure
55          Point15 = data.n7_Point15__Z.y_values.values';
56          Point16 = data.n8_Point16__X.y_values.values';
57          Point17 = data.n9_Point17__Y.y_values.values';
58          Point18 = data.n0_Point18__Z.y_values.values';
59          Point19 = data.n1_Point19__Z.y_values.values';
60          % Cargo hold 3
61          Point20 = data.n2_Point20__Z.y_values.values';
62          % Central measurement unit
63          Point21 = data.n3_Point21__X.y_values.values';
64          Point22 = data.n4_Point22__Y.y_values.values';
65          Point23 = data.n5_Point23__Z.y_values.values';
66          % Strain Measurments -- not Calibrated
67          Point27 = data.n9_Point27.y_values.values';
68          Point28 = data.n0_Point28.y_values.values';
69          Point29 = data.n1_Point29.y_values.values';
70          Point30 = data.n2_Point30.y_values.values';
71          Point31 = data.n3_Point31.y_values.values';
72          Point32 = data.n4_Point32.y_values.values';
73          % Stearing gear room
74          Point33 = data.n5_Point33__Z.y_values.values';
75          Point34 = data.n6_Point34__Y.y_values.values';
76          Point35 = data.n7_Point35__X.y_values.values';
77          Point36 = data.n8_Point36__Z.y_values.values';
78
79  dataMat = [Point1 Point2 Point3 Point5 Point6 Point7 Point8 Point9 ...
80                  Point11 Point12 Point13 Point14 Point15 Point16 Point17
                        Point18 Point19...
81                  Point20 Point21 Point22 Point23 Point27 Point28 Point29
                        Point30...
82                  Point31 Point32 Point33 Point34 Point35 Point36];
83
84  end
85
86  %% Channel setup 2 Start:2013 12 08 (31 Channels) *Change made to Point
        12
87
88  if channelSetup == 2
89          % Stern thruster
90          Point1 = data.n_Point1__Z.y_values.values'; % C1
91          Point2 = data.n_Point2__Z.y_values.values'; % C2
```

```
92          % Central measurement unit
93          Point3 = data.n_Point3__Z.y_values.values'; % C3
94          Point5 = data.n_Point5__Y.y_values.values'; % C4
95          Point6 = data.n_Point6__Z.y_values.values'; % C5
96          % Cargo hold 3
97          Point7 = data.n_Point7__Z.y_values.values'; % C6
98          Point8 = data.n0_Point8__Z.y_values.values'; % C7
99          Point9 = data.n1_Point9__Z.y_values.values'; % C8
100         % Bow
101         Point11 = data.n3_Point11__Z.y_values.values'; % C9
102         Point12 = data.n6_Point12__Y.y_values.values'; % C10
103         Point13 = data.n5_Point13__Z.y_values.values'; % C11
104         % Dummy Channel
105         Point14 = zeros(length(Point1),1); % C12
106         % Superstructure
107         Point15 = data.n7_Point15__Z.y_values.values'; % C13
108         Point16 = data.n8_Point16__X.y_values.values'; % C14
109         Point17 = data.n9_Point17__Y.y_values.values'; % C15
110         Point18 = data.n0_Point18__Z.y_values.values'; % C16
111         Point19 = data.n1_Point19__Z.y_values.values'; % C17
112         % Cargo hold 3
113         Point20 = data.n2_Point20__Z.y_values.values'; % C18
114         % Central measurement unit
115         Point21 = data.n3_Point21__X.y_values.values'; % C19
116         Point22 = data.n4_Point22__Y.y_values.values'; % C20
117         Point23 = data.n5_Point23__Z.y_values.values'; % C21
118         % Strain Measurments -- not Calibrated
119         Point27 = data.n9_Point27.y_values.values'; % C22
120         Point28 = data.n0_Point28.y_values.values'; % C23
121         Point29 = data.n1_Point29.y_values.values'; % C24
122         Point30 = data.n2_Point30.y_values.values'; % C25
123         Point31 = data.n3_Point31.y_values.values'; % C26
124         Point32 = data.n4_Point32.y_values.values'; % C27
125         % Stearing gear room
126         Point33 = data.n5_Point33__Z.y_values.values'; % C28
127         Point34 = data.n6_Point34__Y.y_values.values'; % C29
128         Point35 = data.n7_Point35__X.y_values.values'; % C30
129         Point36 = data.n8_Point36__Z.y_values.values'; % C31
130
131         dataMat = [Point1 Point2 Point3 Point5 Point6 Point7 Point8
                Point9 ...
132                 Point11 Point12 Point13 Point14 Point15 Point16 Point17
                        Point18 Point19...
133                 Point20 Point21 Point22 Point23 Point27 Point28 Point29
                        Point30...
134                 Point31 Point32 Point33 Point34 Point35 Point36];
135
136 end
137
138 %% Channel setup 3 Start:2013 12 10 (31 Channels) * Added synchronisation
        channel Point14
139
140 if channelSetup == 3
141         % Stern thruster
142         Point1 = data.n_Point1__Z.y_values.values';
143         Point2 = data.n_Point2__Z.y_values.values';
144         % Central measurement unit
145         Point3 = data.n_Point3__Z.y_values.values';
```

```
146         Point5 = data.n_Point5__Y.y_values.values';
147         Point6 = data.n_Point6__Z.y_values.values';
148         % Cargo hold 3
149         Point7 = data.n_Point7__Z.y_values.values';
150         Point8 = data.n0_Point8__Z.y_values.values';
151         Point9 = data.n1_Point9__Z.y_values.values';
152         % Bow
153         Point11 = data.n3_Point11__Z.y_values.values';
154         Point12 = data.n6_Point12__Y.y_values.values';
155         Point13 = data.n5_Point13__Z.y_values.values';
156         % Synchronisation channel
157         Point14 = data.n6_Point14.y_values.values';
158         % Superstructure
159         Point15 = data.n7_Point15__Z.y_values.values';
160         Point16 = data.n8_Point16__X.y_values.values';
161         Point17 = data.n9_Point17__Y.y_values.values';
162         Point18 = data.n0_Point18__Z.y_values.values';
163         Point19 = data.n1_Point19__Z.y_values.values';
164         % Cargo hold 3
165         Point20 = data.n2_Point20__Z.y_values.values';
166         % Central measurement unit
167         Point21 = data.n3_Point21__X.y_values.values';
168         Point22 = data.n4_Point22__Y.y_values.values';
169         Point23 = data.n5_Point23__Z.y_values.values';
170         % Strain Measurments -- not Calibrated
171         Point27 = data.n9_Point27.y_values.values';
172         Point28 = data.n0_Point28.y_values.values';
173         Point29 = data.n1_Point29.y_values.values';
174         Point30 = data.n2_Point30.y_values.values';
175         Point31 = data.n3_Point31.y_values.values';
176         Point32 = data.n4_Point32.y_values.values';
177         % Stearing gear room
178         Point33 = data.n5_Point33__Z.y_values.values';
179         Point34 = data.n6_Point34__Y.y_values.values';
180         Point35 = data.n7_Point35__X.y_values.values';
181         Point36 = data.n8_Point36__Z.y_values.values';
182
183         dataMat = [Point1 Point2 Point3 Point5 Point6 Point7 Point8
                Point9 ...
184                 Point11 Point12 Point13 Point14 Point15 Point16 Point17
                    Point18 Point19...
185                 Point20 Point21 Point22 Point23 Point27 Point28 Point29
                    Point30...
186                 Point31 Point32 Point33 Point34 Point35 Point36];
187
188 end
189
190 end
```

Appendix D

Multivariate Statistical Analysis

Table D.1: Factor analysis in open water.

Variable	Factor 1	Factor 2	Factor 3	Factor 4	Factor 5
Port Prop Motor Power	0.759373	0.058685	-0.114965	0.460389	0.199763
Rudder Position Port	-0.172258	-0.208592	0.715603	0.160262	0.135227
Propeller Pitch Port	0.906424	-0.116558	0.000106	0.082813	0.254394
Longitude	0.142432	0.313606	0.579686	-0.462221	-0.278280
Latitude	-0.262449	-0.223906	-0.171975	-0.792441	-0.310868
Airtemp	0.190322	0.295630	0.256191	0.844972	0.086596
WindSpeedRel	0.116367	0.140397	-0.032355	0.256875	0.855764
WindDirRel	0.087696	0.197038	0.751830	-0.035960	-0.112319
Heading	-0.065242	0.828536	0.017668	0.046911	0.287650
GpsSOG	0.967342	-0.126551	0.058680	0.044275	0.003346
Wave height	0.214677	0.051106	-0.049153	0.057135	0.902036
Wave Direction Rel	-0.133847	0.875274	0.082063	0.105596	-0.055780
Draft Mid	0.054497	-0.185802	-0.342514	0.844121	0.050637

Table D.2: Factor analysis in ice.

Variable	Factor 1	Factor 2	Factor 3	Factor 4	Factor 5
S10 Bow	-0.0821	0.6580	-0.3063	-0.1924	-0.1463
S12 Bow Shoulder	0.0919	0.7489	-0.0036	0.0005	0.0681
S15 Stern Shoulder	0.1345	0.7333	0.0117	0.0337	-0.1119
Port Prop Motor Power	0.6408	0.3642	0.0991	-0.0576	-0.3162
Rudder Position Port	-0.0025	-0.1466	-0.0686	-0.1040	0.4358
Propeller Pitch Port	-0.8103	0.1068	-0.1438	-0.1470	0.2118
Longitude	-0.3105	-0.0470	0.7550	0.0350	-0.2148
Latitude	0.7292	0.0994	-0.3520	0.0791	0.1108
Airtemp	-0.0972	0.1486	0.3720	-0.6914	0.1482
WindSpeedRel	0.2235	-0.1204	0.6519	0.0407	0.1347
WindDirRel	0.0732	-0.0025	0.2715	0.7219	0.0352
Heading	-0.4818	0.0659	0.1143	0.4725	0.3594
GpsSOG	-0.8576	0.0626	-0.0089	-0.0067	-0.2334
Ice Thickness	0.7222	0.1354	0.0243	0.0802	0.0445
Ice Concentration	0.8210	0.1049	-0.1429	0.0311	0.2487
Floe Size	0.3499	0.0548	0.1144	0.1753	0.7014
Draft Mid	0.7279	0.0777	0.2072	-0.3322	0.3007

Table D.3: Correlation matrix in open water.

	Bow		Steering Gear			Bridge		
Variable	P13	P12	P36	P34	P35	P16	P17	P18
	Port(+Z)	Centre(+Y)	Port(+Z)	Stb(-Y)	Stb(+X)	Stb(+X) HW	Stb(+Y) HW	Stb(+Z) HW
Port Prop Motor Power	0.4046	0.5147	0.3775	0.5187	0.3859	0.6343	0.7355	0.6870
Rudder Position Port	0.0183	0.0291	0.0260	0.0262	0.0216	-0.0258	-0.0764	-0.0504
Propeller Pitch Port	0.2316	0.3437	0.2216	0.3365	0.2081	0.4421	0.5195	0.4807
Longitude	-0.3521	-0.2948	-0.3423	-0.3140	-0.3676	-0.2559	-0.2997	-0.2876
Latitude	-0.6424	-0.6711	-0.6504	-0.6843	-0.6459	-0.6444	-0.6797	-0.6523
Airtemp	0.5851	0.6017	0.5996	0.6132	0.5985	0.5415	0.5382	0.5376
WindSpeedRel	0.8462	0.8110	0.8467	0.8233	0.8289	0.8512	0.8095	0.8420
WindDirRel	-0.2304	-0.2336	-0.1993	-0.2256	-0.2439	-0.1812	-0.1920	-0.2124
Heading	0.2978	0.2336	0.2881	0.2413	0.2828	0.3135	0.2040	0.2741
GpsSOG	-0.0763	0.0545	-0.0834	0.0494	-0.1020	0.1873	0.3253	0.2402
Wave height	0.7258	0.7607	0.7368	0.7669	0.7100	0.8232	0.8485	0.8304
Wave Direction Rel	0.0836	0.0162	0.0781	0.0133	0.0796	0.0434	-0.0920	0.0042
Draft Mid	0.3075	0.3291	0.2702	0.3300	0.3315	0.2376	0.2934	0.2815

Table D.4: Correlation matrix in ice.

	Bow		Steering Gear			Bridge		
Variable	P13	P12	P36	P34	P35	P16	P17	P18
	Port(+Z)	Centre(+Y)	Port(+Z)	Stb(-Y)	Stb(+X)	Stb(+X) HW	Stb(+Y) HW	Stb(+Z) HW
S10 F134 Bow	0.5501	0.6309	0.3816	0.3236	0.2847	0.6715	0.6385	0.5694
S12 F113 Bow Shoulder	0.2947	0.4295	0.2908	0.3298	0.2770	0.3751	0.4329	0.3565
S15 F41 Stern Shoulder	0.2486	0.4254	0.2817	0.3433	0.2905	0.3634	0.3718	0.3355
Port Prop Motor Power	-0.0051	0.3111	0.6354	0.7778	0.7196	0.2131	0.2423	0.3672
Rudder Position Port	-0.0721	-0.0269	-0.0247	0.0062	-0.0137	-0.0666	-0.0387	-0.0578
Propeller Pitch Port	0.4484	0.1951	-0.3707	-0.5497	-0.5899	0.2942	0.3144	0.0668
Longitude	-0.2215	-0.1558	-0.1688	-0.1070	-0.1558	-0.1268	-0.0988	-0.2146
Latitude	-0.1992	0.0515	0.1727	0.3480	0.3516	-0.0405	-0.0272	0.0236
Airtemp	0.0799	0.1012	0.0289	0.0312	0.0022	0.0057	0.0279	0.0234
WindSpeedRel	-0.3566	-0.2560	-0.1784	-0.0569	-0.1069	-0.3123	-0.2829	-0.2864
WindDirRel	-0.1348	-0.1280	0.0631	0.0932	0.1220	-0.1459	-0.1454	-0.0643
Heading	0.0900	-0.0425	-0.0708	-0.1576	-0.1249	0.0247	0.0211	0.0041
GpsSOG	0.5402	0.2751	-0.0177	-0.2566	-0.2792	0.3445	0.3621	0.2672
Ice Thickness	-0.2330	0.0066	0.2263	0.3925	0.4072	-0.0496	-0.0805	0.0111
Ice Concentration	-0.1935	0.0304	0.2634	0.4185	0.4200	-0.0789	-0.0927	0.0527
Floe Size	-0.2508	-0.1834	-0.1267	-0.0190	0.0103	-0.1962	-0.1871	-0.1964
Draft Mid	-0.2880	-0.0597	0.0790	0.2876	0.2578	-0.2867	-0.2455	-0.1353

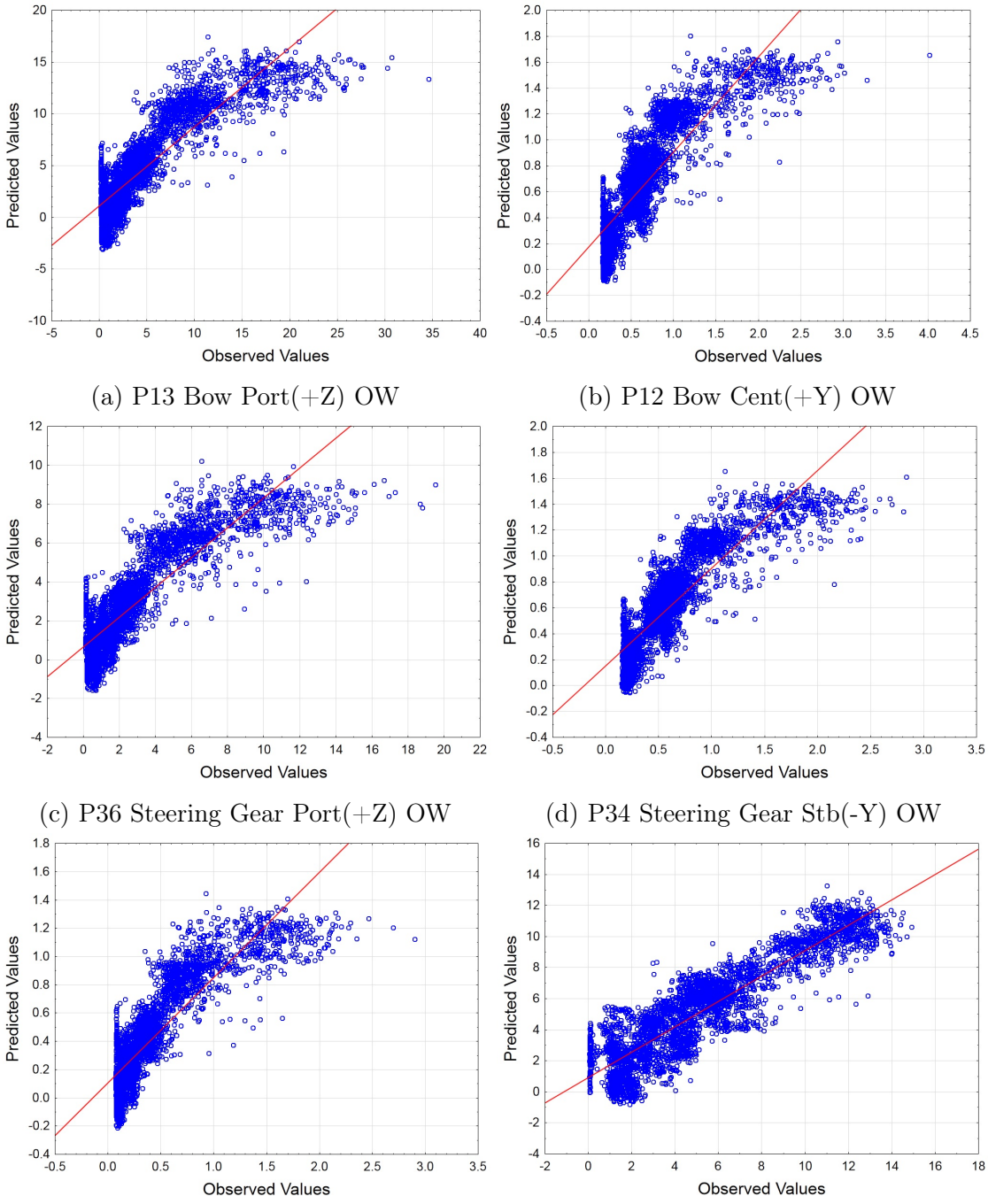

(a) P13 Bow Port(+Z) OW

(b) P12 Bow Cent(+Y) OW

(c) P36 Steering Gear Port(+Z) OW

(d) P34 Steering Gear Stb(-Y) OW

(e) P35 Steering Gear Stb(+X) OW

(f) P16 Bridge stb(+X) OW

Figure D.1: Predicted vs observed values.

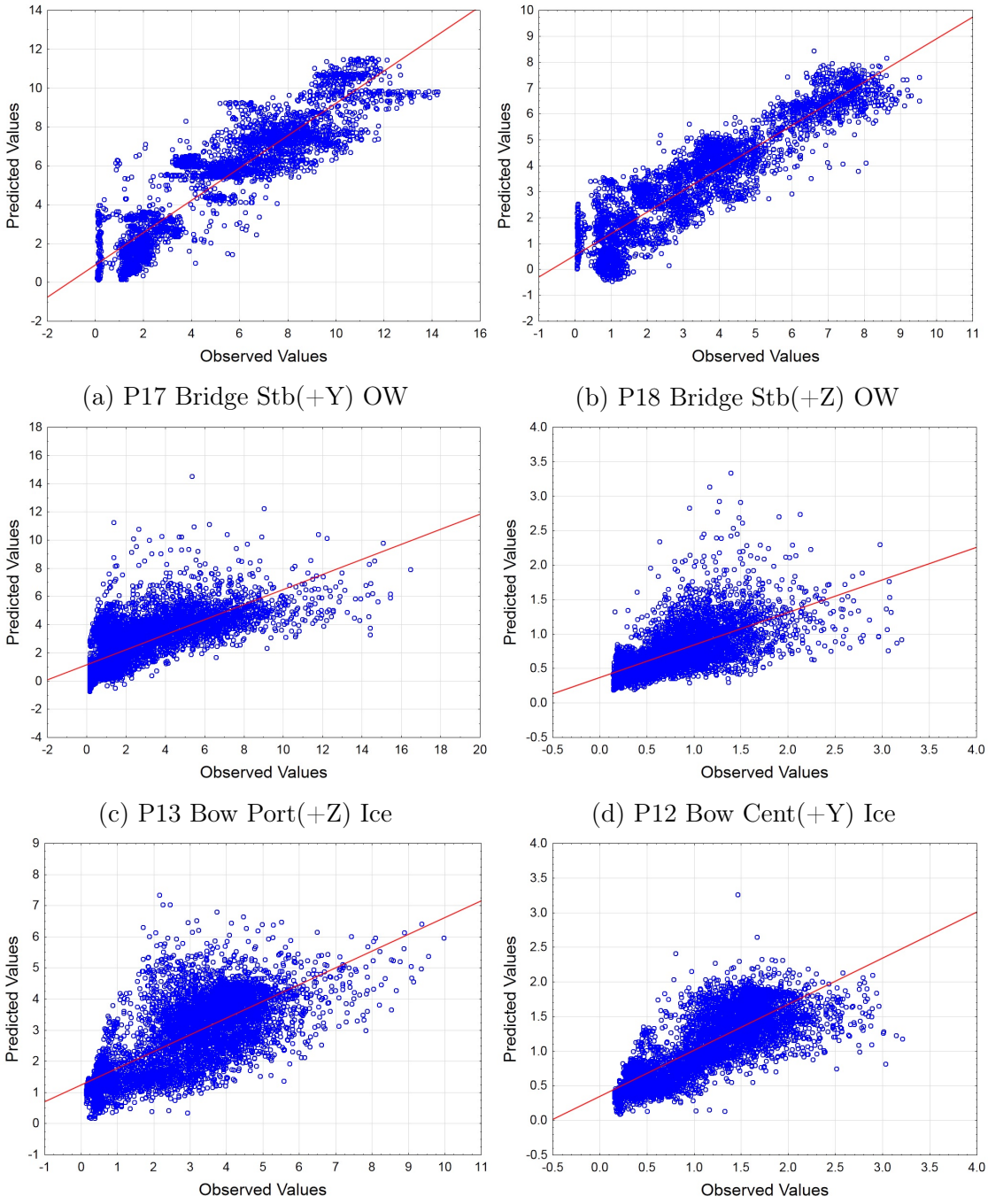

(a) P17 Bridge Stb(+Y) OW

(b) P18 Bridge Stb(+Z) OW

(c) P13 Bow Port(+Z) Ice

(d) P12 Bow Cent(+Y) Ice

(e) P36 Steering Gear Port(+Z) Ice

(f) P34 Steering Gear Stb(-Y) Ice

Figure D.2: Predicted vs observed values.

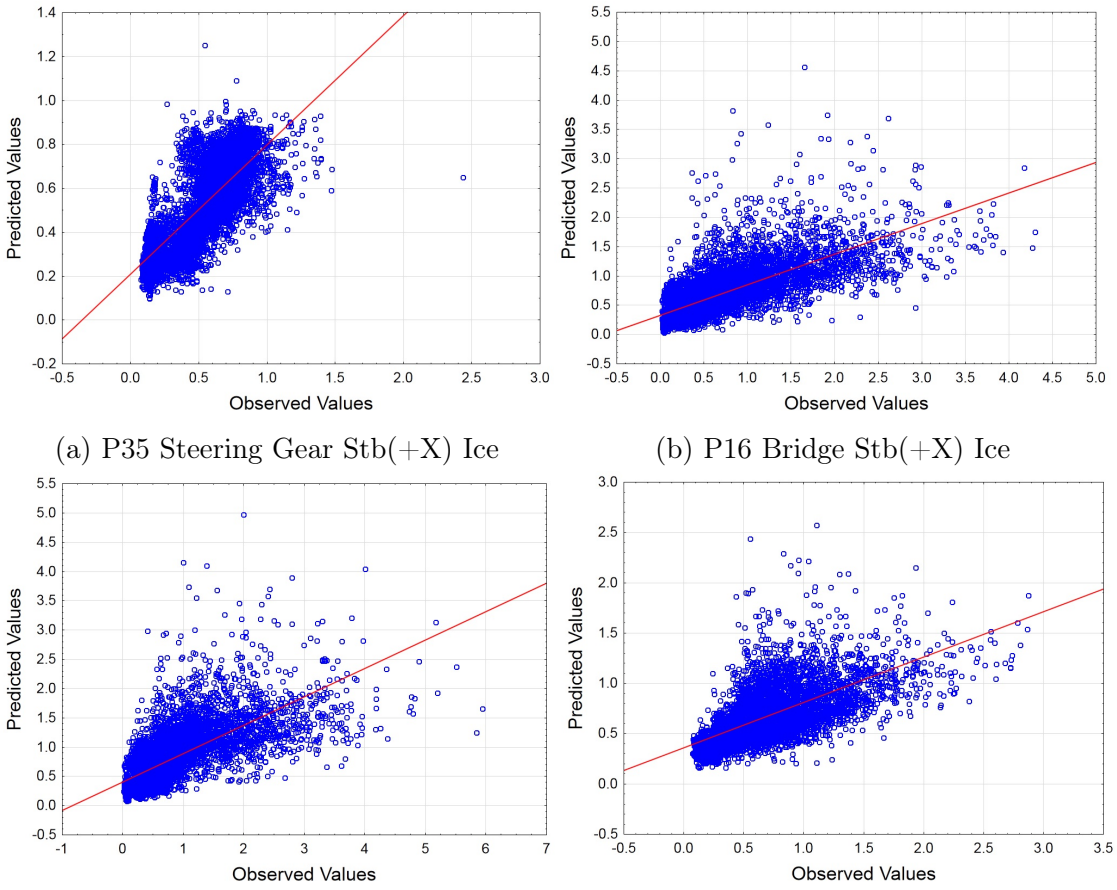

(a) P35 Steering Gear Stb(+X) Ice

(b) P16 Bridge Stb(+X) Ice

(c) P17 Bridge Stb(+Y) Ice

(d) P18 Bridge Stb(+Z) Ice

Figure D.3: Predicted vs observed values.

Appendix E

Operational Modal Analysis

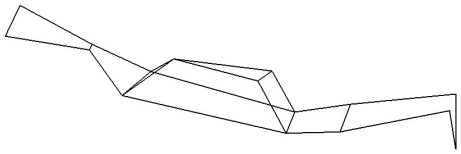

(a) f=1,94 Hz, 2-node, iso view.

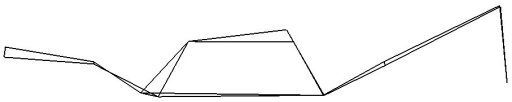

(b) f=1,94 Hz, 2-node, side view.

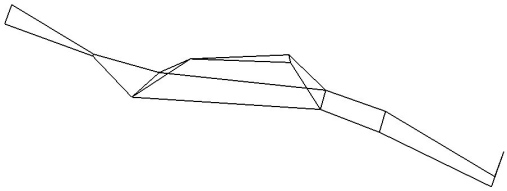

(c) f=3,37 Hz, 3-node, iso view.

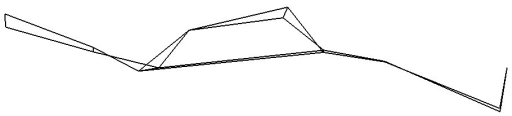

(d) f=3,37 Hz, 3-node, side view.

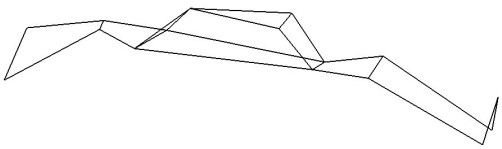

(e) f=4,72 Hz, 4-node, iso view.

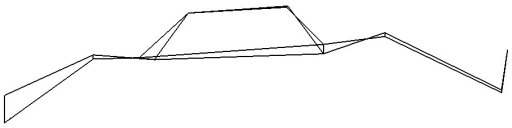

(f) f=4,72 Hz, 4-node, side view.

Figure E.1: Mode shapes of the first three vertical bending modes, showing isometric and side views.